DNA-damage-mediated remodeling of normal and tumor microenvironments modulates cell survival

By

Luke A. Gilbert
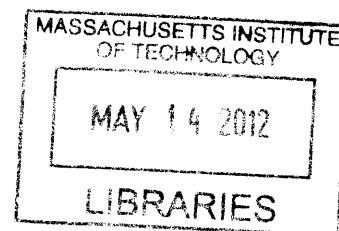
B.S. Microbiology, Immunology and Molecular Genetics
University of California Los Angeles, 2006

SUBMITTED TO THE DEPARTMENT OF BIOLOGY IN PARTIAL
FULFILLMENT OF THE REQUIREMENTS FOR THE DEGREE OF:

DOCTOR OF PHILOSOPHY IN BIOLOGY

AT THE
MASSACHUSETTS INSTITUTE OF TECHNOLOGY
June 2012

Signature of Author _____
April 24, 2012

Certified by: _____
Dr. Michael Hemann
Thesis Advisor

Accepted by: _____
Dr. Robert Sauer
Chairperson, Graduate Committee

1

Table of contents:

DNA-damage-mediated remodeling of normal and tumor microenvironments modulates cell survival

By Luke A. Gilbert

Submitted to the Department of Biology on May 11, 2012 in Partial Fulfillment of the requirements for the degree of Doctor of Philosophy in Biology

Abstract:

Chemotherapeutic regimens involve the systemic administration of genotoxic compounds that induce cancer cell death via well-established DNA damage response signaling networks. While modern chemotherapeutic regimens can be curative, chemotherapeutic drug resistance remains a major clinical problem. This drug resistance can be cancer cell intrinsic or extrinsic. Mechanisms of cancer cell intrinsic drug resistance include apoptotic defects, DNA repair mechanisms, drug efflux pumps, and cell cycle defects. Less well understood is how cancer cell extrinsic drug resistance occurs and whether this process is modulated by DNA damage associated with chemotherapy.

Here, I have used the *Eμ-myc* lymphoma model to study cancer cell extrinsic drug resistance. In this model, I see that certain tumor microenvironments such as the thymus are chemoresistant and that DNA damage in thymic endothelial cells induces an acute secretory response that promotes lymphoma cell chemotherapeutic resistance. Mechanistically, DNA damage induces the rapid activation of a p38-dependent stress response in endothelial cells resulting in the acute release of many proteins including IL-6 and Timp-1. Together these two proteins promote lymphoma cell resistance to apoptosis through the induction of Bcl-XL. While this acute secretory response includes some of the same secreted proteins as the senescence-associated secretory phenotype it differs substantially in both kinetics and mechanism suggesting the two are distinct cellular processes. Furthermore, we see in these chemoresistant microenvironments that drug response requires activation of death-receptor-activated apoptosis suggesting an unexpected complexity to therapeutic response in drug-resistant tumor microenvironments. Thus, local pro-survival signaling may present a fundamental barrier to tumor clearance by genotoxic agents, suggesting that effective treatments need to target both cancer cells and the tumor microenvironment.

Long-lived metazoans have evolved complex mechanisms of tissue protection and repair. To better understand the physiological importance of secretory phenotypes in response to sterile injuries such as DNA damage, we investigated whether IL-6 promotes progenitor cell survival and tissue repair. Here, I have identified a role for the acute DNA-damage-mediated secretory phenotype in the protection of hematopoietic stem cells and in thymic regeneration. Together these observations suggest that tissue repair and response to chemotherapy can be similar processes with different therapeutic windows.

Thesis Supervisor: Michael Hemann
Title: Associate Professor of Biology

Acknowledgements

Chapter 1:

Introduction

Tumor development and treatment occur in the context of an endogenous tissue, with neoplastic cells surrounded by a diverse set of non-transformed cells (1). In fact, for some tumors, the stromal tissue constitutes the majority of the overall tumor mass (2,3). Tumor cells interact with normal cells in the tumor microenvironment through secreted and surface-bound proteins, and these interactions are critical for tumor progression. For example, tumor–stromal interaction is essential for numerous processes that occur during tumor development, including neovascularization, immune surveillance and evasion, and metastasis. Furthermore, it is well established that normal cells in the tumor microenvironment secrete a variety of factors that promote tumor cell survival and growth during various stages of tumor development. Less well understood is how the tumor microenvironment modulates the response to genotoxic chemotherapy. This thesis describes how the tumor microenvironment modulates tumorigenesis and the response to frontline cancer therapy in the *Eμ-myc* lymphoma model.

Chemotherapeutic efficacy, resistance and relapse in the clinic

The use of chemotherapeutic agents to treat cancer is a mainstay of cancer therapy. Modern combinatorial chemotherapeutic regimens are the product of decades of research. The idea of using a specific chemical to treat

5

human disease was described in the early 1900's by Paul Ehrlich who coined the term chemotherapy and performed some of the first treatments of animal models of disease using specific chemical compounds (4). This seminal work also described important concepts such as a therapeutic window for toxic chemicals based on disease-intrinsic differences between normal cells and target cells.

Several decades later, it was accidentally discovered that nitrogen mustards potently ablate the bone marrow and lymphatic tissues of humans suggesting that perhaps they could be of use in the treatment of blood cancers (5,6). In 1946, Goodman, Gilman and Linskog were the first to use a chemotherapeutic to treat a cancer patient (7,8). Here they administered the nitrogen mustard, mustine, to a non-Hodgkins lymphoma patient. In this patient they observed significant disease remission, suggesting that systemic administration of genotoxic compounds could be used to kill cancer cells and improve patient prognosis. By 1948, Farber and colleagues used the anti-folate, aminopterin, to achieve near complete remission in children with advanced acute leukemias. Here for the first time they described the clinical phenomenon of minimal residual disease in which a patient in complete remission following the cessation of therapy exhibited leukemic nodules in the scalp (9).

While chemotherapy was initially used primarily in unresectable cancers such as blood cancer by the 1960's, it became apparent to oncologists that local radiation and surgery could only achieve partial cure rates (10). This realization

that micrometastatic disease could be disseminated throughout the body at the time of treatment suggested that systemic chemotherapy would be an important adjuvant therapy in resectable solid tumors (11). Excitingly, the introduction of combinatorial chemotherapeutic regimes quickly resulted in high long-term cure rates in 10 types of tumors by 1978 (10,12,13).

Currently, nearly all tumors are treated with chemotherapy. This therapy can take the form of conventional genotoxic chemotherapeutics or newer targeted therapeutics. Each year, new progress is made utilizing new chemotherapeutics or new combinations of existing chemotherapeutics. For example, bendamustine, a new nitrogen-mustard derivative, was recently approved for the treatment of chronic lymphocytic leukemia (14). Alternatively, using existing chemotherapeutics, a novel combinatorial chemotherapeutic regime termed FOLFIRINOX was recently developed for the treatment of metastatic pancreatic adenocarcinoma (15).

Modern molecular biology has created many new targeted chemotherapies that attempt to fulfill the "magic bullet" hypothesis described by Paul Ehrlich over 100 years ago. He hypothesized that the perfect therapeutic agent would be a chemical targeting a process in diseased cells not required for the survival of normal cells (4). New chemotherapeutics that inhibit oncogenic Bcr-Abl, ErbB-1, Eml4-Alk and B-Raf proteins fulfill this requirement (16-19). Due

in part to the success of targeted and conventional chemotherapeutics, mortality from cancer has decreased every year since 1990 (11).

Drug resistance and minimal residual disease in cancer therapy

Despite the many successes using chemotherapy, intrinsic and acquired resistance to chemotherapy remains a major clinical problem. In intrinsically drug-resistant tumor types, such as glioblastoma, hepatocellular carcinoma and pancreatic adenocarcinoma, the current standard of care confers a modest survival advantage of only weeks to months (15,20,21). Two major subtypes of intrinsic drug resistance occur in the clinic. Drug resistance can arise from apoptotic defects, low mitochondrial priming, detoxifying enzymes, or high levels of multidrug efflux pumps, as is the case in hepatocellular carcinoma (22,23). Alternatively, resistance may arise due to physical barriers, which limit drug delivery. Tumor cells in the brain are highly resistant to chemotherapy, as the blood brain barrier is a physical barrier to drug delivery (24). In other tumors types, such as pancreatic adenocarcinomas, the tumors are poorly vascularized, highly fibrotic and have very high levels of negative interstitial fluid pressure, presenting a physical barrier, which limits drug delivery (25).

Acquired drug resistance is a clinical phenomenon seen in most tumor types in which a tumor initially regresses in response to chemotherapy but at relapse is insensitive. Here, many genetic alterations, which confer resistance to traditional chemotherapeutics, have been described. These include up-regulation

8

of detoxifying enzymes or drug transporters, alterations to DNA repair processes, apoptotic defects, or the acquisition of stem-cell-like characteristics (26-31). New forms of acquired resistance have emerged with increased use of targeted therapeutics. In this case, resistance most frequently occurs due to mutations in the biochemical target of the therapeutic or in proteins of the downstream pathway (32-34).

Effective cancer therapy using surgery, radiotherapy, or chemotherapy results in the absence of macroscopic disease either at the site of the primary tumor or at common distal sites of disease dissemination. However, despite this initial tumor clearance, many patients who have undergone such therapy will relapse (35). Thus, small cohorts of tumor cells can survive in cryptic anatomic loci following therapy. This fundamental problem has been recognized as the major limiting factor in curing patients since the initiation of systemic chemotherapy (36,37). These surviving cancer cells represent minimal residual disease (MRD) (38). Patients in disease remission can be further sub-classified as MRD-positive or -negative with the use of high-resolution tumor detection techniques, including flow cytometry and PCR (36). Not surprisingly, patients who are MRD-positive have a significantly poorer prognosis than those who are MRD-negative.

The mechanisms by which MRD survives chemotherapy despite the effective elimination of bulk tumor cell populations remain unclear (39). Tumor

drug resistance at relapse is classically associated with cell-intrinsic processes, including apoptotic defects, up-regulation of multidrug efflux pumps, decreased proliferation rates, and defects in DNA damage recognition (40-42). However it is not clear when during relapse this resistance arises. More recently, it has been suggested that cancer stem or initiating cells are more resistant to conventional chemotherapy, and it is this population of tumor cells that fuels disease relapse (43). However, these putative resistance mechanisms for MRD have not been examined in relevant therapeutic settings, largely due to the absence of established preclinical models of MRD persistence. Thus, it is unclear whether MRD survives therapy in a stochastic or cell-autonomous manner, or if response to therapy is specific to the tumor microenvironment. Although the persistence of residual disease is a well-established contributor to disease recurrence and treatment failure, preclinical animal models of cancer therapy have generally failed to interrogate how these cancer cells survive and relapse.

Mouse models of cancer therapy

Cancer is a genetic disease in which the normal function and regulation of a cell is lost. Historically, cancer cells have been described as having several hallmark traits, including deregulated growth, resistance to cell death, and immortalization (44). However, this cell-intrinsic view of the genetic alterations leading to the onset of a frank tumor does not account for the complexity of a cell in the context of an organism (1). Therefore, to study tumor development, progression, metastasis and therapy *in vivo,* scientists have developed *in vivo,*

cancer models in several model organisms, including *D. rerio, D. melanogaster, M. musculus* and *R. norvegicus* (45-47). Here I will discuss both xenograft and genetically engineered mouse models of cancer with an emphasis on cancer therapy.

While mice have been widely used to study tumor development, progression, and metastasis, the use of mice to study cancer therapy has lagged behind. Historically, our understanding of how chemotherapeutic agents kill tumor cells is derived from cell-culture models (48). Cell-culture models of chemotherapy are important in understanding cancer-cell-intrinsic resistance and sensitivity; however, they fail to account for the complexity of a tumor within an organism. Thus, to study cancer therapy in a relevant microenvironment, therapy studies must be carried out *in vivo*. Here rodents, as mammals, are particularly important in the study of cancer therapy as they enable interrogation of the pharmacodynamics, pharmacokinetics and toxicology of novel chemotherapeutic agents (49).

Xenograft mouse models of cancer therapy

Early experimental models of drug treatment *in vivo* demonstrated that mice xenografted with human tumors could recapitulate the resistance and sensitivity seen in the patients from which these xenografts were derived. In a seminal study, 2-3mm tumor samples from bronchial carcinoma patients were xenografted subcutaneously into immune-suppressed mice. These mice were

then treated with the same chemotherapeutic agents as the patients had received (50). Here, the tumor response in mice was very similar to what was seen in the corresponding patients, suggesting that xenograft models are a useful tool for studying cancer therapy. These data have been recapitulated in a number of types of cancer, suggesting that primary patient samples xenografted into mice have significant pre-clinical value as a model for cancer therapy (51-53).

These data has also been cited as evidence for the reverse pre-clinical relationship. Here, mice xenografted with human tumors derived from cancer cells lines are treated with a novel therapeutic agent, and partial or complete responses are often sufficient to begin a clinical trial. Disappointingly, it has been observed retrospectively that pre-clinical efficacy for novel therapeutics using only data from cell lines xenografted into immunodeficient mice generally fails to correctly predict efficacy in the clinic (48,52,54). This is most likely due to the common practice of using human tumor cell lines rather than primary patient samples in mice. Improvements to xenografts have been implemented, including the addition of human stromal cells, human growth factors/extracellular matrix, and the use of mice with a human immune system; however, it remains unclear whether these improvements will translate to improved clinical transition of novel therapeutics (55). While these improvements do more closely mimic an autochthonous tumor, they fail to account for autochthonous vascular and immune contributions to the tumor microenvironment. Thus, it has been

suggested that improved pre-clinical data will be derived using genetically engineered mouse models of cancer.

Increasing evidence suggests that, when compared directly, genetically engineered mouse models (GEM) are indeed a better pre-clinical model than either cell culture or xenografts for the evaluation of novel therapeutics. In one widely cited example, a class of drugs known as thiazolidinediones, which are agonists of peroxisome proliferator-activated receptor-γ, showed strong anti-tumor activity against colon cancer cell lines and xenografted tumors but no efficacy in a genetically engineered model of colon cancer and subsequently showed no activity in a Phase II clinical trial (56-58). In another example, a class of drugs designed to treat Ras-driven tumors, the farnesyltransferase inhibitors, were extremely effective *in vitro* and in xenografts. However, they were shown not to be k- or n-Ras specific *in vivo* in a GEM model of breast cancer, suggesting the efficacy was not related to the inhibition of Ras signaling (59). Unfortunately, this proved to be correct, as this class of drugs failed to significantly improve patient prognosis in clinical trials (60). In both of these examples, while it is not entirely clear why the GEM models provided the more accurate data, the results support the idea that studying cancer therapy in autochthonous tumors provides better pre-clinical data.

Genetically engineered mouse models of cancer

Genetically engineered mouse models have been fundamental to the progress made in all areas of cancer research. Genetically engineered mouse models of cancer have been essential in functionally validating putative oncogenes and tumor suppressors *in vivo*. Here, hypothesis-driven genetic experiments have proven much of the theory behind tumor development. These models also enable the dissection of how tumor cells interact with untransformed cells of the immune system, the vasculature, stromal cells, and the extracellular matrix within the tumor microenvironment (61). Evidence for the relevance of these mice as tools comes from the observation that primary autochthonous and syngeneic transplantable tumors models more faithfully recapitulate the complex histopathology seen in human tumors than do cell line xenografts (62). These models arise in the correct tumor microenvironment with an appropriate complement of stromal, endothelial and immune cells (63). The creation of models syngeneic with the host has also enabled the study of how the immune system modulates tumorigenesis in ways not possible with human tumors (64,65). Thus, for many types of human cancer, mouse models have been constructed that model the genetics, histopathology, and disease progression seen in the clinic.

Mice are the most tractable mammalian organism for modeling human disease due to their small size, short generation time and large litter sizes (66). Even more important is the ability to easily generate transgenic mice, thus creating a genetic model organism for rapidly testing hypotheses. In the 1980's,

the ability to generate transgenic and gene-targeted mice by genetic manipulation of mouse embryonic stem cells resulted in the creation of the first genetic models of cancer (67-70). More recently, mouse models have become increasingly sophisticated due to the development of conditional and inducible alleles in which genes are manipulated in a developmentally and temporally restricted manner (71,72). This has enabled the construction of models that more closely mimic the penetrance and timing of human disease.

The ability to create tumors in mice from a specific cell of origin with complex or inducible genotypes has enabled the causal interrogation of correlative genetic data from patient cohorts. Many studies have stratified patients by outcome following therapy and performed expression profiling, genomic copy number analysis, or sequencing to identify alterations associated with prognosis (73). Every year new transgenic mouse models are created to functionally test the causality of these genetic associations (74-77).

Broadly, genetically engineered mouse models can be divided into two groups. In the more stringent and classic class of cancer models, mice are born with germ-line genetic alterations that predispose them to cancer. Here, tumors develop in a truly autochthonous manner and mimic the variability in latency and metastasis seen in human tumors (61). As all such GEM tumor models have variable latency, mice must be staged using advanced imaging techniques such as PET or CT scans prior to therapy. Such GEM mice are considered a gold

standard for therapy studies, but it is difficult and expensive to generate sufficient numbers of appropriately staged mice for therapy studies.

In a second approach, transplantable genetically engineered mouse models of cancer have been developed. Here, tumor cells or progenitor cells are transplanted into multiple recipient mice such that tumors arise in a more synchronous manner for therapy studies (78). These tumors, while not truly autochthonous, can give rise to tumors in "autochthonous" tumor microenvironments with the correct complement of stromal, endothelial and immune cells. The main limitation in these models is whether transplanted cells form a tumor in tumor microenvironments that resembles autochthonous disease. Leukemia and lymphoma are particularly amenable to transplantation, although lung, breast, pancreatic, and liver cancer models have also been constructed (79-85). For solid tumors, injection of tumor cells into orthotopic sites or into the spleen or portal vein may be required for proper tumor seeding.

Recently, RNAi has enabled, transplantable models of cancer to be increasingly used as tools for the rapid validation of pools of genes putatively involved in cancer. Here, tumor cells or progenitor cells can be genetically modified ex-vivo using viral transduction with vectors expressing stable shRNAs prior to transplantation into recipient mice (86-88). This process of functionally validating large numbers of genes correlated with outcome following cancer therapy is a crucial step in drug discovery, as it provides a biochemical target for

novel therapeutics. Unfortunately, the use of GEM models of cancer to study

therapeutic response has lagged behind the study of primary tumor initiation,

growth, and metastasis (49). Here, I will discuss in detail seminal work on cancer

therapy in two cancer models: the $E\mu$-myc lymphoma model and the k-$Ras^{G12D/+}$

model of non-small-cell lung cancer.

Understanding the genetics of therapeutic response using the $E\mu$-myc

mouse

One of the first pre-clinical GEM models used to study the genetics of

therapeutic response to conventional chemotherapeutic agents was the $E\mu$-myc

mouse, a model of human Burkitt's lymphoma. In this transgenic mouse model,

the Ig heavy chain enhancer drives expression of high levels of c-myc during B

cell development (89). This models the t(8;14)(q24;q32) translocation most

commonly associated with human Burkitt's lymphoma. $E\mu$-myc mice develop

spontaneous pre/pro- and immature B cell lymphomas with complete penetrance.

Seminal studies by Schmitt and colleagues utilized the $E\mu$-myc mouse to

dissect how the p53 pathway modulates response to therapy *in vivo* (78,90).

Here, they saw that loss of p16/p19 or p53, or overexpression of Bcl-2, promoted

resistance to the conventional chemotherapeutic cyclophosphamide. Using this

model, they showed that all of these mutations, which disable the apoptotic

program, promote both tumorigenesis and resistance to therapy, suggesting that

these processes are linked. They also were able to uncouple the role for p53 in

cell-cycle arrest and genomic stability from its role in apoptosis by comparing *Eμ-myc p53$^{+/-}$* to *Eμ-myc p53$^{+/-}$ Bcl-2* or *Eμ-myc p53$^{+/-}$ Caspase 9^{DN}* mice. Here, prior to transformation, *Eμ-myc p53$^{+/-}$ Bcl-2* and *Eμ-myc p53$^{+/-}$ Caspase 9^{DN}* pre-malignant B cells are less apoptotic and the resulting tumors retain the wild-type p53 allele and a normal ploidy (91). This result suggests that apoptosis is the only function of p53 that is selected against during lymphomagenesis. In a crucial validation of GEMs as preclinical models, Schmitt and colleagues also showed that in the *Eμ-myc* tumor model, Bcl-2 overexpression promotes resistance to a variety of conventional chemotherapeutic agents, including doxorubicin, cyclophosphamide and docetaxel, *in vivo*. In contrast, a long-term, lymphoma-cell-culture model of this same *Eμ-myc Bcl-2* tumor showed no chemoresistance in a standard clonogenic survival assay (92). These experiments provided much of the early proof that GEM models are important pre-clinical therapeutic models for dissecting the genetics of cancer therapy.

Using the *Eμ-myc* lymphoma model, it was shown that constitutive activation of survival signaling also promotes both lymphomagenesis and chemoresistance. Here *Eμ-myc Akt* lymphomas are quantitatively and pathologically indistinguishable from *Eμ-myc Bcl2* or *Eμ-myc p53$^{-/-}$* lymphomas. In the *Eμ-myc Akt* lymphomas, the authors saw no p53 pathway mutations, suggesting that activation of pro-survival pathways during tumorigenesis eliminates the selective pressure to inactivate apoptosis. In these *Eμ-myc Akt* lymphomas the combination of doxorubicin and rapamycin was shown to be an

effective combination therapy, while neither single agent provided a survival

advantage (93). In that study and a later study it was shown that activation of

eIF4E downstream of Akt overexpression or Pten haploinsufficiency was

sufficient to induce resistance to therapy, and a proof-of-principle experiment

showed that a novel translation inhibitor silvestrol sensitized *Eμ-myc Pten*$^{+/-}$

lymphomas to doxorubicin-induced apoptosis (93,94).

The genetics of resistance to other novel therapeutic agents such as the

histone deacetylase inhibitor vorinostat have also been studied in the *Eμ-myc*

model. Here, loss of the pro-apoptotic Bcl-2 family members Bid and Bim, but not

p53, promote resistance to vorinostat (95). This model has also been used to

identify spontaneous recurrent chromosomal aberrations that confer resistance

or sensitivity in lymphomas (96) The *Eμ-myc* model has also proven to be an

excellent pre-clinical model for predicting cell-intrinsic genetic determinants of

therapeutic response in other tumor types. In one seminal example of this, Jiang

and colleagues used the *Eμ-myc* lymphoma model to show that loss of the tumor

suppressor ATM promotes resistance to therapy if the cells express functional

p53, while it promotes drug sensitivity if cells are p53-defective (97). This initial

observation was then retrospectively confirmed in human breast, lung and colon-

cancer patients.

Cancer therapy in the *k-Ras*$^{G12D/+}$ mouse model of non-small cell lung
cancer

Another mouse model that has been used extensively to study response to chemotherapy is the k-Ras$^{G12D/+}$ mouse model of non-small-cell lung cancer (98). Using this model, Oliver and colleagues demonstrated that lung cancers are initially sensitive to cisplatin independent of p53 or p21 status but rapidly develop resistance to cisplatin. Here, these chemoresistant tumors have increased genomic alterations, a more aggressive tumor pathology, and an up-regulation of genes involved in DNA repair and cell-cycle control (28). This theme of acquired resistance is not unique to conventional chemotherapeutics. Using the same model of non-small-cell lung cancer, Xue and colleagues showed that k-Ras$^{G12D/+}$ p53$^{-/-}$ but not k-Ras$^{G12D/+}$ p53$^{+/+}$ tumors respond to multiple different NFκB inhibitors, but over time they develop resistance (99). In this lung-cancer model, both cisplatin and NFκB inhibitors induce apoptosis in responsive tumors but not in resistant tumors, suggesting that resistant tumors have evolved to avoid apoptosis associated with DNA damage or the deprivation of survival signals. Interestingly, they also suggest that basal NFκB activity is predictive of response and should be used as a clinical biomarker. An interesting approach to circumventing the problem of acquired resistance to therapy was proposed by Doles and colleagues. They showed using the k-Ras$^{G12D/+}$ p53$^{-/-}$ model of non-small-cell lung cancer and the Eμ-myc p19$^{Arf-/-}$ lymphoma model that the error-prone DNA polymerases Rev 1 and Rev 3 promote the acquisition of therapy-associated mutations and both intrinsic and acquired resistance to cyclophosphamide and cisplatin (84,100).

The k-$Ras^{G12D/+}$ lung-cancer model has also been used as a model to identify new therapeutic strategies for Ras-driven tumors. In two GEM examples, the k-$Ras^{G12D/+}$ $p53^{-/-}$ lung-cancer model and a $Nf1^{+/-}p53^{+/-}$ malignant peripheral-nerve-sheath tumor model, De Raedt and colleagues described an exciting new therapeutic strategy that takes advantage of the Ras-driven endoplasmic-reticulum stress in these tumors. Tumor-bearing mice from both GEM models were treated with a combination of HSP90 inhibitors and rapamycin, resulting in irreversible damage to the endoplasmic reticulum and mitochondria and tumor regression (101). Here, they see that normal cells were largely unaffected by this combination, suggesting a novel therapeutic window based on Ras-induced cell stress. Recently, Chen and colleagues have used the k-$Ras^{G12D/+}$ lung-cancer model to attempt to predict the outcome of an ongoing clinical trial assessing the efficacy of combining the MEK inhibitor selumetinib with docetaxel. Here they see that mice with k-$Ras^{G12D/+}$ and k-$Ras^{G12D/+}$ $p53^{-/-}$ tumors have a significant survival advantage when treated with a combination of selumetinib and docetaxel (102). In contrast, mice with k-$Ras^{G12D/+}$ $Lkb1^{-/-}$ tumors show no response. This approach predicts that with sufficient pre-clinical mouse-model data, clinicians may be able to selectively enroll only patients whom they would predict should see a survival benefit from new therapeutic agents and reduce the incidence of clinical trials enrolling all patients with a particular disease, which can result in false-negative reports.

The k-$Ras^{G12D/+}$ model of non-small-cell lung cancer and the $E\mu$-myc

lymphoma model have revolutionized how GEM models are used to study

chemotherapy. This success has spurred construction or use of other GEM

models of cancer to study resistance to conventional chemotherapeutics and to

develop novel therapeutic strategies. In all genetically engineered mouse models

of cancer, durable response to therapy is rarely observed, and mice are almost

never cured. This models what is seen in the clinic. Thus, it has been suggested

that a better understanding of where and how tumor cells survive in the various

microenvironments could inform new clinical advances.

A role for organ physiology and normal cells in cancer: discovery of the

tumor microenvironment

A better understanding of how the tumor microenvironment modulates

tumor growth, metastasis and resistance to therapy is a major goal in oncology.

The idea that a tumor is not an autonomous entity originated as early as the

1880's when surgeons realized that patterns of metastasis were not random.

Paget and colleagues interpreted this as meaning that normal tissue

microenvironments modulate tumor cell seeding and growth during metastasis.

(103). Extensive later work used a variety of models to show that tumor cells

have an inherent propensity to metastasize to select tissues independent of

vascular physiology (104-106). This work highlights how tissue-specific physical

or genetic factors, which create a local microenvironment, dictate the ability for a

cancer cell to form a metastasis. This seminal work also proved that there are

specific interactions between cancer cells and normal cells required for tumor progression (107). Thus, normal cells are critical effectors of tumor metastasis and tumor initiation. In contrast, a frank tumor is not a normal tissue and untransformed cells within a tumor are thought to be altered (108,109). Thus, the microenvironment surrounding a cancer cell may actually represent a continuum, with neoplastic cells in contact with physiologic tissue or within a tumor in a range of malignant transformation.

Dissection of the soluble microenvironment: growth and survival factors

Soluble paracrine signals emanating from many cell types in the tumor microenvironment can promote tumor progression, metastasis, and drug resistance in various tumor types (110). The establishment of cell culture techniques initially proved that both normal and tumor cells can have diverse paracrine growth or survival requirements. For example, most cancer cell lines proliferate robustly in response to soluble factors present in serum (111). Early research also showed that paracrine factors act in a context-specific manner. Here, normal human fibroblasts proliferate robustly in response to human serum combined with chick embryo extract, while human epithelial cell growth is inhibited by the addition of chick-embryo extract (112). In 1954, Cohen and colleagues identified the first specific growth factor, Nerve Growth Factor (113). They identified a soluble protein secreted by a mouse sarcoma cell line that induced the growth of chick embryo sympathetic ganglia *in vivo* and *in vitro*. Importantly, they also showed that this effect was context-specific, as the

sarcoma failed to induce chick ganglion outgrowth *in vitro* if the sarcoma cells were first grown in a mouse rather than a chick embryo.

In the 1980's many paracrine factors, including interleukins 1-6, were identified and later cloned as growth factors secreted by non-transformed cells that induced proliferation of cancer cells (114-118). Work by Orin and colleagues also showed that in other cell lines these same growth factors, such as IL-6, were required not for growth but for survival following induction of apoptosis. This early work suggests that a single protein can have context-specific functions in cancer cell growth and survival (119). In contrast, other inducible molecules, such as IFN-λ or TRAIL, can strongly inhibit proliferation or induce apoptosis in cells (120). Thus *in vitro,* both normal and cancer cells respond to paracrine signaling with specific and diverse phenotypes depending on the combination of extracellular cues.

The tumor microenvironment in cancer therapy and tumor development

While seminal *in vitro* work deconstructing how paracrine and autocrine signals control cell cycle and apoptosis have advanced our understanding of cancer, it is important to study paracrine signaling *in vivo* in an actual tumor microenvironment. Soluble paracrine factors have been shown to promote resistance to both conventional cytotoxic chemotherapeutics and to targeted therapeutics. One type of resistance occurs when non-transformed cells within the tumor microenvironment secrete factors that prevent tumor cell apoptosis.

One example of this is multiple myeloma, in which IL-6 secreted by bone marrow stromal cells promotes tumor cell resistance to dexamethasone, bortezomib and lenalidomide in the bone marrow microenvironment (121). Multiple myeloma cells are also reliant on stromal IGF-1, which activates both AKT and NFκB, suggesting that bone-marrow-stromal cells secrete multiple factors that modulate tumor-cell survival (122). Paracrine factors can also promote resistance to targeted therapeutics. In a GEM model of BCR-ABL-positive acute lymphoblastic leukemia, Williams and colleagues showed that paracrine IL-7 promotes resistance to imatinib in the bone marrow of mice (123).

An emerging theme in cancer therapy is that damage associated with conventional chemotherapeutics acutely remodels the tumor microenvironment. Using the MMTV breast-cancer model, Denardo and colleagues recently showed that paclitaxel acutely induces tumor cells to secrete Csf1 and IL-34, resulting in the rapid recruitment of macrophages to the tumor (124). They showed paclitaxel combined with a Csf1R antagonist reduced the growth and metastasis of surviving tumor cells and promoted the anti-tumor activity of CD8$^+$ T cells. In another example, Shaked and colleagues showed that treating mice with paclitaxel resulted in the rapid mobilization of circulating endothelial progenitor cells. Here, egress of the endothelial progenitor cells is dependent on SDF1α released by platelets. This induction is specific, as paclitaxel treatment acutely increases the serum concentration of SDF1α, while it decreases VEGF and GM-CSF levels in both mice and humans. Using mouse models of lung cancer and

melanoma they also suggested that circulating endothelial progenitor cells were able to seed the tumors and promote both angiogenesis and tumor regrowth. (125-127). Similarly, in humans and mice, Roodhart and colleagues observed that cisplatin therapy induces mobilization of mesenchymal stem cells from the bone marrow (128). Here, following administration of cisplatin, mesenchymal stem cells acutely release two unusual fatty acids, that promote COX1-dependent resistance to cisplatin in tumor cells.

Contact-dependent interactions between cancer cells and the extracellular matrix, stromal, immune, or endothelial cells can also promote resistance to apoptosis (129). Adhesion-mediated survival signaling is required for the survival of both untransformed cells and cancer cells within the tumor microenvironment (130). For example, cell adhesion to the extracellular matrix activates integrin-mediated survival signaling required for normal cell growth and in some tumor types, such as multiple myeloma, promotes resistance to chemotherapy (131). In one non-therapy-related example of this, Quintana and colleagues showed that human melanomas have many more tumor-initiating cells than was previously appreciated, suggesting in this tumor type that cancer stem cells do not drive tumor progression (132). To prove this they injected primary human melanoma cells with human extracellular matrix into NOD/SCID/γ-chain-deficient mice, and they saw that 27% of mice injected with a single melanoma cell developed tumors.

Juxtacrine or direct cell-cell-contact-mediated signaling also promotes tumorigenesis and drug-resistance. For example, juxtacrine Notch signaling supports tumorigenesis and drug resistance in pancreatic adenocarcinoma, multiple myeloma and T cell acute lymphoblastic leukemia (133-135). Here, γ-secretase inhibitors have been used in combination with conventional cytotoxic chemotherapeutic agents to successfully treat GEM models of multiple myeloma and pancreatic adenocarcinoma.

The tumor microenvironment can also present physical barriers to effective cancer treatment. Perhaps the most well understood physical barrier affecting cancer therapy is the blood-brain barrier (BBB). This structure is composed of endothelial cells joined by extensive tight junctions. Thus, the BBB is physical barrier within the cerebral capillaries that excludes the transfer of polar molecules, proteins and cells into the brain (24). The BBB physically occludes chemotherapeutic agents from brain tumors and brain metastasis, making tumor cells in the brain highly refractory to systemic chemotherapy.

This classic problem of delivering drugs across the blood–brain barrier is only one example of a physical aspect of a tumor microenvironment that can influence cancer therapy. Other examples of physical barriers include negative interstitial-fluid pressure in the tumor, aberrant tumor vasculature, and fibrosis (43). Using a k-$Ras^{G12D/+}$ $p53^{-/-}$ mouse model of pancreatic adenocarcinoma, Olive and colleagues demonstrated that physical barriers can be targeted for

therapy. Here the authors showed that inhibition of Hedgehog signaling could decrease stromal fibrosis and increase vascular permeability and intratumoral gemcitabine delivery, resulting in increased tumor cell apoptosis and improved survival (25). This was not a cancer-cell-autonomous effect, as lineage-tracing experiments showed that expression of activated Smoothened in mesenchymal but not epithelial cells promotes tumorigenesis (136). In another proof-of-principle experiment using the same tumor model, enzymatic disruption of this physical barrier was achieved using PH20, a hyaluronidase (2). Here, tumors treated with PH20 showed decreased interstitial fluid pressure, vascular normalization and increased gemcitabine delivery. Thus, the tumor microenvironment dynamically modulates the response to therapy, suggesting that if we understood how the tumor microenvironment affects therapy we could promote the efficacy of conventional chemotherapeutics using novel targeted therapies.

Secretory phenotypes associated with transformation and DNA damage

It has long been appreciated that secretory processes are tightly controlled during the immune response, as uncontrolled inflammation can lead to tissue destruction and death (137). More recently, there has been renewed interest in secretory phenotypes associated with oncogenic transformation and DNA damage. Early work by Senger and colleagues showed that oncogenic transformation induces the secretion of specific proteins (138). Here, cells that are virally transformed at a permissive temperature secrete a phosphorylated 58,000 Dalton protein only at the transforming temperature. High levels of this

protein, osteopontin, are also secreted by normal fibroblasts following DNA

damage. Pazolli and colleagues later showed that osteopontin acts as a

paracrine mitogen, inducing tumor formation in a cancer model of transformation

(139). Here, in a xenograft model, osteopontin secreted by senescent fibroblasts

induces the transformation of pre-neoplastic immortalized keratinocytes. This

work suggests that both transformation and DNA damage can induce a secretory

phenotype that remodels the tumor microenvironment *in vitro* and *in vivo*.

This finding has recently been extended with the discovery that such

inducible secretory responses are a common feature during cancer development

and cancer therapy. During tumor development, oncogene activation can induce

an irreversible state of cell-cycle arrest termed cellular senescence. In four

hallmark papers, Acosta, Coppe, Kuilman and Wajapeyee showed in four

different *in vitro* models that oncogene-induced senescence is associated with

the induction of a complex secretory phenotype (140-143). Here, senescent cells

secrete very high levels of many growth factors, chemokines and cytokines. In

these papers, IL-6 and IL-8 were shown to be important autocrine tumor

suppressors required for the maintenance of senescence. The senescence

associated secretory phenotype (SASP) is also induced at replicative

senescence and by DNA-damage-mediated senescence associated with

radiation or chemotherapy (144). The question of why IL-6 signaling is activated

in many human cancers but also can act as an autocrine tumor suppressor that

reinforces senescence is unclear. Interestingly, two earlier reports demonstrated

that IL-6 and IL-8 are rapidly up-regulated during Ras-induced transformation in a variety of cell types and are required for tumorigenesis and angiogenesis (145,146). Further complicating the matter is the observation that IL-6 inhibits the growth of some fully transformed melanoma and breast cancer cell lines (147).

The SASP is postulated to play a variety of roles but has been shown to promote tumor cell migration, immune infiltration and the clearance of senescent cells (148,149). While the SASP clearly occurs *in vitro* it has been difficult to pinpoint whether this occurs broadly *in vivo*. A process similar to the SASP has also been described in a model of liver fibrosis (150). Here chemical insults induce senescence in hepatic stellate cells, resulting in the up-regulation of chemokines, cytokines, and natural killer cell ligands. In this case, senescent cells are rapidly cleared by natural killer cells and macrophages, which may prevent the accumulation of high levels of these secreted factors. Thus, senescence induced by oncogene activation or systemic chemotherapy may result in the dynamic remodeling of normal and tumor microenvironments.

Pro-survival signals in tissue homeostasis, development and cancer: IL-6 as a model cytokine

The concept of pro-survival signaling is well described in developmental biology and occurs during both adult and embryonic development. For example, during B-cell development, IL-7 is critically required for cell survival during the transition of pre-pro to pro B cells (151,152). Other paracrine signals, such as the

30

Notch, Wnt, and Hedgehog pathways, similarly support self-renewal and repopulation of stem or progenitor populations in the skin, blood, gut, and nervous system (153). In fact, metazoans have developed many evolutionarily conserved processes to modulate and repair tissues, ensuring the survival of the organism even when widespread cell death occurs in a tissue (154). For example, Notch signaling from endothelial cells within the bone marrow is required for hematopoietic renewal and repopulation of stem cells following irradiation (155).

These processes can be activated by diverse physiologic stresses, including ischemia, wounds, and pathogens. Here, recognition by the innate immune system of pathogen- or damage-associated molecular patterns can induce the activation of specific inflammasomes that tailor the response to a given insult. Additionally, it has long been appreciated that wounds or infections induce inflammation in which numerous cytokines are secreted locally and systemically (156). Here, IL-6 is a critical pro-survival signal that is induced acutely following tissue injury and acts primarily to activate immune cells. Recently it was shown that IL-6 is acutely released from endothelial cells during influenza infection and that this precedes and is required for immune-cell recruitment and activation (157). Indeed, this cytokine release is required for recruitment of immune and stromal cells and activation of processes required for physiologic tissue restoration.

Emerging literature suggests that IL-6 can act as a potent pro-survival signal in many contexts. For example, viral IL-6 encoded by Kaposi sarcoma herpes virus (KSHV) promotes B-cell survival following KSHV infection (158). IL-6 promotes T cell survival during development and is critically required for T cell survival and expansion during chronic viral infections (159,160). IL-6 is also required for liver regeneration, as shown by the fact that $IL-6^{-/-}$ mice die due to massive necrosis following partial hepatectomy (161). Importantly, this survival signaling must be acute, as mortality occurs within 24 hours of liver damage in $IL-6^{-/-}$ animals. In the colon, IL-6 is also required for the survival of colonic epithelial cells and the maintenance of mucosal integrity in mouse models of colitis (162).

In cancer patients, the IL-6/Jak/Stat signaling pathway is frequently activated by overexpression or activating mutations. In hepatocellular adenomas, lymphomas, and all three myeloproliferative disorders; polycythemia vera, essential thrombocythemia, and idiopathic myelofibrosis, most patients have activating mutations in gp130, MYD88, or Jak2, which induce high levels of Jak2/Stat3 signaling and drive proliferation (163-165). Mechanistically, our data and those of others indicate that IL-6 or activation of Jak2/Stat3 signaling can induce up-regulation of anti-apoptotic Bcl-2 family members. Indeed, constitutively active Stat3 is an oncogene in mouse models (166). In mouse models, IL-6 promotes the development of pancreatic adenocarcinomas, hepatocellular carcinoma, colitis-associated cancer and glioblastomas,

melanoma and plasmocytomas (145,162,167-171). Thus, IL-6 is a potent pro-survival factor that can affect both tumorigenesis and response to tissue injury.

Advances in cancer therapy and our understanding of the tumor microenvironment have opened more questions than they have answered. One thing is clear: the interplay between normal and tumor cells is complicated and context-dependent. Efforts to understand these processes will undoubtedly continue to uncover how survival signals govern tissue homeostasis, the immune response, and cancer therapy.

This thesis contains my work attempting to understand how the tumor microenvironment modulates tumorigenesis and response to therapy in the *Eµ-myc* lymphoma model. It is divided into 6 chapters.

Chapter 1: Introduction

Chapter 2: DNA-damage-mediated induction of a chemoresistant niche

This paper details our discovery of chemoresistant microenvironments and how they promote minimal residual disease following therapy in the *Eµ-myc* lymphoma model. We show that DNA damage induces an acute secretory response required for normal tissue repair, which is co-opted by lymphoma cells.

Chapter 3: DNA damage induces distinct acute and senescence associated secretory phenotypes in a context-specific manner

This unpublished chapter delves further into the molecular details of the acute secretory response in an attempt to discover how the senescence-associated secretory phenotype is related to the acute secretory-associated phenotype. We

33

also uncover a role for the unfolded-protein response in the senescence-associated secretory phenotype.

Chapter 4: BCL-2 family genetic profiling reveals microenvironment-specific determinants of chemotherapeutic response

In this paper, Justin Pritchard and I developed a novel bead-based hybridization technique to measure enrichment and depletion of shRNAs within a pool of shRNAs in a semi-high-throughput manner. We proceeded to use this technique to ask how the Bcl-2 family modulates therapeutic response *in vitro* and *in vivo*. Here, we uncover a novel role for the extrinsic death pathway in promoting response to doxorubicin treatment.

Chapter 5: Developmentally specified roles for paracrine IL-6 in lymphomagenesis

This unpublished chapter is under re-review. Here, we describe how IL-6 modulates tumorigenesis in the *Eμ-myc* lymphoma model. We see that IL-6 loss actually promotes lymphomagenesis. In the absence if IL-6, we see widespread changes in the bone-marrow microenvironment which retard B-cell development in *IL-6$^{-/-}$* and *IL-6$^{-/-}$ Eμ-myc*. Here, IL-6 and IL-10 promote the transition between pro/pre-B cells and immature B cells. Interestingly, we see that IL-6 acts directly as a survival factor in hematopoietic stem cells but not in developmental intermediates. Once transformed, the resulting B-cell lymphomas again utilize paracrine IL-6 signaling as a survival signal, highlighting the ability of tumor cells to co-opt pathways utilized for stem-cell protection.

Chapter 6: Discussion

Chapter 2:

DNA-damage-mediated induction of a chemoresistant niche

Luke A Gilbert[1] and Michael T Hemann[1*]

[1] The Koch Institute for Integrative Cancer Research at MIT, Massachusetts Institute of Technology, Cambridge, MA 02139, USA.

Abstract

While numerous cell-intrinsic processes are known to play decisive roles in chemotherapeutic response, relatively little is known about the impact of the tumor microenvironment on therapeutic outcome. Here, we use a well-established mouse model of Burkitt's lymphoma to show that paracrine factors in the tumor microenvironment modulate lymphoma cell survival following the administration of genotoxic chemotherapy. Specifically, IL-6 and Timp-1 are released in the thymus in response to DNA damage, creating a "chemo-resistant niche" that promotes the survival of a minimal residual tumor burden and serves as a reservoir for eventual tumor relapse. Notably, IL-6 is released acutely from thymic endothelial cells in a p38-dependent manner following genotoxic stress,

and this acute secretory response precedes the gradual induction of senescence in tumor-associated stromal cells. Thus, conventional chemotherapies can induce tumor regression while simultaneously eliciting stress responses that protect subsets of tumor cells in select anatomical locations from drug action.

Introduction

While significant progress has been made in the application of chemotherapy over the past 40 years, most chemotherapeutic regimens ultimately fail to cure cancer patients (172). Even tumors that show dramatic initial responses to therapy frequently relapse as chemoresistant malignancies. This chemoresistance is thought to arise as a consequence of cell-intrinsic genetic changes including up-regulation of drug-efflux pumps, activation of detoxifying enzymes or apoptotic defects (77,173). However, recent data suggests that resistance to chemotherapy can also result from cell-extrinsic factors such as cytokines and growth factors (123,174). Additionally, other studies have suggested that rare cancer stem cells are the source of eventual tumor relapse following therapy, as these cells are thought to be drug-resistant due to increased genomic stability, decreased oxidative stress or the presence of multiple drug-resistance transporters (175).

Modern combinatorial chemotherapeutic regimes can reduce patient tumor burdens to undetectable levels, yet in many cases these tumors will relapse (176). Thus, even when a patient is classified as being in complete

remission, surviving cancer cells can persist in particular anatomical locations.

This remnant population of cancer cells has been described as Minimal Residual

Disease (MRD). MRD, is generally not macroscopic and may not be at the site of

the primary tumor, making this phenomenon difficult to dissect experimentally

(177). While MRD is a significant clinical problem, few models exist to study

residual tumor burden following therapy. Thus, it remains unclear whether the

cancer cells that compose the MRD burden are surviving following chemotherapy

due to stochastic events, intrinsic drug-resistance, or microenvironmental cues.

Efforts to experimentally recapitulate the response of human tumors *in*

vivo to chemotherapy have generally relied upon xenografts of human tumors

transplanted into immunodeficient mice (48). These models have proven

ineffective in predicting drug efficacy, likely due to a failure to reproduce the

complexity of a tumor with its associated complement of stromal, immune and

endothelial cells. This autochthonous tumor microenvironment includes a

complex mixture of pro- and anti- neoplastic factors (178). Both malignant and

untransformed cells within a tumor influence the balance of growth factors,

chemokines and cytokines found in the tumor microenvironment. These factors

play key roles in regulating tumor-cell proliferation, and survival through the

activation of diverse signaling pathways, including the Jak/Stat, NFκB, Smad,

and PI3K pathways (179).

While numerous studies have addressed the role of tumor-proximal factors in tumor growth or metastasis, relatively few have addressed the role of the tumor microenvironment in chemotherapeutic outcome (44). Here we show that two cytokines, IL-6 and Timp-1, protect lymphoma cells from cell death induced by genotoxic chemotherapy, such that small-molecule inhibition of cytokine-induced signaling potentiates chemotherapeutic efficacy. We further show that IL-6 release occurs as a result of activation of p38 MAP kinase in tumor-associated endothelial cells acutely following DNA damage. This acute cytokine release also occurs in treated human endothelial and hepatocellular carcinoma cells, suggesting that acute secretory responses may occur in numerous contexts. In the thymus, rapid cytokine release precedes the induction of senescence – a process recently shown to promote sustained cytokine release in cultured cells (140-143). Thus, genotoxic drugs can, paradoxically, elicit pro-survival signaling in select anatomical sites, providing a reservoir of minimal residual disease that subsequently fuels tumor relapse.

Results

The thymus represents a chemoprotective tumor microenvironment

To investigate the dynamics of lymphoma response and relapse following chemotherapy, we used a well established preclinical model of human Burkitt's lymphoma – the $E\mu$-myc mouse (70,78). Tumors from these mice can be transplanted into immunocompetent, syngeneic, recipient mice, and the resulting tumors are pathologically indistinguishable from autochthonous tumors (180). Six

to 8 week-old mice were tail-vein-injected with GFP-tagged *Eμ-myc p19$^{Arf-/-}$* B lymphoma cells. At tumor onset all mice displayed a characteristic disseminated pattern of disease with lymphoma cells in the peripheral lymph nodes, spleen and mediastinum. Mice were treated with the maximum tolerated dose of the front-line chemotherapeutic doxorubicin at the time of lymphoma manifestation. Three days after administration of doxorubicin, all mice displayed tumor regression and peripheral tumor clearance, measured by lymph-node palpation. These mice were sacrificed at four days post treatment and sites of minimal residual disease were identified by GFP imaging. Interestingly, the majority of surviving lymphoma cells were in the mediastinal cavity (Figure 1A), a central component of the thoracic cavity that encapsulates the heart, esophagus, trachea and a large amount of lymphatic tissue including the mediastinal lymph nodes and the thymus.
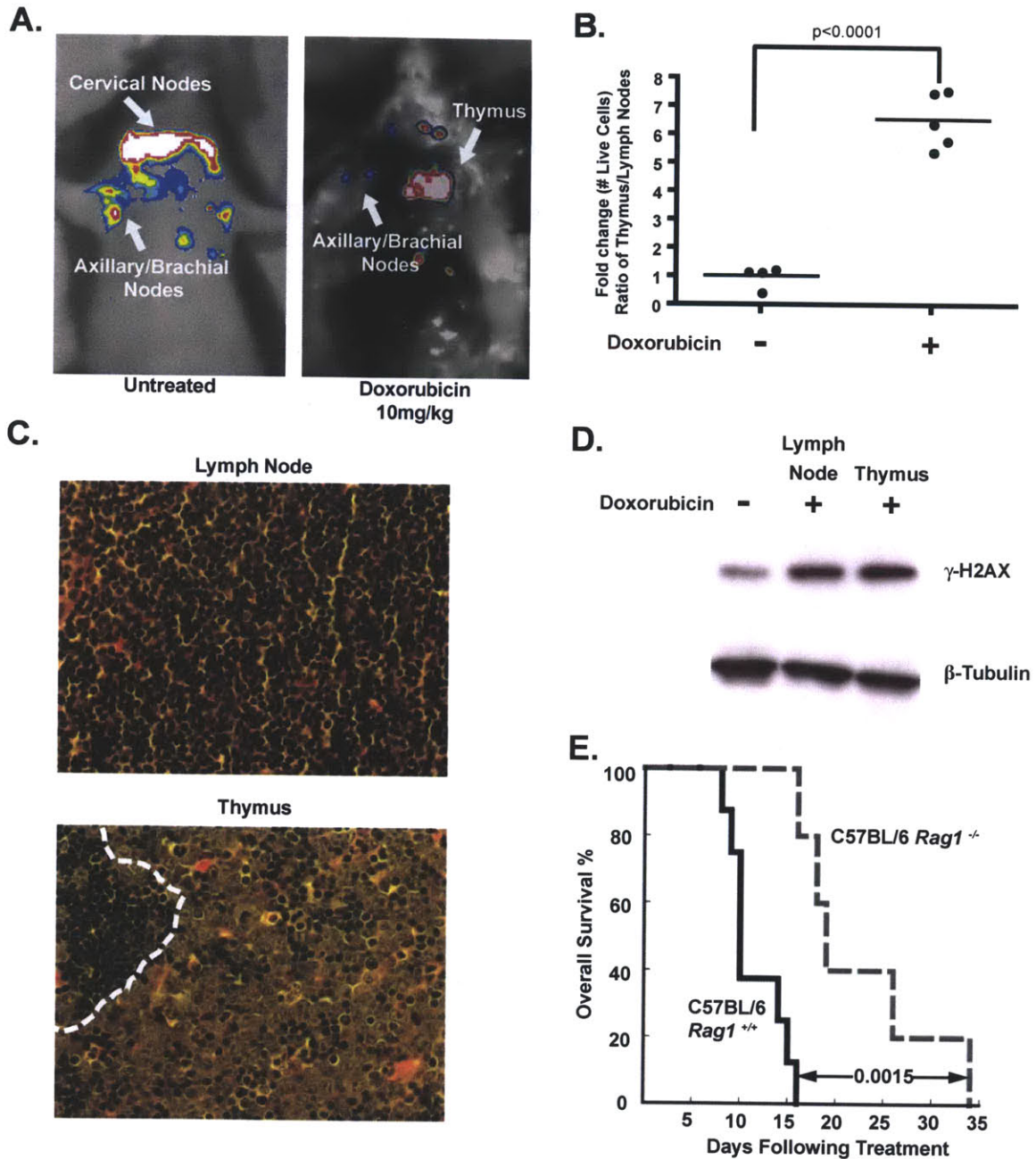
Figure 1. The thymus represents a chemoprotective niche that harbors surviving lymphoma cells following doxorubicin treatment. (A) Lymphoma-bearing mice were imaged for whole-body fluorescence prior to treatment and 4 days following a single dose of 10mg/kg doxorubicin. Representative mice are shown. **(B)** Ratios of live GFP-tagged *Eµ-myc p19^{Arf-/-}* B lymphoma cells in the thymus versus peripheral lymph nodes were quantified by flow cytometry, before (n=4 mice) and 48 hours after (n=5 mice) doxorubicin treatment. Average ratios are indicated with a line. **(C)** Hematoxylin and eosin (H&E) stained sections of lymph node and thymus from a tumor-bearing mouse 48 hours after doxorubicin treatment. The dotted line in the thymus demarcates a small region of infiltrating

40

lymphocytes neighboring a larger region of surviving lymphoma cells. Representative fields are shown at 40x magnification. **(D)** A western blot showing γ-H2AX levels in FACS-sorted, GFP-positive, lymphoma cells from the thymus and peripheral lymph nodes following doxorubicin treatment. β-Tubulin serves as a loading control. The untreated sample is a lysate from cultured lymphoma cells. **(E)** A Kaplan-Meier curve showing the overall survival of tumor-bearing C57BL/6 (n=8) or C57BL/6 *Rag1*$^{-/-}$ (n=5) mice following doxorubicin treatment. The p value was calculated using a log rank test. See also Figure S1.

To analyze the effect of drug treatment on specific tumor niches, we harvested all primary lymphoid organs, including peripheral lymph nodes, thymus, spleen and bone marrow, following doxorubicin treatment. All tissues sampled showed extensive lymphoma cell apoptosis and restoration of normal organ architecture. Peripheral lymph nodes, spleen and bone marrow exhibited nearly complete tumor clearance with rare surviving lymphoma cells (Figure 1C and Supplemental Figure 1A). In contrast, many surviving B lymphoma cells could be seen in the thymus. To quantify this phenotype, cells were harvested from peripheral lymph nodes and the thymus following treatment, and the number of surviving GFP-positive lymphoma cells was assessed by flow cytometry. The number of viable lymphoma cells in the thymus relative to the lymph nodes increased 6.5 fold following doxorubicin treatment (Figure 1B). Thus, the thymus represents a chemoprotective niche that protects lymphoma cells from doxorubicin-induced cell death.

To rule out the possibility that the selective survival of tumor cells in the thymus was due to the specific exclusion of doxorubicin from the mediastinum, we sorted live GFP-positive tumor cells from the lymph nodes and thymus 12

hours after doxorubicin treatment and blotted for γ-H2AX, a marker of DNA

damage (181). Western blot analysis showed that cells in both anatomical

locations undergo the same amount of DNA damage (Figure 1D). Additionally,

flow cytometry of mediastinal lymphoma cells failed to identify any sub-population

of lymphoma cells with decreased γ-H2AX fluorescence (Supplemental Figure

1B). These data suggest that the thymus offers no physical barrier to drug

delivery.

A.

	Lymph Node	Thymus	Spleen	Bone Marrow
Untreated				
Doxorubicin				

B.

C.

D.

E.
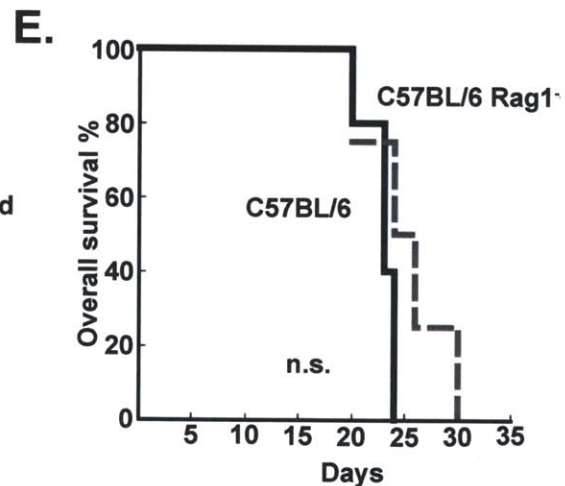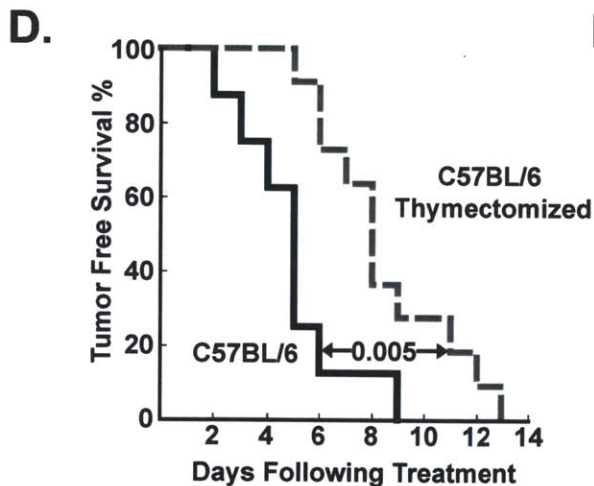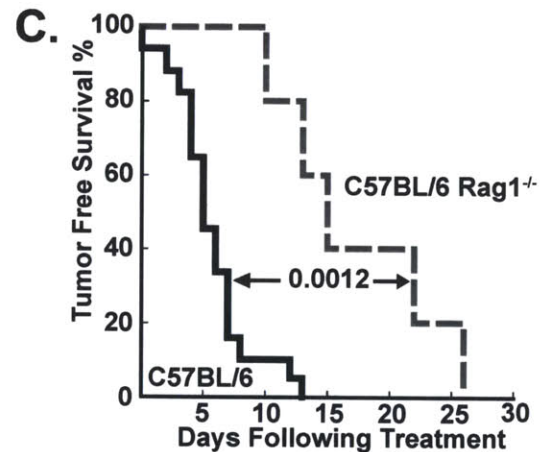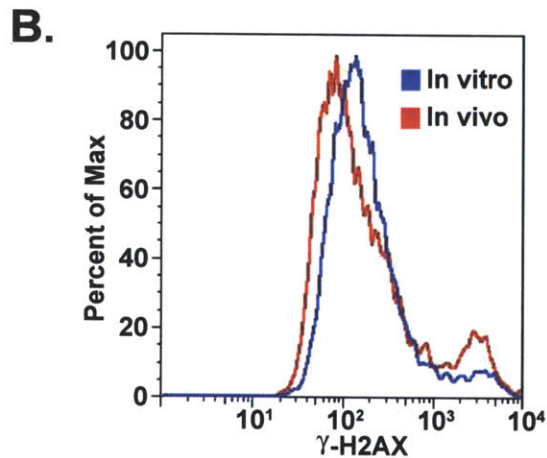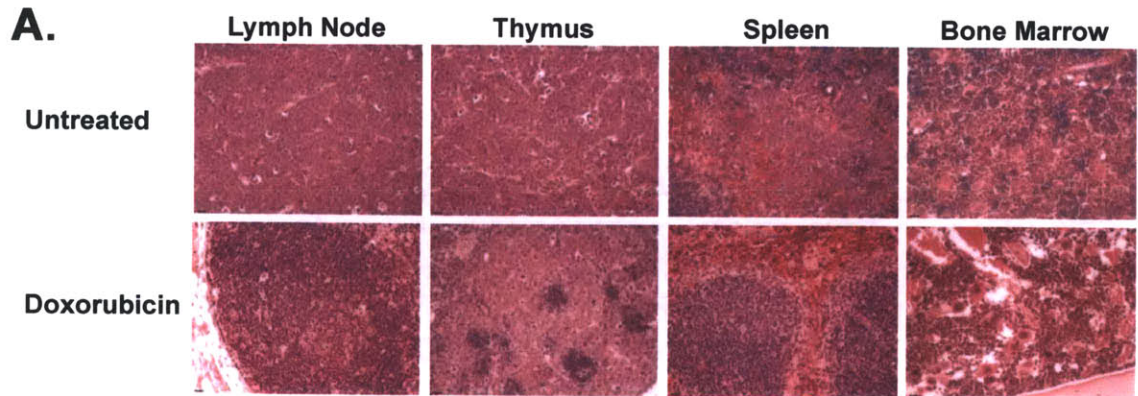
Supplemental Figure 1. Athymic mice show improved tumor-free survival following treatment with doxorubicin. (A) Hematoxylin and eosin (H&E) stained sections of lymph node, spleen, bone marrow and thymus from mice bearing $E\mu$-myc p19$^{Arf-/-}$ tumors. Mice were untreated or treated with a single dose of 10mg/kg doxorubicin for 72 hours. Surviving lymphoma cells are absent in the lymph node, spleen and bone marrow but present in the thymus. Scale bars indicate 35 microns on all panels. **(B)** A histogram showing γH2AX levels across a population of $E\mu$-myc p19$^{Arf-/-}$ lymphoma cells treated *in vitro* and *in vivo*

in the thymus. **(C)** A Kaplan-Meier curve showing the tumor-free survival of $E\mu$-myc $p19^{Arf-/-}$ tumor-bearing C57BL/6 (n=8) or C57BL/6 $Rag1^{-/-}$ (n=5) mice following treatment with 10mg/kg doxorubicin. The p value was calculated using a log rank test. **(D)** A Kaplan-Meier curve showing the tumor-free survival of $E\mu$-myc $p19^{Arf-/-}$ tumor-bearing C57BL/6 (n=8) or C57BL/6 thymectomized (n=11) mice following treatment with 10mg/kg doxorubicin. The p value was calculated using a log rank test. **(E)** A Kaplan-Meier curve showing the overall survival of $E\mu$-myc $p19^{Arf-/-}$ tumor-bearing C57BL/6 (n=5) or C57BL/6 $Rag1^{-/-}$ (n=4) mice. The p value was calculated using a log rank test.

Minimal residual tumor burden in the thymus fuels tumor relapse following chemotherapy

Given the persistence of tumor cells in the thymus following chemotherapy, we next sought to determine whether tumor cells in the thymus contributed to lymphoma relapse. To this end, we examined therapeutic response in genetically and surgically athymic mice. We injected control or *Rag1*-deficient mice, which have severely atrophic thymuses, with lymphoma cells and then treated tumor-bearing recipient animals with doxorubicin. Overall survival and tumor-free survival were significantly extended in tumor-bearing *Rag1* deficient mice, relative to control animals, suggesting that the presence of a functional thymus promotes relapse and disease progression (Figure 1E and Supplemental Figure 1C). Similarly, surgically thymectomized tumor-bearing mice also showed extended tumor-free and overall survival following therapy relative to control animals (Supplemental Figure 1D and data not shown). Notably, overall survival in untreated tumor-bearing *Rag1*-deficient or thymectomized mice was indistinguishable from that in control animals (Supplemental Figure 1E). Thus, the thymus harbors minimal residual disease that contributes to tumor relapse following therapy in this model.

Cultured thymuses secrete pro-survival factors *in vitro*

Preferential lymphoma cell survival in the thymus following doxorubicin

treatment suggests that specific anatomical microenvironments may contain pro-

survival factors absent in other lymphoid organs. There is precedent for this

phenomenon in multiple myeloma, where the bone-marrow microenvironment

promotes myeloma cell survival (178). To address this possibility, we derived

conditioned media from the thymus (TM, for Thymic Media), bone marrow (BMM)

and lymph nodes (LNM) of mice treated with doxorubicin. Cultured lymphoma

cells were then treated with doxorubicin, along with TM, LNM or BMM. Addition

of TM provided a significant survival advantage, with 10-fold more cells surviving

48 hours following treatment (Figure 2A). This effect was specifically pro-survival,

as opposed to pro-proliferative, as these same conditioned medias had little

effect on lymphoma cell growth (Figure 2B). In contrast, conditioned media

derived from peripheral lymph nodes had only a minimal effect on lymphoma cell

survival (Figure 2A). Thus, soluble pro-survival factor(s) present in the thymic

microenvironment protect tumor cells from genotoxic chemotherapy.

A. Doxorubicin 20nM

p<0.0001

Fold Change (# Live Cells) vs No CM, TCM, BMM, LNM

B. Untreated

Fold Change (# Live Cells) vs No CM, TCM, LNM

C.

Lymph Node   Thymus

Normalized Signal Intensity (x10⁶)

MCP-1
MCP-5
IL-16
KC
IL-6
IL-1α
IL-1ra
MIP-2
TIMP1
G-CSF
MIP-1α
sICAM
C5a
TNFα
M-CSF
CXCL-1
SDF-1
TARC
TREM-1
IL-2
CXCL-9
GM-CSF
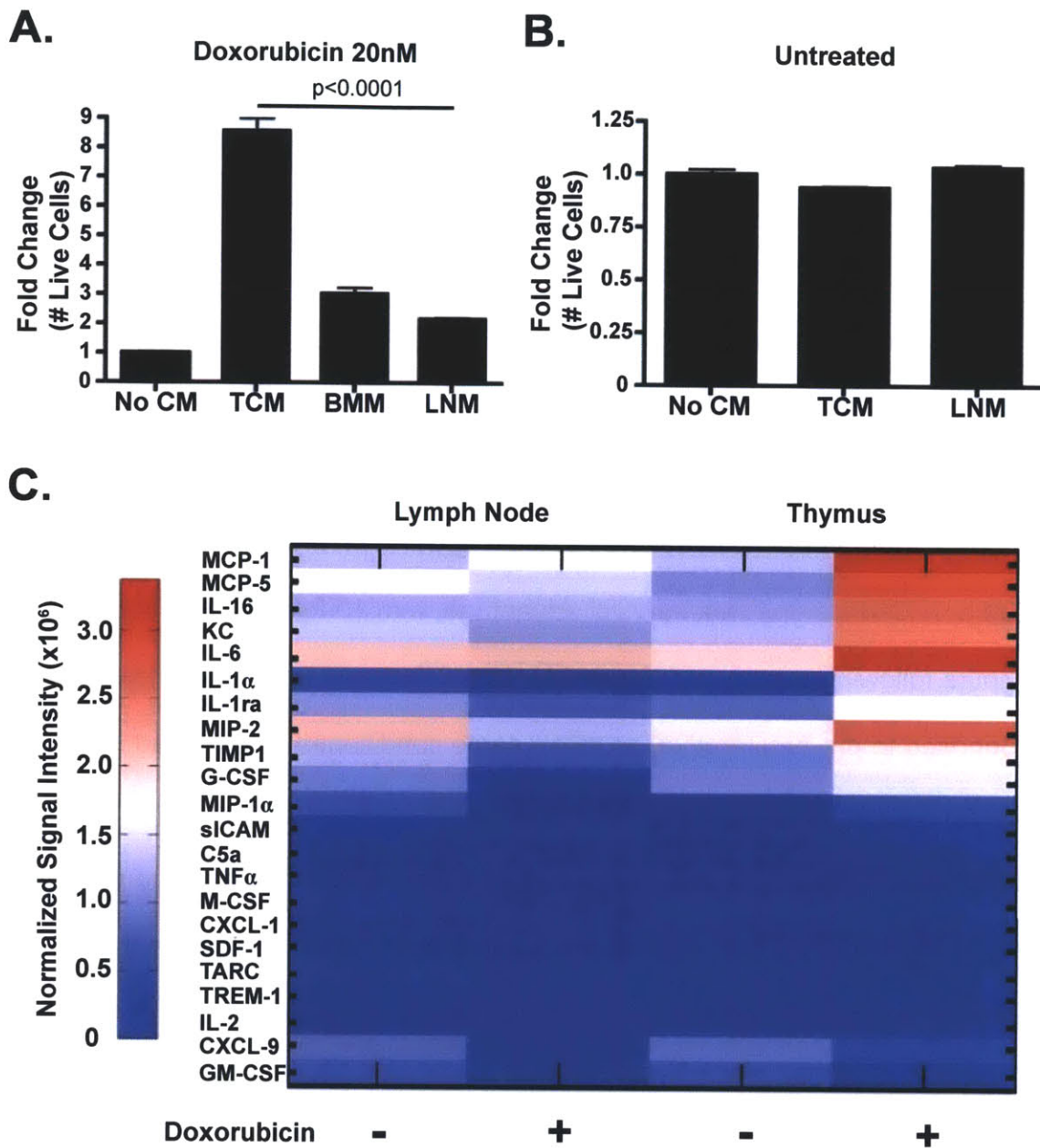
Doxorubicin   −   +   −   +

Figure 2. Thymic conditioned medium contain soluble chemoprotective factors. (A) A graph showing lymphoma cell survival in the presence of doxorubicin alone or in the presence of conditioned media. The data are represented as mean +/- standard error of the mean (SEM) (n=3). **(B)** A graph showing the growth of lymphoma cells cultured in the absence or presence of conditioned media. The data are represented as mean +/- SEM (n=3). **(C)** Cytokine array analysis of conditioned media from untreated and doxorubicin treated lymph nodes and thymus. The data are represented graphically as

normalized signal intensity. Conditioned media were pooled from 3 or 4 mice for each array.

Cytokine levels vary between tumor-bearing anatomical locations

To identify the factor(s) contributing to survival of lymphoma cells in the thymus, we performed cytokine arrays analyzing the abundance of 40 cytokines and chemokines in conditioned media from doxorubicin-treated and untreated tumors (Figure 2C and data not shown). Analysis of cytokine expression showed significant differences between the thymic and lymph node tumor microenvironments. Multiple factors related to cell migration and cell-cycle control were acutely up-regulated in thymic lymphomas, but not in peripheral lymphomas or cultured lymphoma cells, following doxorubicin treatment. These included the cytokines G-CSF, IL-1α, IL-1ra, IL-6, IL-16 and the chemokines and growth factors KC, MCP-1, MCP-5, MIP-2 and Timp-1 (Figure 2C).

Each of the up-regulated factors was tested *in vitro* for the ability to promote doxorubicin resistance. Of the 10 recombinant proteins examined, only two produced a significant effect on survival of lymphoma cells following doxorubicin treatment *in vitro*. Recombinant Interleukin-6 (IL-6), as a single agent, was able to promote a 2.8-fold increase in the number of surviving lymphoma cells 72 hours following doxorubicin treatment (Figure 3A and Supplemental Figure 2A). Similarly, addition of Tissue inhibitor of metalloproteases 1 (Timp-1) resulted in a 3-fold increase in surviving lymphoma cells following doxorubicin treatment (Figure 3B). These factors had a

combinatorial effect (Figure 3B), as addition of both recombinant IL-6 and Timp-1 resulted in a 4.5-fold increase lymphoma cell number following treatment (Figure 3B). Importantly, neither factor alone or in combination affected the growth of lymphoma cells, suggesting that this increase in cell number was not due to enhanced cell proliferation (Supplemental Figure 2B). Additionally, recombinant IL-6 had no effect on lymphoma cell motility in this setting (Supplemental Figure 2C).
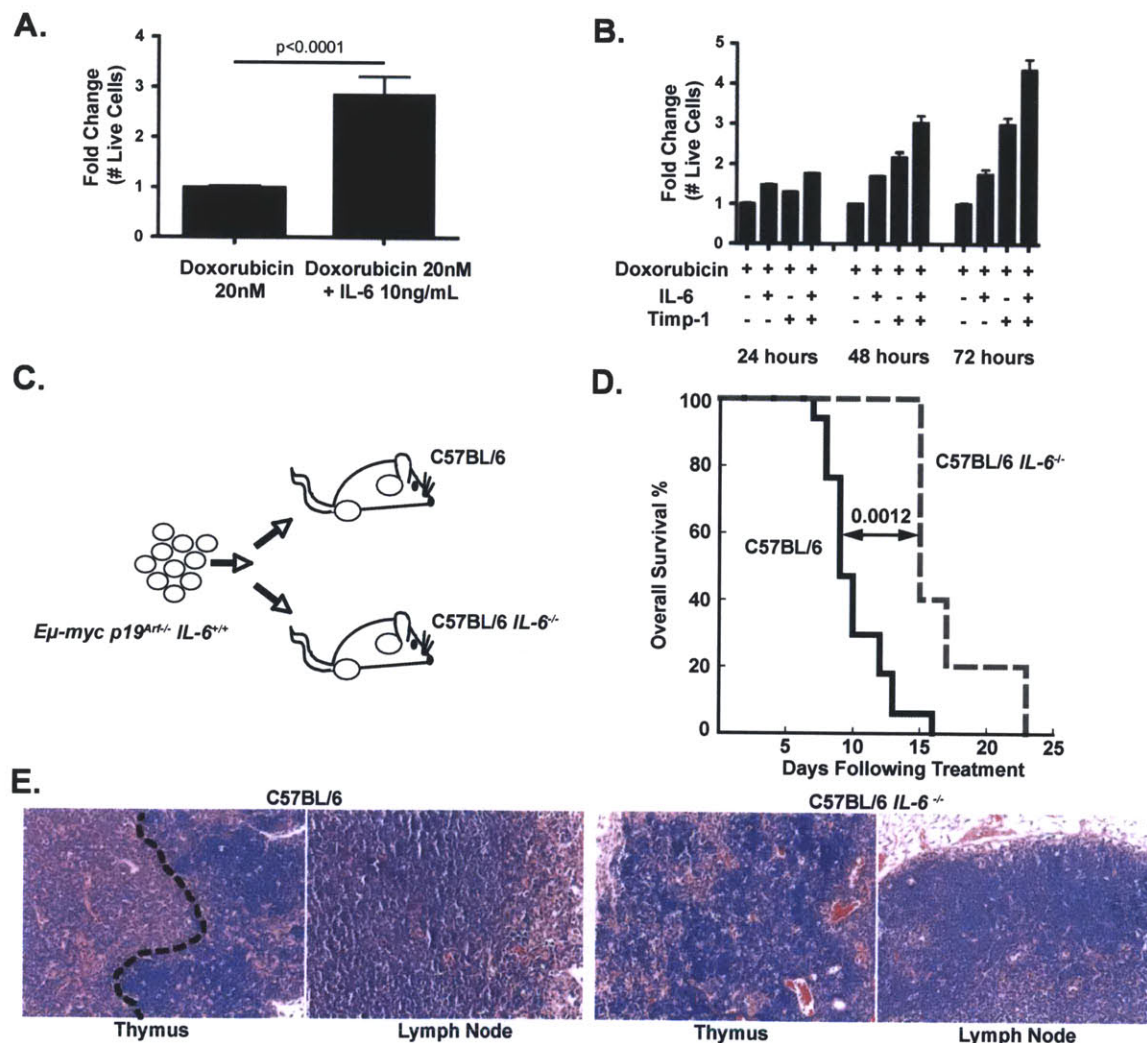

Figure 3. IL-6 and Timp-1 are chemoprotective *in vitro* and *in vivo*. (A) A graph showing the fold change in lymphoma cell number 72 hours after treatment

with doxorubicin as a single agent or doxorubicin plus recombinant IL-6. The data are represented as mean +/- SEM (n=4 independent experiments). **(B)** A graph showing the relative survival of cultured lymphoma cells at 24-hour intervals following treatment with doxorubicin alone, doxorubicin plus recombinant IL-6 or Timp-1, or doxorubicin plus both IL-6 and Timp-1. The data are represented as mean +/- SEM (n=3 independent experiments). **(C)** A schematic diagram of the lymphoma transplant experiment, showing injection of IL-$6^{+/+}$ lymphoma cells into both IL-$6^{+/+}$ and IL-$6^{-/-}$ recipients. **(D)** A Kaplan-Meier curve showing post-treatment survival of IL-$6^{+/+}$ (n=17) or IL-$6^{-/-}$ (n=5) mice bearing IL-$6^{+/+}$ lymphomas. All mice were treated with a single dose of 10mg/kg doxorubicin. The p value was calculated using a log rank test. **(E)** H&E stained sections of lymphomas 72 hours following doxorubicin treatment. The black dotted line shown in the thymus from the IL-$6^{+/+}$ recipient mouse demarcates a zone of surviving lymphoma cells that is absent in the other sections. Representative fields are shown at 20x magnification. See also Figure S2.

While these data suggest that both Timp-1 and IL-6 promote chemoresistance in the thymus, we decided to focus our efforts on the contribution of IL-6 to therapeutic response. To determine whether IL-6 was acting to promote cell survival in an autocrine fashion following release from lymphoma cells or a paracrine fashion following release from surrounding thymic cells, we performed lymphoma transplant experiments in the presence or absence of IL-6. Specifically, IL-$6^{+/+}$ lymphomas were transplanted into IL-$6^{+/+}$ or IL-$6^{-/-}$ mice (Figure 3C and Supplemental Figure 2D). Tumor-bearing recipient mice were then treated with the maximum tolerated dose of doxorubicin and monitored for tumor-free survival and overall survival. Notably, while IL-$6^{-/-}$ and IL-$6^{+/+}$ recipient mice developed pathologically indistinguishable tumors, IL-$6^{-/-}$ recipients displayed significantly longer tumor-free survival and overall survival following treatment than their IL-$6^{+/+}$ counterparts (Figure 3D and Supplemental Figure 2F-G). Additionally, histological analysis confirmed the lack of surviving lymphoma cells in the thymus of IL-$6^{-/-}$ mice following treatment (Figure 3E).

Thus, IL-6 release from the tumor microenvironment, rather than from the tumor

itself, promotes tumor-cell survival.
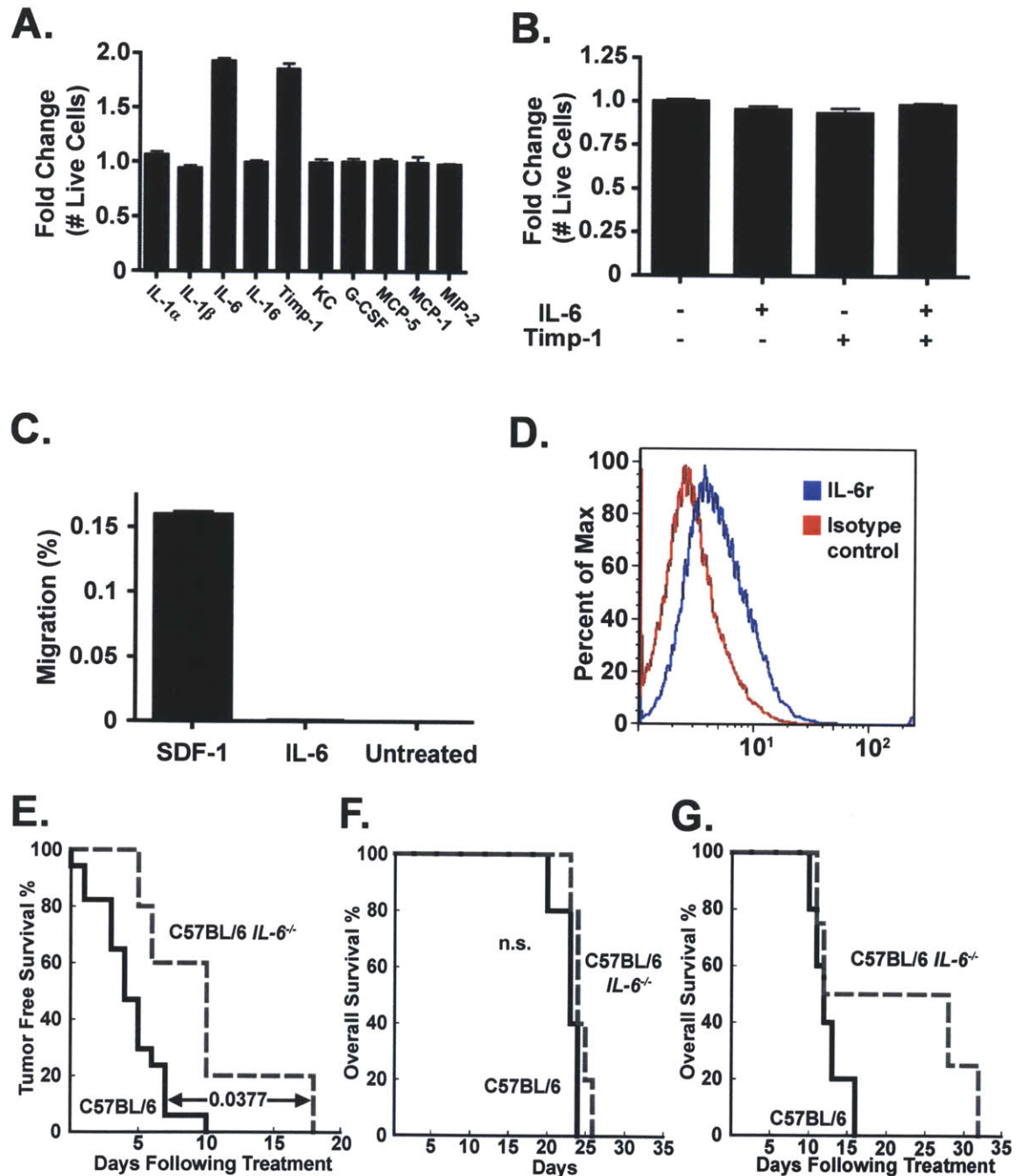
Supplemental Figure 2. Soluble factors in the thymic tumor microenvironment modulate doxorubicin-induced lymphoma cell death but do not affect growth. (A) A bar graph depicting lymphoma cell survival following

treatment with doxorubicin alone or doxorubicin and recombinant cytokines as indicated. The data are represented as mean +/- SEM **(B)** A graph showing lymphoma cell number at 72 hours. Lymphoma cells are untreated or treated with IL-6 or Timp-1 as indicated. The data are represented as mean +/- SEM **(C)** A graph of $E\mu$-myc $p19^{Arf-/-}$ lymphoma cell migration in response to no stimulation, IL-6 or SDF-1. SDF-1 serves as a positive control. The data are represented as mean +/- SEM **(D)** A histogram showing surface IL6r expression on $E\mu$-myc $p19^{Arf-/-}$ lymphoma cells. **(E)** A Kaplan-Meier curve showing the tumor-free survival of $E\mu$-myc $p19^{Arf-/-}$ tumor-bearing C57BL/6 (n=17) or C57BL/6 $IL-6^{-/-}$ (n=5) mice following treatment with 10mg/kg doxorubicin. **(F)** A Kaplan-Meier curve depicting overall survival of $E\mu$-myc $p19^{Arf-/-}$ tumor-bearing C57BL/6 (n=5) or C57BL/6 $IL-6^{-/-}$ (n=5) mice. **(G)** A Kaplan-Meier curve showing the tumor-free survival of $E\mu$-myc $p19^{Arf-/-}$ tumor-bearing C57BL/6 (n=5) or C57BL/6 $IL-6^{-/-}$ (n=4) mice following treatment with a fractionated dose of 20mg/kg doxorubicin. The p values for all Kaplan-Meier curves were calculated using a log rank test.

To further investigate the source of thymic IL-6, IL-6 levels were examined in thymic lymphomas from doxorubicin-treated $IL-6^{+/+}$ and $IL-6^{-/-}$ recipient mice, as well as doxorubicin-treated lymphoma cells *in vitro* (Figure 3C). No IL-6 was detected in either $IL-6^{+/+}$ lymphoma cells *in vitro* or in thymic or peripheral tumors from $IL-6^{-/-}$ lymphoma-bearing mice (data not shown). This result strongly suggests that the IL-6 present in the tumor microenvironment following genotoxic stress is secreted in a paracrine manner from resident thymic cells.

Genotoxic chemotherapy induces the release of pro-survival cytokines *in vivo*

Recent work has shown that DNA damage can induce a secretory phenotype in cultured cells (144). To determine whether IL-6 is similarly induced as a consequence of genotoxic chemotherapy *in vivo*, we treated mice lacking tumors with the maximally tolerated dose of doxorubicin. 18 hours later we assayed IL-6 levels by ELISA in untreated and doxorubicin-treated mice. As

suggested by the cytokine array data, IL-6 was present at a constitutively higher

level in the thymus versus the lymph nodes of mice (Figure 4A). Additionally,

doxorubicin treatment significantly increased the amount of IL-6 in the thymus but

not in peripheral lymph nodes or the spleen (Figure 4A and Supplemental Figure

3A). Thus, genotoxic chemotherapy induces a stress response in the thymus that

includes the release of IL-6, a pro-survival cytokine. Notably, IL-6 induction in

the thymus occurred within 18 hours of treatment, much more acutely than has

been reported for secretory phenotypes in cultured cells (144).
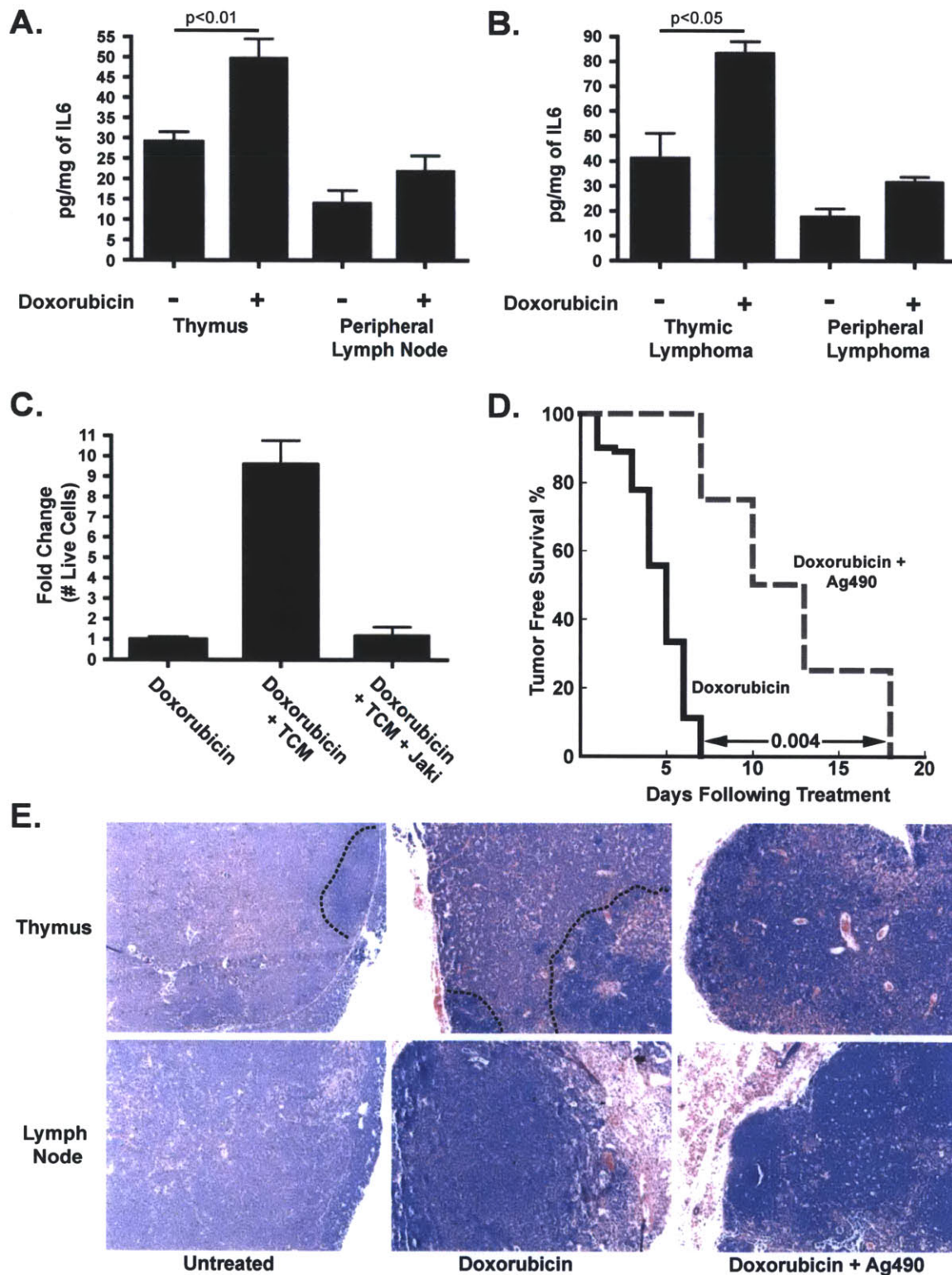
Figure 4. Doxorubicin induces the release of IL-6, and inhibition of this cytokine signaling sensitizes tumor cells to chemotherapy. (A) Quantification of IL-6 levels in conditioned media from the thymus or lymph nodes of untreated mice (n≥10) or mice treated for 18 hours with 10mg/kg
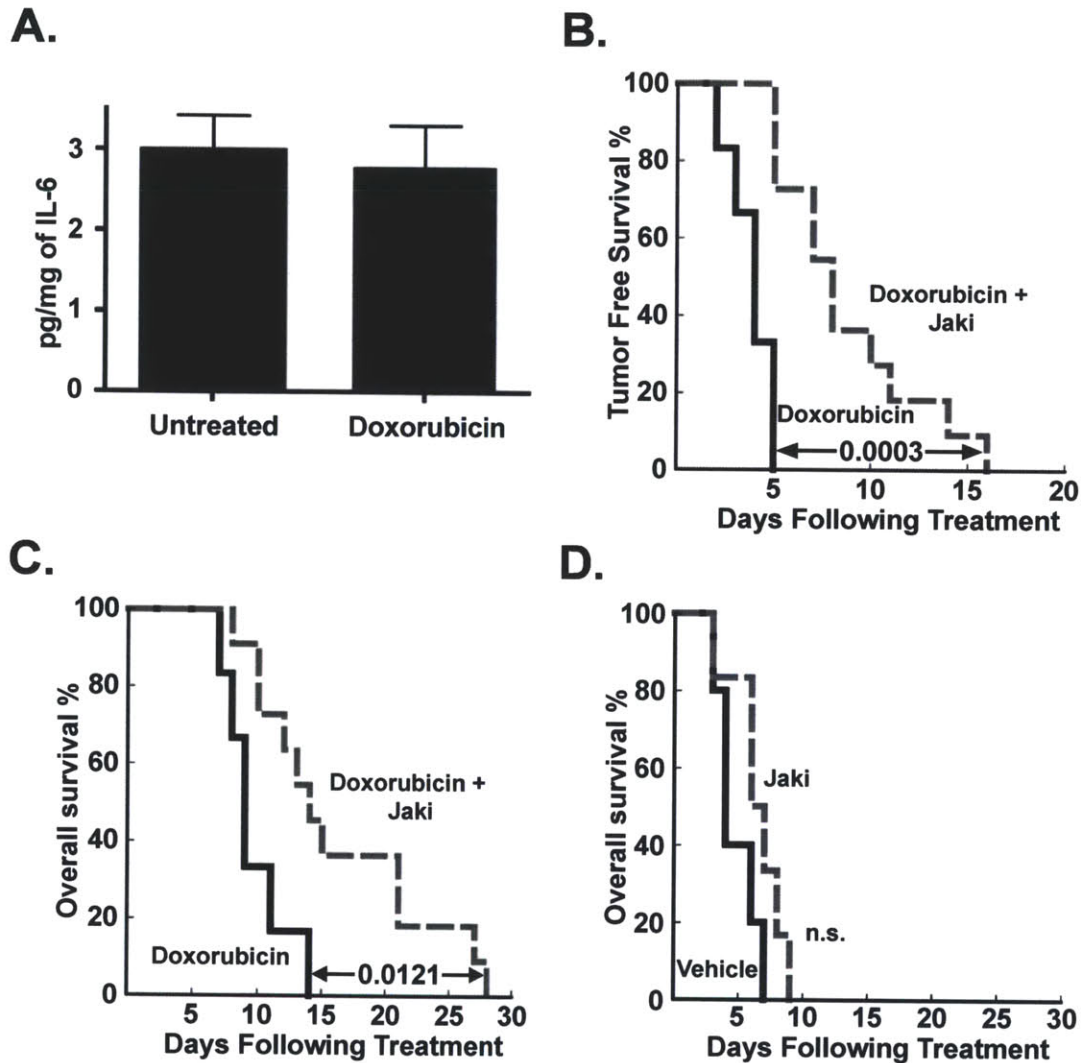
doxorubicin (n≥7). Values were normalized by tissue weight. The data are represented as mean +/- SEM. **(B)** Quantification of IL-6 levels in conditioned media derived from tumor-bearing thymuses or lymph nodes of doxorubicin-treated (n=3) or untreated (n=3) mice. The data are represented as mean +/- SEM. **(C)** A bar graph showing the fold change in number of live cells following treatment with doxorubicin alone or in combination with conditioned media plus or minus a Jak2 inhibitor. The data are represented as mean +/- SEM (n=3). **(D)** A Kaplan-Meier curve showing tumor-free survival of lymphoma-bearing mice treated with doxorubicin (n=9) or doxorubicin plus two doses of 50mg/kg AG-490 m-CF$_3$ (n=4). The p value was calculated using a log rank test. **(E)** H&E sections of lymphomas 72 hours after treatment with doxorubicin or doxorubicin plus AG-490 m-CF$_3$. Black dotted lines distinguish surviving lymphoma cells, which are largely absent in the presence of AG-490 m-CF$_3$, from infiltrating immune cells. Representative fields are shown at 20x magnification. See also Figure S3.

To confirm that this acute DNA-damage-induced secretory response also occurs in thymuses with substantial lymphoma infiltration, we examined IL-6 levels in tumor-bearing mice. Again, IL-6 was constitutively present at a higher level in the thymic tumor microenvironment versus the peripheral tumor microenvironment, and treatment with doxorubicin resulted in a rapid and significant increase in IL-6 levels in thymic lymphomas but not in peripheral lymphomas (Figure 4B). As chemotherapy rapidly induces apoptosis in lymphoid malignancies, these data are consistent with the idea that acute cytokine release following DNA damage may directly impact therapeutic response.

Supplemental Figure 3. Inhibition of cytokine signaling sensitizes lymphoma cells to doxorubicin but does not affect growth. (A) IL-6 levels were quantified by ELISA for conditioned media from spleen of untreated mice (n=3) or mice treated for 18 hours with 10mg/kg doxorubicin (n=3). Values were normalized by tissue weight. The data are represented as mean +/- SEM **(B)** A Kaplan-Meier curve depicting tumor-free survival of $E\mu$-myc $p19^{Arf-/-}$ tumor-bearing C57BL/6 mice treated with either a single dose of 10mg/kg doxorubicin (n=6) or a single dose of both 10mg/kg doxorubicin and 50mg/kg AG-490 m-CF$_3$ (n=11). **(C)** A Kaplan-Meier curve showing overall survival of $E\mu$-myc $p19^{Arf-/-}$ tumor-bearing C57BL/6 mice treated with either a single dose of 10mg/kg doxorubicin (n=6) or a single dose of both 10mg/kg doxorubicin and 50mg/kg AG-490 m-CF$_3$ (n=11). **(D)** A Kaplan-Meier curve showing overall survival of $E\mu$-myc $p19^{Arf-/-}$ tumor-bearing C57BL/6 mice treated with vehicle control (n=5) or 50mg/kg AG-490 m-CF$_3$ (n=6). The p values for all Kaplan-Meier curves were calculated using a log rank test.

Jak2 signaling is required for lymphoma cell survival following doxorubicin treatment *in vivo* and *in vitro*

Both IL-6 and Timp-1 have been shown to signal through Jak2 and Stat3 (182,183), suggesting that doxorubicin efficacy could be potentiated if Jak signaling were chemically inhibited. We tested this hypothesis by treating lymphoma cells with doxorubicin and TM or doxorubicin and TM plus a Jak2/Jak3 inhibitor. Addition of the Jak inhibitor completely ablated the protective effect of TM (Figure 4C). Importantly, the Jak inhibitor had a minimal effect on lymphoma cell growth in the presence of TM (data not shown). Thus, Jak2/Jak3 signaling promotes the chemoprotective effect of TM *in vitro*.

To determine whether this effect could be recapitulated *in vivo*, we treated lymphoma-bearing mice with either doxorubicin, Ag490 (a Jak2/3 inhibitor previously used in murine *in vivo* studies) (184), or with a combination of both doxorubicin and Ag490. Mice treated with doxorubicin and Ag490 showed significantly longer tumor-free survival and overall survival than mice treated with doxorubicin alone (Figure 4D and Supplemental Figure 3B and C). Histological analysis of the thymus in mice treated with both drugs showed few surviving lymphoma cells, in sharp contrast with those treated with doxorubicin alone (Figure 4E). Importantly, this was not due to a simple additive effect of doxorubicin and Ag490-induced cytotoxicity, as mice treated with Ag490 alone exhibited no tumor-free survival or extended overall survival when compared to mice treated with a vehicle control (Supplemental Figure 3D and data not

shown). Thus, Jak2/Jak3 inhibition can eliminate pro-survival signaling in the thymic niche and potentiate doxorubicin cytotoxicity.

IL-6 is released from thymic endothelial cells

To identify the cell type(s) responsible for IL-6 release from the thymic stroma, we disassociated thymuses from untreated mice and sorted known resident cells by characteristic surface markers. Sorted cells were then plated in normal growth media, and IL-6 levels were assessed after 48 hours. Notably, the vast majority of IL-6 secreted following thymic disassociation was released from thymic endothelial cells, while B, T, dendritic and thymic epithelial cells failed to produce any IL-6 levels above background (Figure 5A). Resident macrophages produced trace levels of IL-6 (Figure 5A and Supplemental Figure 4A). However, they did so at a level that was more than ten-fold less than endothelial cells. Similar results were seen for Timp-1, which was released almost exclusively from thymic endothelial cells (Figure 5B).

Importantly, in mice treated with doxorubicin, IL-6 levels were significantly induced in thymic endothelial cells (Figure 5F). While IL-6 levels were also elevated in treated macrophages (Supplemental Figure 4A), this increase was not significant and represented less than one tenth of the amount released from treated endothelial cells - even when adjusted for total cell number. Additionally, no significant increase in infiltrating macrophages or dendritic cells was seen acutely following treatment (data not shown). Consistent with the central role of

endothelial cells in this secretory response, pretreatment of mice with an inhibitor

of VEGFR1/2 – receptors necessary for endothelial cell proliferation - partially

inhibited doxorubicin-induced IL-6 release (Supplemental Figure 4B). These data

suggest that resident endothelial cells are largely responsible for the

accumulation of pro-survival factors following chemotherapy in this model. To

directly assess the relevance of endothelial cells to tumor cell survival, we co-

cultured purified endothelial cells and lymphoma cells in the presence of

doxorubicin (Figure 5C). The presence of endothelial cells dramatically increased

lymphoma cell survival following treatment, with a 15-fold increase in lymphoma

cell number in co-cultured populations relative to lymphoma cell-only populations

72 hours post-treatment.

Several studies have indicated that cytokines, including IL-6, may exert a

pro-survival benefit in target cells through induction of anti-apoptotic Bcl2 family

members, including Bcl2, Bcl-XL and Mcl-1 (185). Thus, we examined the protein

levels of Bcl2 family members in lymphoma cells treated with thymic conditioned

media. While Bcl2 and Mcl-1 levels were unaffected (data not shown), Bcl-XL

was consistently induced 2-4 fold (Figure 5D). To further examine whether Bcl-

XL contributes to cell survival in this context, we treated cells expressing a Bcl-

XL shRNA with doxorubicin alone or doxorubicin plus IL-6 (Figure 5E).

Suppression of Bcl-XL blocked the ability of IL-6 to promote doxorubicin

resistance, suggesting that IL-6 mediated induction of Bcl-XL may be necessary

for its role in cell survival. This does not, however, preclude that other factors

may contribute to cell survival following exposure to IL-6, as cytokines are known

to activate numerous pro-survival pathways.

A.

B.

C.

| Lymphoma | + | + | + | + |
| Endothelial | - | + | - | + |

48 hours   72 hours

D.

Bcl-XL

Vinculin

Untreated   TCM

E.

p<0.0001   p<0.0001

	Vector	shBcl-XL	shBcl-XL
Doxorubicin	+	+	+
IL-6	-	-	+

F.

Untreated   Doxorubicin   Doxorubicin + SB203580

G.

p<0.0001

Untreated   Doxorubicin

H.

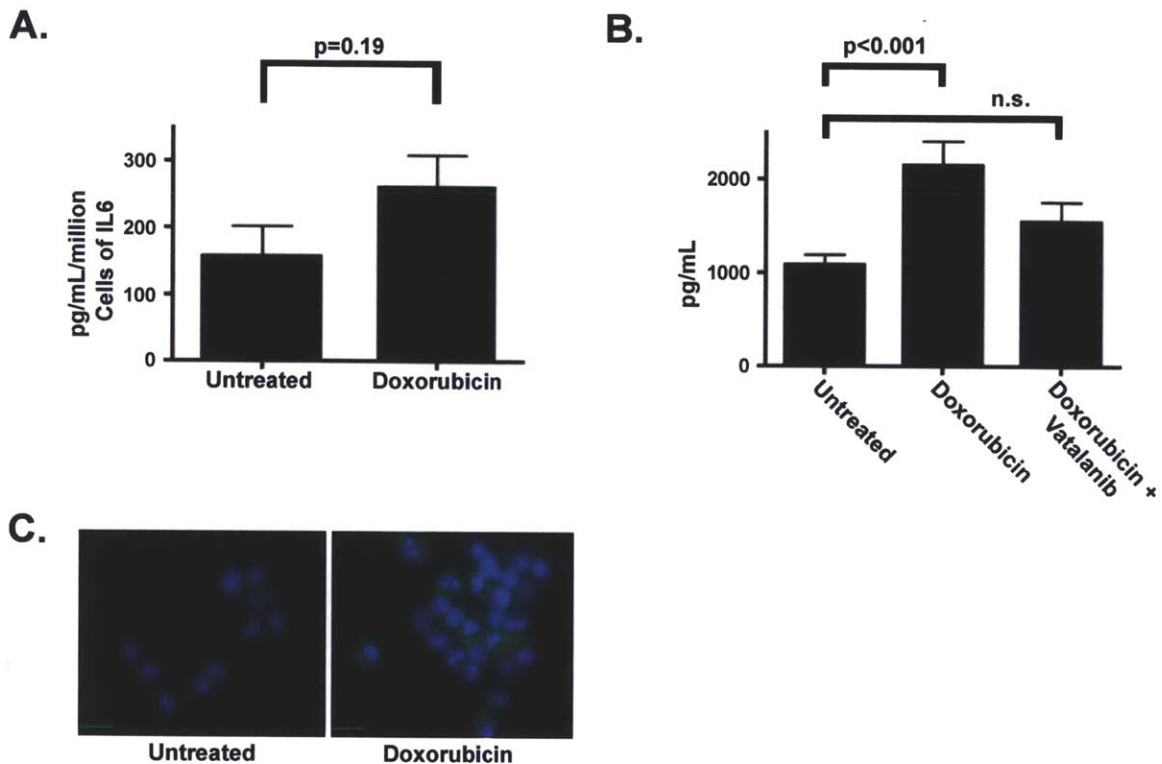| Untreated | + | - | - | + | - | - |
| SB203580 | - | + | - | - | + | - |
| KU55933 | - | - | + | - | - | + |

Untreated   Doxorubicin
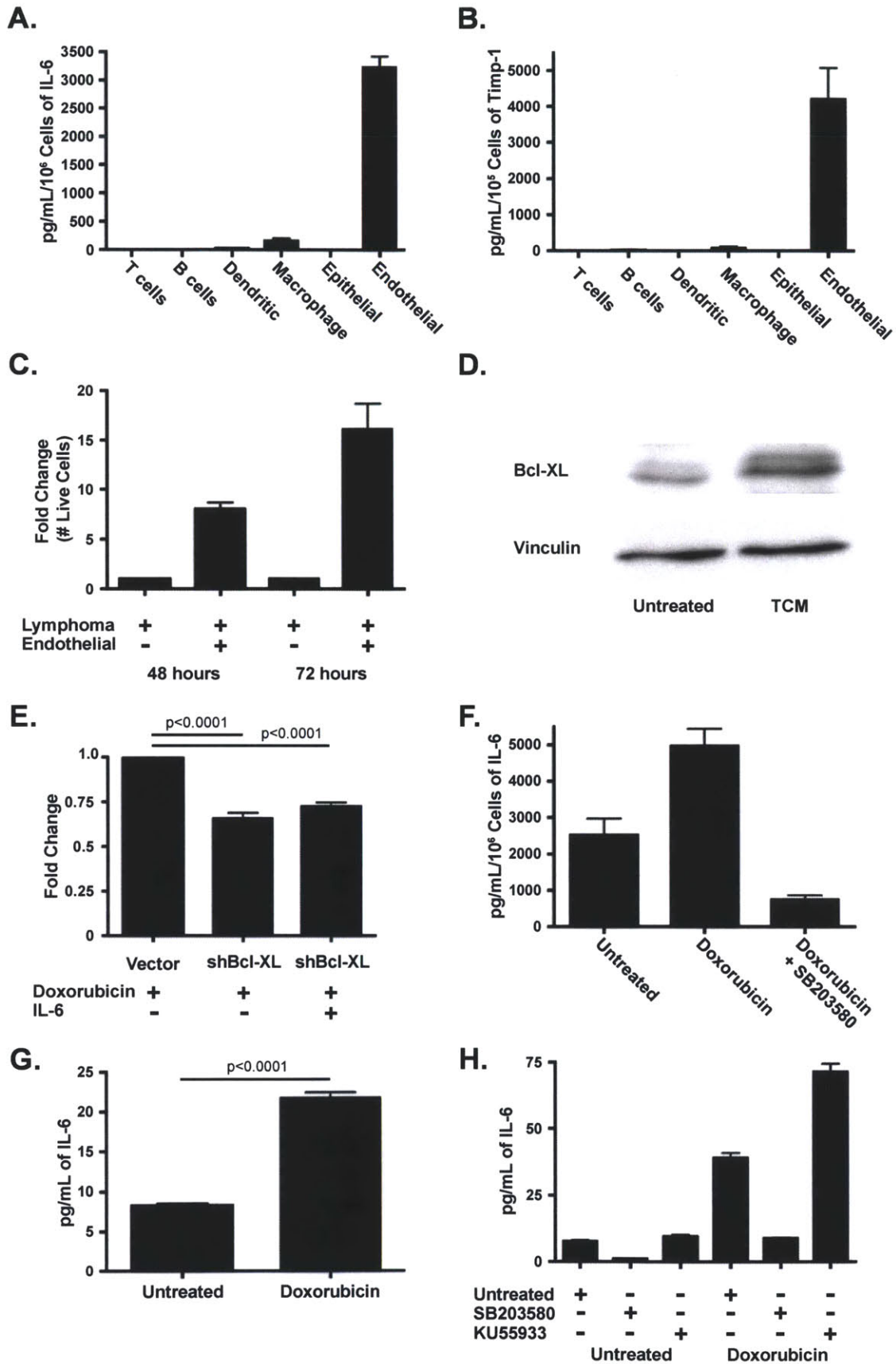
Figure 5. Endothelial cells secrete IL-6 and Timp-1 in response to DNA damage in a p38 MAP kinase dependent manner. (A) IL-6 and **(B)** Timp-1 levels were quantified by ELISA in conditioned media derived from sorted thymic cell populations. The data are represented as mean +/- SEM (n≥3 independent experiments). Values were normalized to the number of cells sorted. **(C)** A graph showing lymphoma cell survival in response to 20nM doxorubicin, with or without endothelial cell co-culture. Fold change in cell number was assessed at 48 and 72 hours post treatment. The data are represented as mean +/- SEM (n=6 independent experiments) **(D)** A western blot for Bcl-XL levels in lymphoma cells in the presence or absence of TCM for 24 hours. The blot is representative of three independent experiments. **(E)** A graph showing the results of a GFP competition assay in cells partially transduced with a Bcl-XL shRNA or a control vector. Fold change in GFP percentage was assessed 48 hours following treatment with 20nM doxorubicin. The data are represented as mean +/- SEM (n=3). **(F)** A bar graph showing the amount of IL-6 in conditioned media from endothelial cells sorted from the thymus of untreated mice (n=5), mice treated with doxorubicin (n=8) or mice treated with doxorubicin plus SB203580 (n=4). Values were normalized to cell number. The data are represented as mean +/- SEM. **(G)** A graph showing the amount of IL-6 present in conditioned media from untreated and treated human vascular endothelial cells (HUVECs). The data are represented as mean +/- SEM (n=3). **(H)** A graph showing the amount of IL-6 present in conditioned media from HUVECs 48 hours after treatment with doxorubicin alone or doxorubicin plus either SB203580 or KU55933. The data are represented as mean +/- SEM (n=3). See also Figure S4.

IL-6 is release from endothelial cells is dependent upon p38 MAP Kinase activity

The p38 MAP Kinase (p38) is known to be a key regulator of the expression of inflammatory cytokines, including IL-6 (186). To determine whether p38 is required for DNA-damage-induced IL-6 release, treated and untreated thymic endothelial cells were purified and probed by immunofluorescence for the presence of activated p38. Notably, treated endothelial cells showed significantly higher phospho-p38 levels than their untreated counterparts (Supplemental Figure 4C). To examine the functional relevance of this p38 activation, we plated thymic endothelial cells from mice treated with doxorubicin in the presence or

61

absence of a p38 inhibitor (Figure 5F). Strikingly, the addition of a p38 inhibitor

not only prevented IL-6 induction, but actually reduced the level of secreted IL-6

to below the level in untreated cells. To investigate whether this DNA-damage-

induced IL-6 release is a conserved characteristic of endothelial cells, we

performed similar experiments in human vascular endothelial cells (HUVECs).

Cultured HUVECs were treated with doxorubicin and conditioned media were

collected 24 hours after treatment. Here, doxorubicin elicited a threefold

increase in the amount of secreted IL-6 (Figure 5G). This process was also

dependent upon p38 activity, as concurrent treatment of HUVECs with

doxorubicin and a p38 inhibitor blocked IL-6 induction (Figure 5F and Figure 5H).

Cell-based studies have implicated the ATM checkpoint kinase in

senescence-associated secretory phenotypes (SASP) (144). To examine the

relevance of ATM to endothelial IL-6 release, we treated HUVECs with

doxorubicin and an ATM inhibitor (Figure 5H). Surprisingly, as opposed to

blocking cytokine secretion, ATM inhibition significantly increased the level of

endothelial IL-6 release. These data suggest that the biology of acute cytokine

release may be distinct from SASP.

A.

B.

C.

| Untreated | Doxorubicin |

Supplemental Figure 4. Endothelial cells release IL-6 via p38 activation in response to DNA damage. (A) IL-6 levels were quantified by ELISA for conditioned media from macrophages sorted from the thymus of untreated mice or mice treated with 10mg/kg for 18 hours. The data are represented as mean +/- SEM. **(B)** IL-6 levels were quantified by ELISA for conditioned media from untreated mice (n=8), mice treated with 10mg/kg doxorubicin for 18 hours (n=15) or mice treated with 100mg/kg vatalanib for 4 days and then 100mg/kg vatalanib and 10mg/kg doxorubicin for 18 hours (n=12). Values displayed are pg/mL per thymus. The data are represented as mean +/- SEM. **(C)** A representative fluorescent image of pospho-p38 levels in endothelial cells from untreated mice or mice treated with 10mg/kg doxorubicin for 18 hours.

**Cytotoxic chemotherapy induces senescence in thymic stromal cells *in vivo***

Recent studies have shown that an autocrine IL-6 signaling loop is induced upon oncogene activation and that this autocrine loop reinforces oncogene-induced senescence (OIS) (141,142). This observation led us to investigate whether IL-6 secretion in the thymus is accompanied by drug-induced

senescence. To determine whether doxorubicin induces senescence *in vivo*, we harvested the thymus and lymph nodes from mice 6 days following treatment with doxorubicin. Tissues were frozen, sectioned and stained for β-Galactosidase activity – a marker of cellular senescence (187). Tissues from untreated mice showed no senescent cells (Figure 6A). In sharp contrast, β-Galactosidase-positive cells were abundant in the thymus, but not the lymph nodes, of doxorubicin-treated mice (Supplemental Figure 5A). Notably, this "senescent" state was transient, as β-Galactosidase-positive cells were no longer present at twelve days following treatment (Supplemental Figure 5B). While the mechanism underlying the transient presence of senescent cells in this context is unclear, these data are consistent with the recognition and removal of senescent cells by the innate immune system (149,150). Thus, doxorubicin can elicit the acute release of pro-survival cytokines from non-tumor cells in the thymus, coincident with a more gradual induction of senescence.

To confirm that a similar "senescent" state also occurs in the thymic tumor microenvironment, lymphoma-bearing mice were treated with doxorubicin. Six days following treatment, mice were sacrificed and tumors were harvested. Again, thymic tumor sites showed the presence of disseminated senescent cells, while the lymph nodes lacked any β-galactosidase positivity (Figure 6A and Supplemental Figure 5A). At least a component of this treatment-induced senescent population was comprised of endothelial cells, as purified CD31+/CD34+ cells showed senescent phenotypes – including β–galactosidase

activity (Supplemental Figure 5C). Notably, tumor-bearing thymuses and lymph nodes showed similar numbers of macrophages and dendritic cells, suggesting that the β-galactosidase-positive cells in the thymus were resident stromal cells as opposed to infiltrating immune cells (Supplemental Figure 5D).

A.
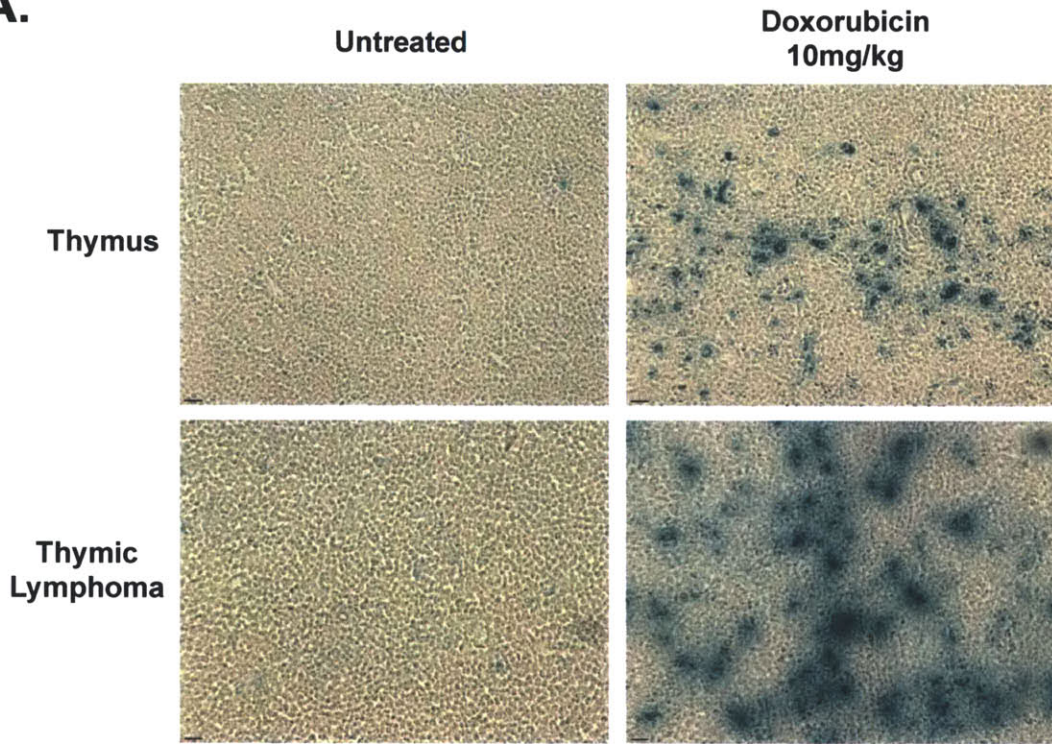
B.
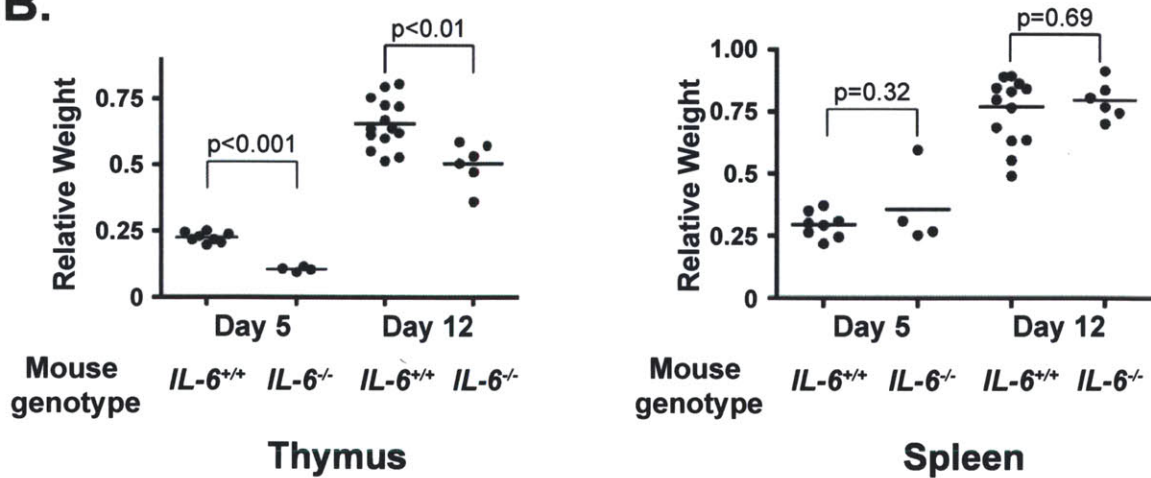
Figure 6. Genotoxic damage promotes cellular senescence in thymic stromal cells and subsequent IL-6 mediated thymic rebound. (A) β-galactosidase staining of normal and tumor-bearing thymuses and lymph nodes in the presence or absence of doxorubicin-induced DNA damage. Representative fields are shown at 20x magnification. **(B)** A graph showing relative thymic and splenic weight following genotoxic damage in the presence (n=14) and absence (n=6) of IL-6. Organ weights are shown as the ratio of individual irradiated thymus or spleen weights relative to the average un-irradiated thymic or spleen weight for each genotype. The data are represented as mean +/- SEM. See also Figure S5.
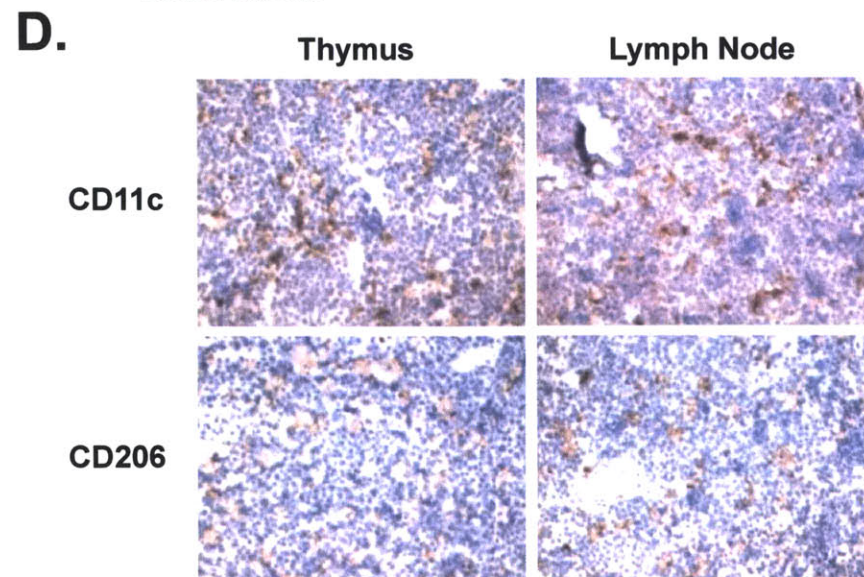

IL-6 modulates a general response to DNA damage in the thymus

The presence of a pro-survival secretory response in the thymus following chemotherapy led us to investigate whether IL-6 is involved more generally in stress-induced thymic homeostasis. Whole-body irradiation, such as that occurring prior to bone-marrow transplantation, induces thymocyte cell death, peripheral leucopenia and thymic involution. This acute wave of thymocyte death is followed by an acute regrowth of the thymus, termed "thymic rebound" (188). To assess whether IL-6 induced by DNA damage is similarly cytoprotective in this setting, we irradiated wild-type and *IL-6*$^{-/-}$ mice. 5 or 12 days later, all mice were sacrificed and the spleen and thymus were harvested and weighed. Thymic regrowth in *IL-6*$^{-/-}$ mice was significantly reduced when compared to wild-type control mice (Figure 6B), while no difference was seen in the spleen. Therefore, IL-6 secretion in the thymus may be critical for thymic growth and repopulation following diverse genotoxic stresses.

A.

Peripheral Lymphoma | Thymic Lymphoma

Doxorubicin 10mg/kg

B.

Day 6 | Day 12

Doxorubicin 10mg/kg

C.

Untreated

Doxorubicin

β-galactosidase positive (%)

Untreated | Doxorubicin

D.

Thymus | Lymph Node

CD11c

CD206
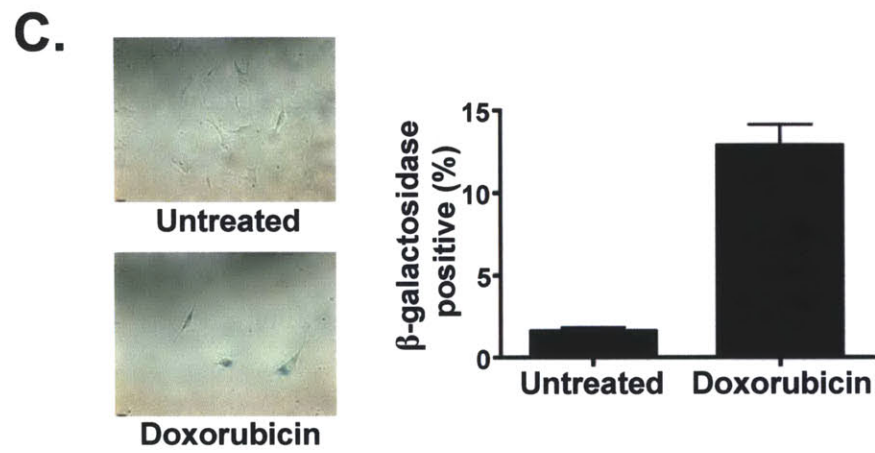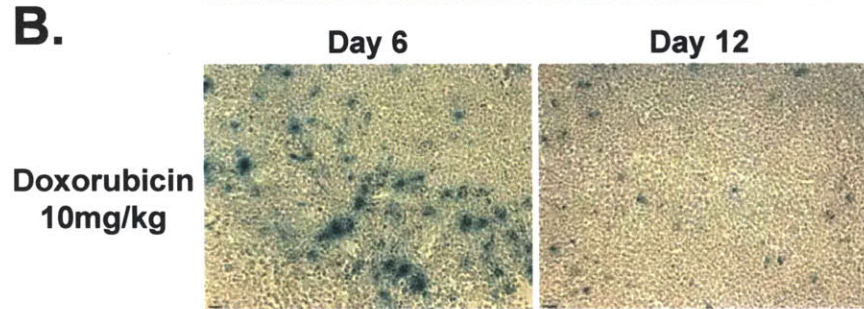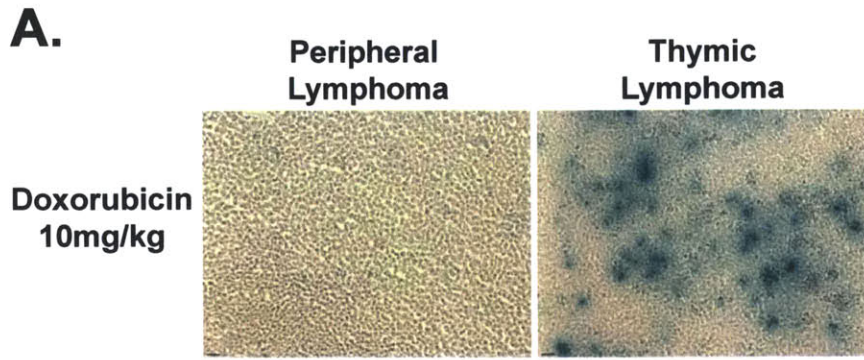
Supplemental Figure 5. Genotoxic damage promotes cellular senescence in thymic stromal cells (A) β-galactosidase staining of peripheral lymphoma and thymic lymphoma 6 days following doxorubicin-induced DNA damage. Representative fields are shown at 20x magnification. **(B)** β-galactosidase staining of *Eμ-myc p19*$^{Arf-/-}$ thymic lymphomas at 6 or 12 days following doxorubicin-induced DNA damage. Representative fields are shown at 20x magnification. **(C)** β-galactosidase staining and quantification of β-galactosidase staining in thymic endothelial cells sorted from untreated mice or mice treated with 10mg/kg doxorubicin for 4 days. The data are represented as mean +/- SEM. **(D)** Immunohistochemistry showing infiltration of CD11C and CD206 positive dendritic cells and macrophages into the tumor following treatment with doxorubicin. Representative fields are shown at 20x magnification.

Genotoxic damage promotes acute IL-6 release and chemoprotection in human liver cancer cells

Previous descriptions of secretory phenotypes have reported a gradual induction of cytokine release following the onset of stress-induced cellular senescence. This suggests that the release of pro-survival cytokines may not occur rapidly enough to impact chemotherapeutic response. The finding that doxorubicin can induce an acute secretory response led us to investigate whether IL-6 induction might be relevant to therapeutic response in contexts other than the thymic microenvironment. Recent reports have implicated IL-6 as a major contributor to the pathogenesis of hepatocellular carcinoma (HCC) (168,189). In humans, activating mutations in gp130, the obligate signal-transducing subunit of the IL-6 receptor, have been recently identified (163). Additionally recent expression profiling identified the presence of an IL-6-induced transcriptional signature in the tumor stroma that is associated with poor prognosis in hepatocellular carcinoma (73).

We treated an HCC cell line, Focus cells, with doxorubicin - a front-line therapy for HCC - and measured the levels of secreted IL-6 after 24 hours. Consistent with our endothelial cell data, IL-6 secretion was increased over 3-fold acutely following treatment (Figure 7A). Notably, treated cells lacked any markers of senescence at this time point, indicating that senescence is not required for acute cytokine release. In contrast with endothelial cells, IL-6 secretion could be partially inhibited by either a p38 or an ATM inhibitor (Figure 7B). Thus, pathway requirements for acute secretory phenotypes may be somewhat variable between cell types.

We then investigated whether inhibition of IL-6 signaling could enhance doxorubicin-induced cell death in HCC cells. We treated Focus cells with doxorubicin alone, Ag490 alone or doxorubicin in combination with Ag490. Treatment with both doxorubicin and Ag490 resulted in more apoptosis and fewer surviving cells in acute survival assays than either single agent alone (Figure 7C). The combination treatment of doxorubicin and Ag490 was also more effective than single-agent therapy when measured in a colony-formation assay (Figure 7D). These data suggest that acute drug-induced IL-6 release is chemoprotective in HCC and may contribute to the intrinsic chemoresistance of these tumors.
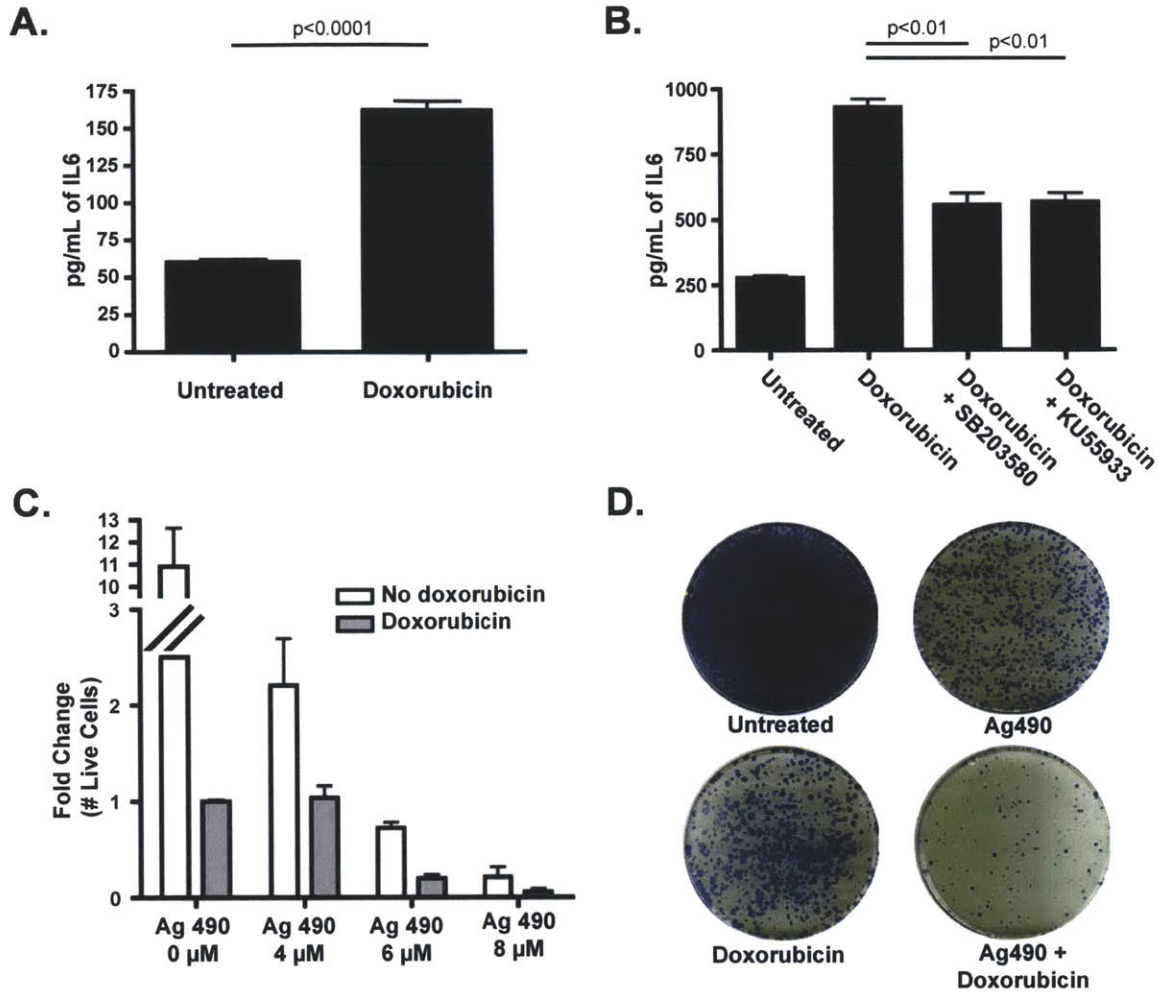
Figure 7. DNA damage acutely induces IL-6 in human hepatocellular carcinoma, promoting both cellular survival and senescence. (A) IL-6 levels were quantified in conditioned media derived from Focus cells treated with 200nM doxorubicin for 24 hours. The data are represented as mean +/- SEM (n=3). **(B)** A graph showing the amount of IL-6 present in Focus cells following treatment with either SB203580 or KU55933, in the presence or absence of doxorubicin. The data are represented as mean +/- SEM (n=3). **(C)** A graph showing the results of an acute cell survival assay in which Focus cells were treated with doxorubicin and increasing doses of Ag490, as indicated, for 4 days. The data are represented as mean +/- SEM (n=3 independent experiments) **(D)** A colony formation assay showing Focus cells that were treated with doxorubicin, Ag490 or both for 24 hours before replating. Results are representative of 3 independent experiments.

Discussion

The persistence of minimal residual disease following anti-cancer therapy is strongly correlated with decreased survival in patients (190). However, the mechanisms by which cells survive in select contexts following chemotherapy are unclear. In a mouse model of Burkitt's lymphoma, we show that a specific anatomical location, the thymus, confers a potent cytoprotective benefit to lymphoma cells treated with genotoxic chemotherapy. This surviving cell population is functionally relevant to disease progression, as ablation of the thymus prolongs both tumor-free survival and overall survival following treatment with chemotherapy. While the importance of the thymic microenvironment to tumor cell survival in human malignancy remains unclear, we expect that factors contributing to drug resistance at this site may also underlie MRD persistence at analogous locations in human cancers.

The establishment of the thymic pro-survival microenvironment occurs, paradoxically, as a response to genotoxic chemotherapy. Specifically, pro-survival chemokines and cytokines are acutely released following DNA-damage. While the complete signaling network leading from a DNA damage response to cytokine release remains unclear, it involves the activation of stress-responsive kinases – most notably the MAP kinase p38. Thus, cells exposed to genotoxic damage *in vivo* can engage well-described cell-cycle arrest and apoptotic programs, as well as a physiological stress-response pathway leading to survival

signaling. Importantly, the resulting secretory response occurs not in the tumor cells themselves, but in proximal endothelial cells. Drug-treated endothelial cells release IL-6 and Timp-1, which promote the induction of Bcl-XL in proximal lymphoma cells. As a result, pro-apoptotic signaling induced by the direct action of chemotherapy on tumor cells is countered by anti-apoptotic signaling emanating from the treated vascular compartment in the tumor microenvironment.

Recent literature has shown that the induction of oncogene-induced cellular senescence elicits a secretory response (141,142). Here we find that IL-6 is induced acutely following DNA damage, prior to the onset of senescence. This difference between a pro-survival response that occurs within one day of treatment and a SASP that is detectable only after 3-4 days is critical. Chemotherapy-induced cell death generally occurs with 48 hours of treatment. Thus, a SASP simply cannot effectively alter treatment response, as it occurs well after tumor cell death decisions are made. However, our data does not preclude a role for senescence in overall tumor survival following therapy. Given that significant levels of senescence occur in the thymus days after doxorubicin treatment, it is possible that elevated IL-6 levels are maintained through the establishment of a SASP. Thus, acute cytokine release and subsequent senescence-related secretory phenotypes may represent a general strategy to promote paracrine cell survival in response to genotoxic stress in select microenvironments.

Secretory and inflammatory processes have been shown to be critical for tissue repair and regeneration (150,162). Thus, chemotherapy in the thymic setting may activate physiological mechanisms of tissue homeostasis. Consistent with this idea, the thymus is known to engage pro-survival and growth mechanisms in response to other cellular stresses. Following radiotherapy and subsequent thymic atrophy (191), the thymus re-grows and replenishes the peripheral T-cell population, leading to significant thymic hyperplasia – even in adults with limited remaining thymic tissue (192). Factors that govern this process have not been previously identified. Here we show that IL-6 modulates thymic recovery in response to DNA damage. This suggests that lymphomas, and perhaps other malignancies, can co-opt organ-specific pro-survival mechanisms.

Interestingly, serum IL-6 levels are elevated in many types of cancer (193), and high IL-6 levels are strongly correlated with poor overall survival and accelerated disease progression in a variety of cancers, including lymphomas (194). Furthermore, IL-6 levels are greatly increased in metastatic disease versus non-metastatic disease (195). Consequently, stromal or tumor up-regulation of IL-6 may contribute to the intrinsic chemoresistance commonly found in both primary and metastatic malignancies. Additionally, tumor-directed inflammatory responses that result in IL-6 release may similarly limit the efficacy of genotoxic agents. These data suggest that both intrinsic genetic alterations as well as

chemoprotective microenvironments can play decisive roles in the cellular response to genotoxic insults. Thus, improved chemotherapeutic regimes may require a combination of cytotoxic agents, which target tumor cells, and targeted therapeutics that inhibit pro-survival signaling from the tumor-adjacent cells.
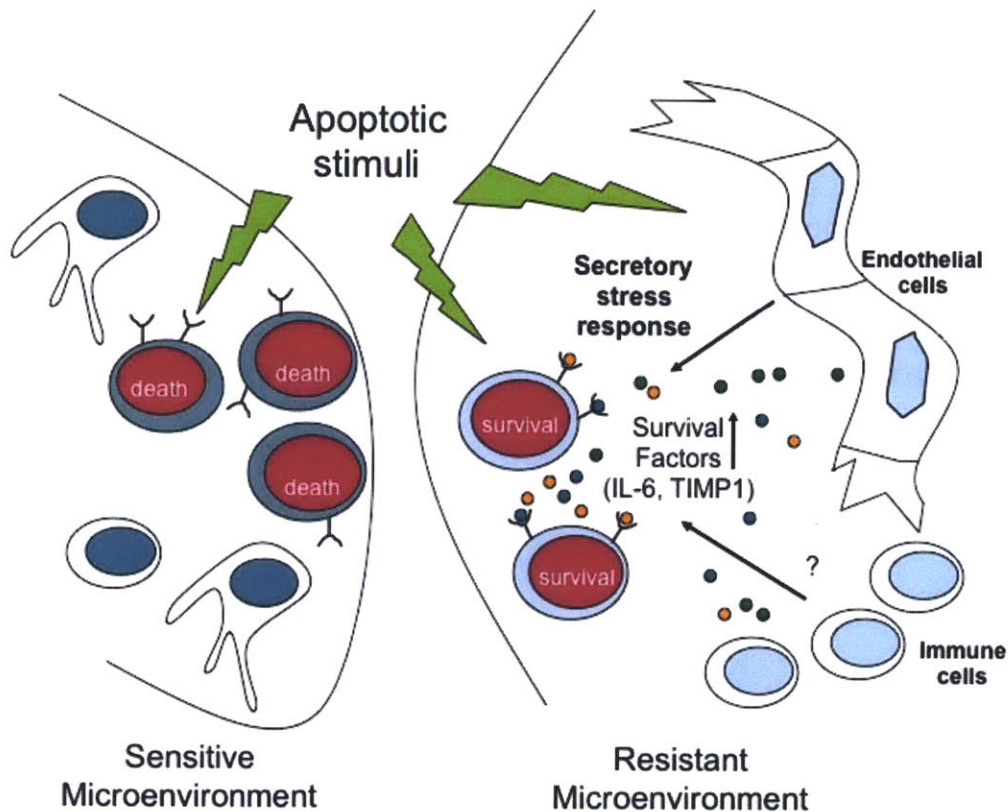
Figure 8. A diagram showing microenvironment-specific responses to chemotherapy. Left, systemic chemotherapy can effectively clear the majority of lymphoid tumor cells. Right, genotoxic damage can also induce organ- and cell-type–specific stress responses. Paracrine prosurvival signaling in select tumor microenvironments can counter the efficacy of anticancer agents, leading to the persistence of MRD.

Experimental Procedures

Cell culture and chemicals

$E\mu$-$Myc;p19^{Arf-/-}$ mouse B cell lymphomas were cultured in B cell medium (45% DMEM/45% IMDM/10% FBS, supplemented with 2mM L-glutamine and

74

5μM β- mercaptoethanol). γ-irradiated NIH 3T3 cells were used as feeder cells. Focus cells were cultured in MEM with 10% FBS. HUVEC cells were cultured in Endothelial Cell Growth Medium 2 (Lonza). Doxorubicin, Jak Inhibitor 1 and Ag490 mCF_3 were purchased from Calbiochem. SB203580 and KU55933 were purchased from Tocris Bioscience. Gefitinib was purchased from LC labs. For *in vivo* studies, Ag490 m-CF3 was dissolved in DMSO and then diluted 3:2 in DMEM plus 10% FBS.

Conditioned media

Conditioned media was made from mouse tissues 18 hours after doxorubicin treatment. Conditioned media for viability assays and cytokine arrays was derived from organs from 3-4 pooled mice, while media for ELISAs was generated from individual mice. All tissues were dissociated manually in B cell media. Thymic, bone marrow and lymph node conditioned media were conditioned for 6 hours at 37°C. To isolate single cell types from the thymus, tissue was manual dissociated and washed two times in serum free DMEM, followed by incubation for 1 hour at 37°C with Liberase™ (Roche, 1.3 Wunsch units/mL) and Dnase I (0.15 mg/mL). To aid in dissociation, samples were manually pipetted at 15-minute intervals. Single cell populations were sorted using FITC conjugated antibodies to the following cell surface markers: CD45, CD19, CD11b, CD11c, MHC II, CD31/CD34 for T cells, B cells, macrophages, dendritic cells, epithelial and endothelial cells, respectively. Cells were plated and allowed to condition media for 48 hours at 37°C and 5% CO_2. All conditioned

medias were cleared of tissue and cells by centrifugation. All values shown for viability assays, ELISAs and cytokine arrays are normalized to the weight of the dissected tissue or the number of sorted cells. For the viability assays, conditioned medias were diluted one to three. IL-6 ELISA kits were purchased from eBioscience. The Timp-1 ELISA kit and mouse cytokine arrays were purchased from R&D Biosystems.

In vitro viability, competition and cell growth assays.

For viability, competition and growth assays $E\mu$-$Myc;p19^{Arf-/-}$ lymphoma cells were split into replicate wells of $\approx$500,000 cells in 24-well plates or $\approx$125,000 cells in a 48-well plate. Every 24 hours, cultured cells were resuspended by pipeting and half of the culture was replaced with fresh medium. Viability and cell number were determined by propidium iodide exclusion. For the competition assay, lymphoma cells were partially infected with the indicated retroviruses. The fold change for the competition assay is calculated by dividing the percentage of GFP positive lymphoma cells in the treated population by the percentage in untreated populations. Murine Timp-1 was purchased from R&D Biosystems and used at 100ng/mL. All other cytokines were purchased from Peprotech and used at 10ng/mL. Jak Inhibitor 1 was used at a final concentration of 500nM, and Gefitinib was used at a final concentration of 3μM.

In vivo response to chemotherapy

All mice were purchased from Jackson Laboratory. For survival assays, 1

x 10^6 $E\mu$-$Myc;p19^{Arf-/-}$ mouse lymphoma cells were injected by tail-vein injection

into syngenic C57BL/6J, C57BL/6J IL-$6^{-/-}$ or C57BL/6J $Rag1^{-/-}$ mice. Lymphoma

burden was monitored by palpation of the axillary and brachial lymph nodes. At

the presentation of a substantial tumor burden (12-13 days after injection), mice

were treated with doxorubicin and/or Ag490 m-CF$_3$. Tumor free survival was

monitored by palpation and *in vivo* GFP imaging using a NightOwl imaging

system (Berthold).

Thymic rebound in response to radiation

Untreated 6 to 8 week old C57BL/6J or C57BL/6J IL-$6^{-/-}$ mice were

sacrificed to establish basal spleen and thymic weight. 6 to 8 week old C57BL/6J

or C57BL/6J IL-$6^{-/-}$ mice were irradiated with 4 or 5 Gray. 5 or 12 days later all

mice were sacrificed and the spleen and thymus were weighed.

Immunohistochemistry

Frozen sections of mouse lymphoid tissue were acetone fixed at -20°C for

20 minutes. Endogenous peroxidases were quenched using 0.3% H$_2$O$_2$ for 30

minutes. Non-specific antibody binding was blocked with 10% goat serum 1%

BSA in PBS for 30 minutes. Samples were then incubated overnight at 4°C in 1%

BSA PBS with anti-CD11c (hampster anti-mouse 1:100 BD Pharmingen) or anti-

CD206 (rat anti-mouse 1:75 AbD Serotec). Secondary antibodies were

horseradish peroxidase-conjugated anti-rat/hampster IgG (Abcam; 1:5,000).

Samples were incubated with secondary antibodies for 1 hour at room temperature. Immune complexes were visualized using the DAB method. Sections were counterstained with hematoxylin. Images were collected on an Axioplan2 (Zeiss) microscope equipped with Openlab software from Improvision.

Flow cytometry

Lymphoma cells were incubated with anti-IL6r (purified rat anti mouse 1:100 BioLegend) or isotype control (rat anti mouse IgG2b 1:100 Ebioscience) in 1% FBS for 30 minutes at room temperature. Cells were washed once in 1% FBS and then stained at 4°C for 30 minutes with Alexaflour 488 conjugated secondary (goat anti rat 1:500 Invitrogen). Cells were washed twice in 1% FBS PBS. Samples were then examined by FACS on a BD Bioscience FACS Scan machine. FloJo was used to further analyze the data.

To assess phospho Serine 139 H2AX levels *in vivo*, mice bearing GFP positive tumors were treated with 10mg/kg doxorubicin. Lymphoma cells (GFP+ PI- cells) were harvested 12 hours later and sorted by FACS using a MoFlo FACS sorting machine. All samples were fixed in 70% ethanol. Cells were washed and rehydrated in 2% FBS PBS. Samples were then stained for 5 hours with anti-γH2AX (monoclonal clone JBW301, 1:1000; Upstate/Millipore) in 2% FBS PBS at 4°C. Cells were washed once in 2%FBS PBS and then stained with Alexaflour 488 secondary antibody (goat anti-mouse 1:500 Invitrogen) for 30 minutes at 4°C. Cells were washed twice in 2% FBS PBS. Samples were then

acquired by FACS on a BD Bioscience FACS Scan machine. FloJo was used to further analyze the data.

Migration Assay

Recombinant murine SDF-1α and IL-6 (Peprotech) were used for migration assays. Lymphoma cells were placed in B-cell medium containing 2.5% FBS for 2 h. Lymphoma cells (250,000) resuspended in low-serum B-cell medium were added to the upper chamber of 24-well Transwell inserts (5-mum pore size, Millipore), and 100ng/mL SDF-1α or 10ng/mL IL-6 was added to the lower chamber. The percentage of lymphoma cells that migrated to the lower chamber was quantified after 5 h by flow cytometry on a BD Bioscience FACS Scan machine.

***In vivo* inhibition of endothelial cell function**

All mice were purchased from Jackson Laboratory. Vatalanib was purchased from LC labs. Vatalanib was dissolved in water with 3% DMSO.

Immunoflourescence

Endothelial cells were fixed in 4% paraformaldeyde at 37°C for 10 minutes. Cells were then chilled on ice for 1 minute and then fixed in 90% ice cold methanol for 30 minutes. Endothelial cells were then washed twice in 10% FBS /PBS, cytospun onto glass slides and allowed to dry overnight. Samples were blocked for 1 hour in 5% goat serum/PBS at room temperature. Samples

were then incubated overnight at 4°C using an anti-phospho-p38 antibody (Clone

3D7 Rabbit anti-mouse 1:50 Cell Signaling). Cells were then stained with

Alexaflour 488 secondary antibody (donkey anti-rabbit 1:3000 Invitrogen) for 60

minutes at room temperature, prior to incubation in 0.3ug/mL DAPI for 20

minutes. Images were collected on an Axioplan2 (Zeiss) microscope equipped

with Openlab software from Improvision.

Clonogenic survival assay

To address clonogenic survival, 400,00 Focus HCC cells were plated in a

6 well plate. Cells were untreated, treated with 90nM doxorubicin, 6μM Ag490

mCF$_3$ or both. After 24 hours of treatment, cells were washed three times with

growth media and three times with PBS, trypsinized and re-plated at a

concentration of 100,000 cells/10cm^2 culture dish. For Ag490 mCF$_3$ treated cells,

fresh Ag490 mCF$_3$ was added for an additional 24 hours, at which point the

growth media was changed. After 10 days cells were fixed and surviving colonies

were stained with 0.1% crystal violet (Sigma-Aldrich).

Histological analysis and β-galactosidase activity staining.

Formalin fixed, paraffin-embedded tissue sections were stained with

hematoxylin and eosin for routine examination. Detection of SA-β-galactosidase

activity *in vivo* was performed as described previously (78). Briefly, frozen

sections of mouse lymphoid tissue or sorted endothelial cells were fixed with

0.5% gluteraldehyde in PBS for 15 min, washed with PBS supplemented with 1

mM MgCl$_2$, and stained for 5 hours in pH 5.5 PBS containing 1 mM MgCl$_2$,

1mg/ml X-Gal, and 5 mM each of potassium ferricyanide II and potassium

ferrocyanide III. Images were collected on an Axioplan2 (Zeiss) microscope

equipped with Openlab software from Improvision.

shRNA constructs

shRNA constructs were designed and cloned as previously described

(86). The hairpin targeting sequence for Bcl-XL is

AGGAGAGCGTTCAGTGATCTAA.

Protein analysis

Protein lysates were run on a 12% SDS-PAGE gel, transferred to PVDF

(Millipore) and detected with the following antibodies: anti-γH2AX (monoclonal

clone JBW301, 1:1000; Upstate/Millipore), anti-Bcl-XL (monoclonal clone 4/Bcl-

XL 1:1000 BD Bioscience) and anti-vinculin (V9131 1:10,000; Sigma). Secondary

antibodies were horseradish peroxidase-conjugated anti-mouse/rabbit/human

IgG (GE Healthcare; 1:5,000).

Statistical analysis

Statistical analysis was performed using GraphPad Prism4 software. Two-

tailed Student's t-tests were used, as indicated. Error bars represent mean +/-

standard error of the mean. For comparison of survival curves, a Kaplan-Meier

test was used.

Acknowledgments

Chapter 3:

DNA damage induces distinct acute and senescence-associated secretory phenotypes in a context-specific manner

Luke A. Gilbert[1] and Michael T. Hemann[1*]

[1] The Koch Institute for Integrative Cancer Research at MIT, Massachusetts Institute of Technology, Cambridge, MA 02139

Abstract

Cancer therapy occurs in the context of a tissue with cancer cells surrounded by a diverse complement of normal cells. How DNA damage induced in normal cells modulates response to therapy is unclear. Recently it has been observed that DNA damage induces a secretory program in both cancer cells and normal cells. Here, we see that DNA damage actually induces two distinct secretory responses. The acute secretory response is dynamic and is required for tissue repair and cellular survival, while the senescence-associated secretory phenotype (SASP) is delayed and is required for the clearance of damaged cells. These two secretory responses differ kinetically, mechanistically and functionally suggesting they are distinct processes. We also show that DNA damage can

activate the unfolded protein response (UPR), an ancient stress response pathway. Once fully activated, the UPR represses both the SASP and senescence. This suggests there may be a balance between survival at a cellular level and tumor suppression at an organismal level.

Introduction

Systemic chemotherapy induces damage in both tumor cells and normal cells. Tumor cells are inherently more sensitive to cell death induced by damage due to increased cell proliferation or oncogenic stress (196). This clinical reality provides a therapeutic window for conventional cytotoxic chemotherapeutic agents. Clinically, it is widely appreciated that chemotherapy also induces normal cell death. In one example of this, modern chemotherapeutic regimens have been designed to avoid overlapping organ-specific toxicity (197). Thus, it has been known for many years that chemotherapy induces stress in normal cells and tissues.

While mammals have not evolved to survive damage associated with cancer therapy, all metazoans have evolved to survive tissue injury and infection (198). During inflammation associated with sterile injury or infection, various cell types release context-specific soluble factors required for tissue repair (137). Here, activation of cells of the innate immune system, fibroblasts, epithelial cells, and endothelial cells are important in the repair process (199). It has been shown that the resolution of inflammation is as important for tissue repair as is the

induction of inflammation (200). Here, the failure to resolve inflammation leads to fibrosis; tissue destruction and can lead to tumor development (201,202).

Recently, it has been realized that in normal fibroblasts, epithelial and endothelial cells, DNA damage induces the production of a secretory response *in vitro* and *in vivo* (142,203). Mechanistically, DNA damage activates NFκB or p38α MAP kinase resulting in the secretion of many proteins including IL-6 (203,204). These secretory phenotypes have been shown to promote resistance to chemotherapy, tumor metastasis and primary tumor growth (142,203,205). DNA damage can also induce secretory responses in cancer cells (124,203). Thus, chemotherapy remodels the tumor microenvironment by inducing secretory phenotypes in both cancer cells and normal cells.

It is unclear whether all DNA-damage-mediated secretory phenotypes are the same. In both cancer cells and normal cells, DNA damage induces apoptosis, cell cycle arrest, and senescence. The onset of senescence has been shown to be associated with a complex secretory phenotype (140-143). The senescence-associated secretory phenotype (SASP) occurs following the onset of classic markers of senescence including β-galactosidase activity, heterochromatic nuclear foci, and the induction of p16, p53, and p21. This process requires 5-7 days to occur. Whether this process occurs *in vivo* is unclear. Other models have shown that damaged senescent cells activate a secretory phenotype that induces the recruitment of cells of the innate immune system resulting in the clearance of

senescent cells (149). In contrast, we have observed a secretory phenotype induced by DNA damage that occurs rapidly following therapy. The acute secretory associated phenotype (ASAP) occurs both *in vivo* and *in vitro* within 18 hours. Thus, these two secretory phenotypes differ significantly in the kinetics of activation. Previous work has shown that while both the ASAP and SASP require p38α activation these two secretory phenotypes differ in their requirement for ATM signaling following DNA damage. Thus, it remains unclear how these two secretory processes are related.

Here, we have investigated how the ASAP and SASP are regulated and related. We see that both *in vivo* and *in vitro*, DNA damage induces an acute secretory phenotype in endothelial cells. This secretory process is dynamic and is resolved within 72 hours. We find that endothelial cells undergo senescence but find no evidence for the SASP. Mechanistically we find that the ASAP is NFκB-independent while the SASP critically relies on NFκB signaling. In addition, we see that DNA damage acutely induces the unfolded protein response. Interestingly, the unfolded protein response restrains the SASP but not the ASAP, suggesting the ASAP may be a physiologically normal process. Thus, the SASP and ASAP differ in their regulation and kinetics suggesting they may represent fundamentally distinct processes.

Results

DNA damage transiently induces IL-6 release in endothelial cells

We had previously shown that IL-6 secretion is acutely induced in the thymus following administration of doxorubicin to mice (203). In the thymus, endothelial cells secrete IL-6. To more closely examine the dynamics of IL-6 release following DNA damage in the thymus, we derived conditioned media from the thymus of mice at different intervals following doxorubicin treatment. Six to 8 week-old female mice were treated with the maximally tolerated dose of doxorubicin. 18 hours, 4 and 8 days later we measured the level of IL-6 in the thymus of untreated and doxorubicin-treated mice by ELISA. Here, as previously published, IL-6 is induced in the thymus acutely following treatment with doxorubicin. Interestingly, 4 or 8 days following treatment, the amount of IL-6 in the thymus is reduced below basal physiologic levels (Figure 1A). Thus, IL-6 induction is transient, suggesting active regulation of IL-6 secretion or clearance of IL-6-producing endothelial cells.
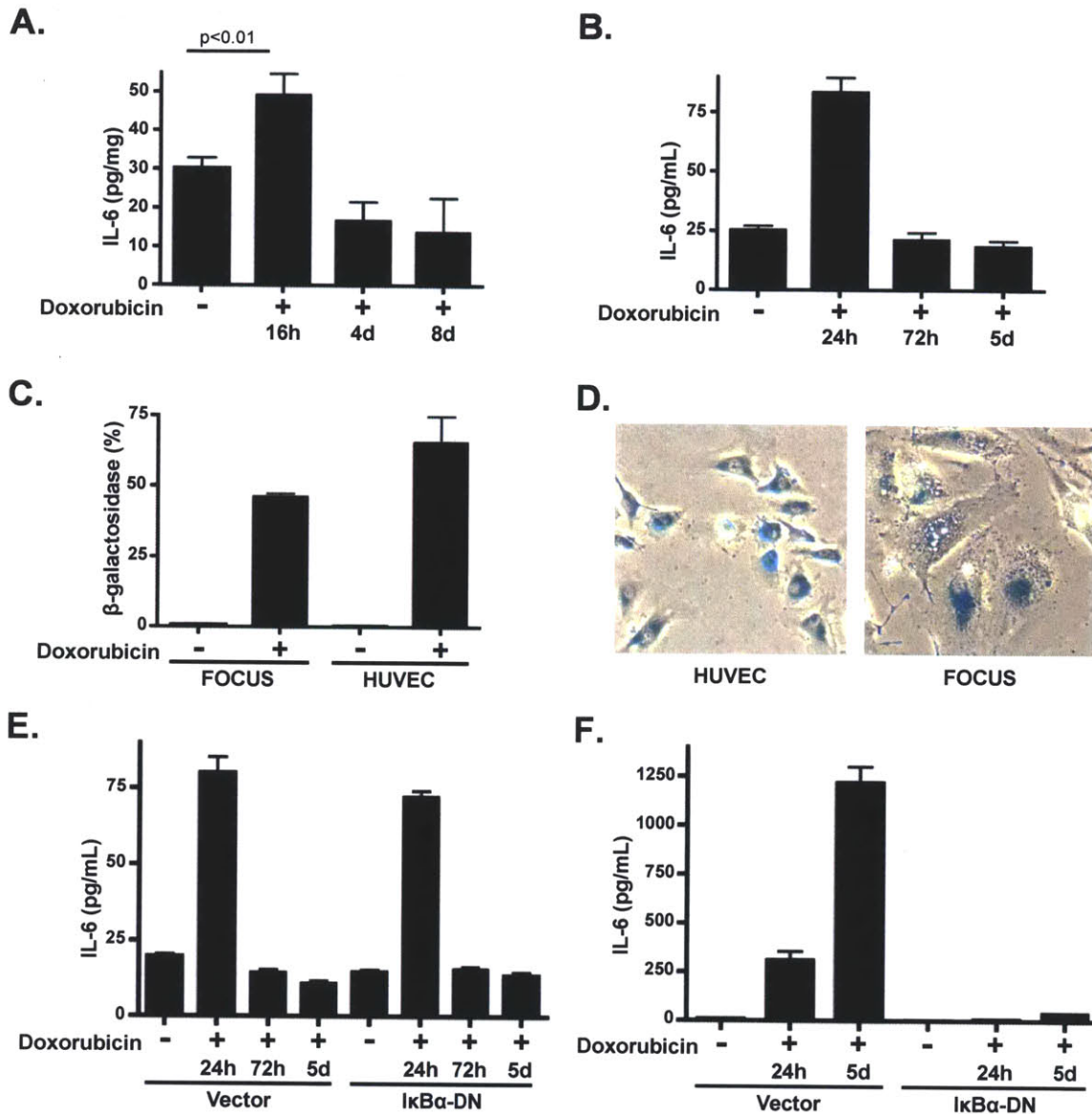
Figure 1. DNA damage induces acute IL-6 release from endothelial cells independent of NFκB activation. (A) Quantification of IL-6 levels in conditioned media from the thymus or lymph nodes of untreated mice (n=10) or mice treated for 18 hours with 10mg/kg doxorubicin (n≥3). Values were normalized by tissue weight. The data are represented as mean +/- SEM. **(B)** A graph showing the amount of IL-6 present in conditioned media from untreated and doxorubicin treated human vein endothelial cells (HUVECs). The data are represented as mean +/- STDEV (n≥6). **(C)** β-galactosidase staining and quantification of β-galactosidase staining in HUVEC and FOCUS cells. Cells were fixed untreated or at 6 days following doxorubicin-induced DNA damage. The data are represented as mean +/- SEM. **(D)** β-galactosidase staining of HUVEC and FOCUS cells at 6 days following doxorubicin-induced DNA damage. Representative fields are shown at 20x magnification. **(E)** A graph showing the amount of IL-6 present in conditioned media from HUVECS expressing a vector control or an IκBα

dominant negative allele either untreated or treated with doxorubicin. The data are represented as mean +/- SEM (n=3). **(F)** A graph showing the amount of IL-6 present in conditioned media from HUVECS expressing a vector control or an IκBα dominant negative allele either untreated or treated with doxorubicin. The data are represented as mean +/- SEM (n=3).

DNA damage also induces acute IL-6 release in human vein endothelial cells (HUVEC) *in vitro*. To ask whether IL-6 release is also transient *in vitro,* HUVECs were treated with doxorubicin for 24, 72 hours or 5 days. We collected IL-6 in conditioned media for each time point for only 24 hours. The amount of secreted IL-6 was then measured by ELISA. As shown previously, doxorubicin acutely induces a three-fold increase in the amount of secreted IL-6. In contrast, IL-6 secretion had returned to basal levels at later time points (Figure 1B). This is not merely a consequence of cell killing as the IL-6 concentration at each time point was normalized to the number of cells present at the end of the assay. Thus, *in vivo* and *in vitro*, endothelial cells acutely and transiently release IL-6 in response to DNA damage. We have termed this process the acute secretory associated phenotype (ASAP).

IL-6 release is not a hallmark of senescence induced by DNA damage

Recent work has shown that DNA damage can induce a senescence-associated secretory phenotype (SASP) the timing of which coincides with the acquisition of classic markers of senescence including β-galactosidase staining, p21, and p16 accumulation, and senescence-associated heterochromatic foci (142). The SASP prominently features IL-6. To ask whether our endothelial ASAP is similar to or different from the SASP, we sought to re-capitulate the

SASP. We asked whether HUVECs and a control cancer cell line, FOCUS cells, senesce following the administration of doxorubicin. HUVECs and FOCUS cells were treated with doxorubicin and 6 days later fixed and stained for senescence-associated β-galactosidase activity. Both cell types exhibited strong β-galactosidase staining indicative of senescence (Figure 1C-D). While the endothelial cells stain β-galactosidase-positive, they assume a less classic "fried egg" senescent cell morphology and do not exhibit significant cytoplasmic expansion, nuclear abnormality, or a highly vacuolated cytoplasm (Figure 1D).

To further understand the SASP and ASAP, we asked whether FOCUS cells, a liver cancer cell line, underwent a SASP-like process using IL-6 release as a proxy. We had previously shown these cells secrete IL-6 in response to DNA damage. FOCUS cells were treated with doxorubicin and conditioned media were collected as before. As described previously, doxorubicin induces the acute release of IL-6 from FOCUS cells. However, this IL-6 release is significantly less than that which is secreted by these cells at the onset of senescence (Supplemental Figure 1). Thus, FOCUS cells release very large amounts of IL-6 at the onset of senescence while endothelial cells do not.
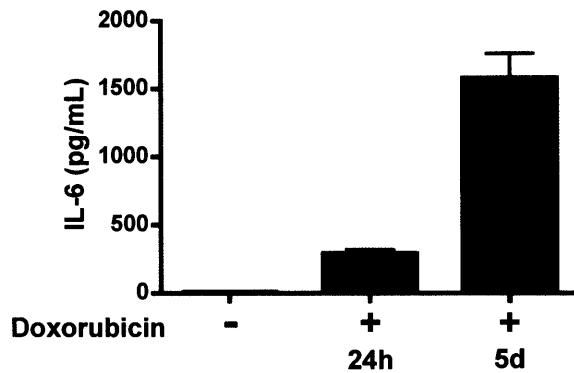
Supplemental Figure 1. IL-6 is secreted acutely and at senescence in FOCUS cells. A graph showing the amount of IL-6 present in conditioned media from untreated and doxorubicin treated FOCUS cells. The data are represented as mean +/- STDEV (n≥6).

IL-6 release from endothelial cells is independent of NFκB

NFκB activation is required for cytokine release in diverse settings including the SASP and in sterile induction of the inflammasome (85,206). To ask if endothelial cells require activation of NFκB for IL-6 release following DNA damage, we infected HUVECs with a vector control or a non-phosphorylatable dominant negative form of IκBα (IκBα-DN). HUVECs were treated with doxorubicin and conditioned media were collected after 24, 72 hours, and 5 days. We see no differences in IL-6 induction following treatment with doxorubicin in HUVEC expressing IκBα-DN compared to the control, strongly suggesting that activation of NFκB is not required for the ASAP (Figure 1E). We see the same results treating HUVEC with doxorubicin and the NFκB inhibitor BAY 11-7085 (Data not shown). In contrast, FOCUS cells require NFκB activity for all forms of IL-6 secretion (Figure 1F).

Endothelial cells do not undergo a SASP

To more formally address whether endothelial cells undergo a SASP-like process, we used a quantitative bead-based ELISA assay to measure the secretion of 65 cytokines, chemokines, and growth factors following doxorubicin treatment. HUVECs treated with doxorubicin for 24 hours or 5 days. Conditioned media were collected for 24 hours for each time point and subjected to analysis. Here, we see acute up-regulation of FLT-3 ligand, Fractalkine, G-CSF, GM-CSF, IL-6, MCP1, PDGF-A, PDGF-B and VEGF (Figure 2A). However, we see no evidence for a pattern indicating a delayed general up-regulation of cytokine secretion indicative of the SASP at senescence. As a control, we performed the same experiment using FOCUS cells. In the FOCUS cells we observe the induction of a potent SASP at the onset of senescence (Figure 2B). Importantly, the lack of a SASP in endothelial cells can not be explained by an inability to up-regulate secreted factors at senescence, as one factor PDGF-B is up-regulated by 3-fold acutely following administration of doxorubicin but 100-fold upon senescence (Supplemental Figure 2).
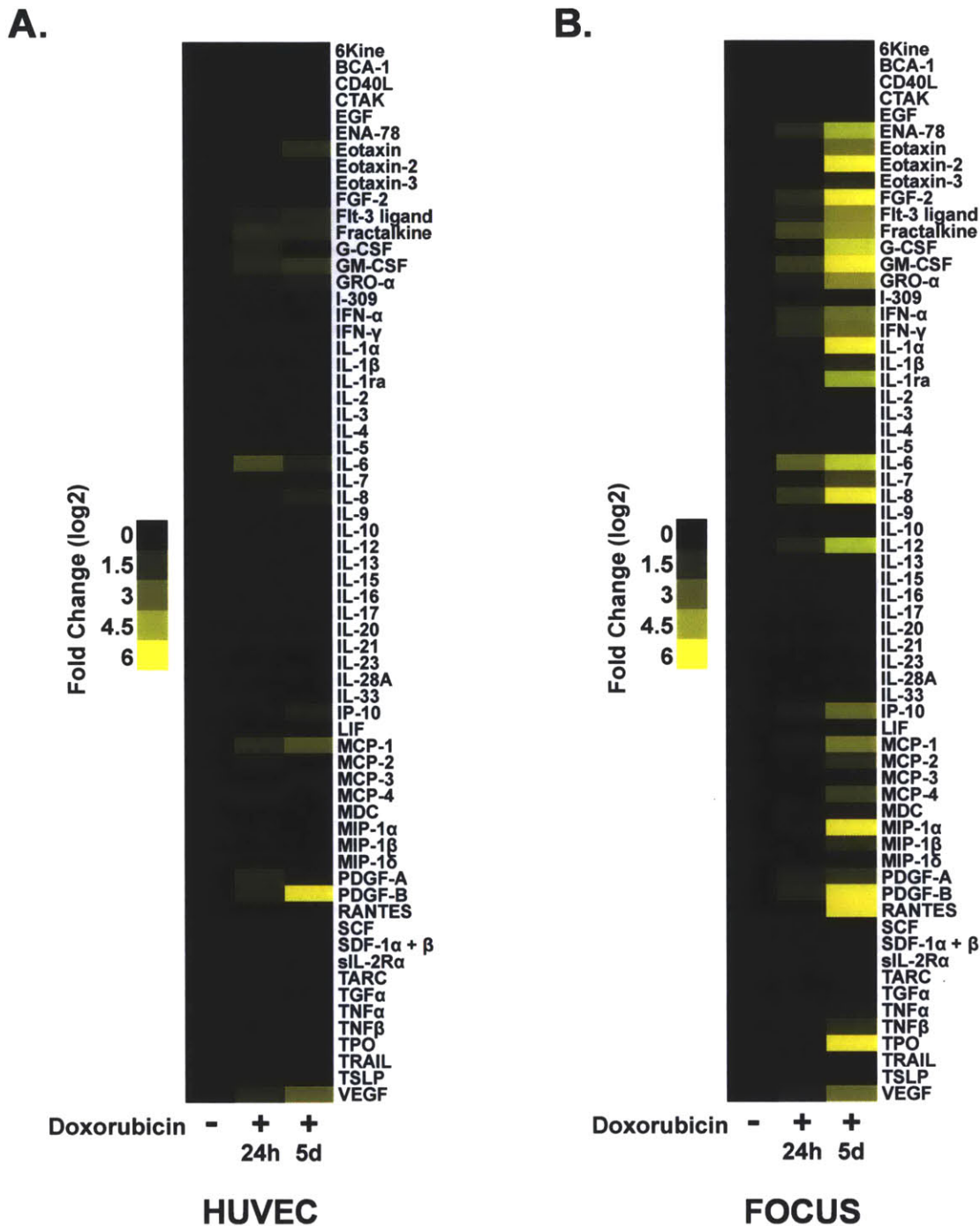
Figure 2. The ASAP and SASP are temporally distinct. (A) A heat map displaying the relative concentration of 65 growth factors, cytokines and chemokines secreted by HUVECs untreated or treated with doxorubicin. The data are displayed as $\log_2$ of the fold change comparing doxorubicin-treated cells over untreated cells (n=3). **(B)** A heat map displaying the relative concentrations of 65 growth factors, cytokines and chemokines secreted by FOCUS cells untreated or treated with doxorubicin. The data are displayed as $\log_2$ of the fold change comparing doxorubicin-treated cells over untreated cells (n=3).

93
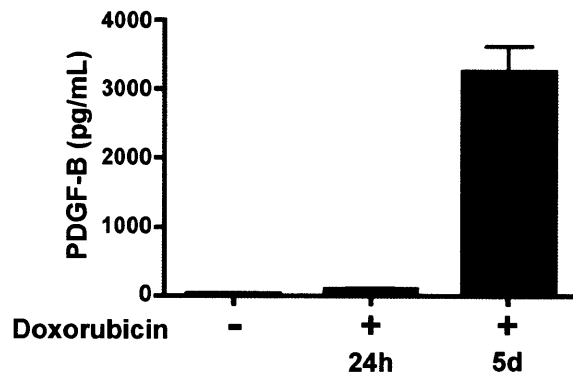
Supplemental Figure 2. PDGF-B is secreted acutely and at senescence in endothelial cells. A graph showing the amount of PDGF-B present in conditioned media from untreated and doxorubicin-treated HUVECs. The data are represented as mean +/- SEM (n=3).

## The unfolded protein response is activated following DNA damage

While the SASP and the ASAP differ mechanistically in a number of signaling pathways, one physical aspect that distinguishes them quantitatively is the magnitude of the secretory response. In normal cell types that have high levels of protein secretion, such as exocrine cells and B cells, the unfolded protein response (UPR) is activated (207-209). We reasoned that very high levels of protein secretion associated with the SASP but not ASAP might activate the unfolded protein response at senescence. To test this hypothesis, we measured XBP1 activation in FOCUS and HUVECs treated with doxorubicin over a time course of 6 days. XBP1 is normally expressed as a mature mRNA containing an intron. This mRNA is not translated until IRE1, a nuclease, is activated during the unfolded protein response resulting in XBP1 splicing and translation. Surprisingly, we see that DNA damage induces XBP1 splicing within

48 hours in both FOCUS and HUVEC cells (Figure 3A-B). This timing suggests

that the unfolded protein response is activated prior to the onset of senescence

or the SASP. Importantly, doxorubicin is a specific topoisomerase II poison which

induces DNA double-strand breaks, strongly suggesting that induction of the

UPR is not due to damage in the endoplasmic reticulum.
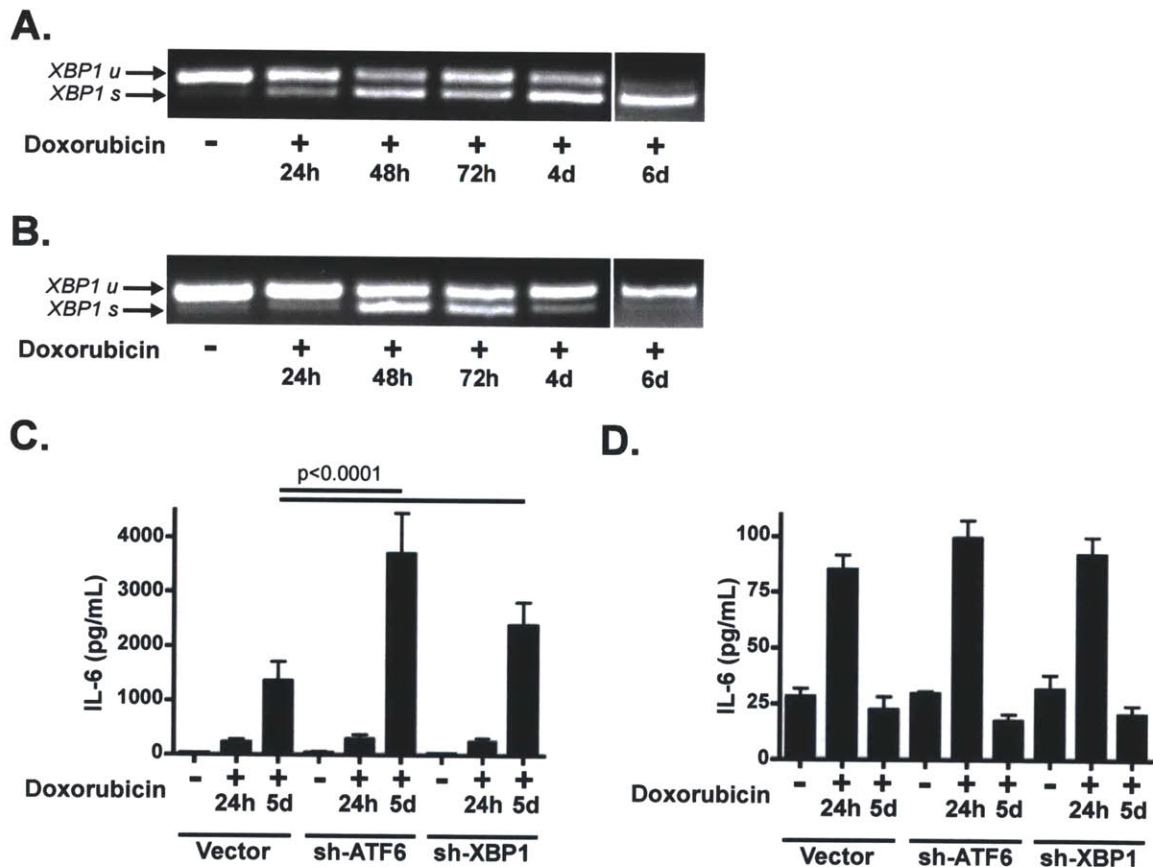
Figure 3. The unfolded protein response is induced by DNA damage. (A) Total RNA from FOCUS cells untreated or treated with doxorubicin for 1-6 days was used for RT-PCR analysis. Primers spanning the splice junction of murine XBP1 were used to amplify products of un-spliced and spliced mRNA. PCR products were separated by electrophoresis on a 3% agarose gel and visualized by ethidium bromide staining. **(B)** Total RNA from HUVECs untreated or treated with doxorubicin for 1-6 days was used for RT-PCR analysis. Primers spanning the splice junction of murine XBP1 were used to amplify products of un-spliced and spliced mRNA. PCR products were separated by electrophoresis on a 3% agarose and visualized by ethidium bromide staining. **(C)** A graph showing the

amount of IL-6 present in conditioned media from FOCUS cells expressing a vector control or shRNAs targeting ATF6 or XBP1. Cells were untreated or treated with doxorubicin. The data are represented as mean +/- STDEV (n≥5). **(D)** A graph showing the amount of IL-6 present in conditioned media from HUVEC cells expressing a vector control or shRNAs targeting ATF6 or XBP1. Cells were untreated or treated with doxorubicin. The data are represented as mean +/- STDEV (n=6).

Here we do see a major distinction between FOCUS, which undergo a SASP, and HUVEC, which do not, in the resolution of unfolded protein stress and XBP1 splicing. FOCUS cells continue to accumulate an increasing ratio of spliced to un-spliced XBP1 such that at the onset of the SASP, nearly all of the XBP1 present is spliced. Thus, at the onset of the SASP, FOCUS cells undergo very high levels of UPR stress (Figure 3A). In contrast, in endothelial cells we see acute activation and then resolution of XBP1 splicing at later time points. This suggests that senescence does not induce the UPR but the SASP does (Figure 3B).

To determine whether the UPR functionally modulates secretory phenotypes, we generated shRNAs to both XBP1 and ATF6, two main branches of the mammalian UPR. Here, FOCUS cells expressing a vector control, shATF6 or shXBP1 were treated with doxorubicin for 24 hours or 5 days. We see that suppression of ATF6 or XBP1 has no effect on IL-6 release basally or at 24 hours. In contrast, we see that suppression of either ATF6 or XBP1 results in much higher levels of secreted IL-6 upon senescence (Figure 3C). This suggests that activation of both of these branches of the UPR reduces the secretory response associated with senescence. We also performed this same experiment

in endothelial cells. Here we see that suppression of ATF6 or XBP1 has no effect

on IL-6 secretion basally, acutely or at senescence (Figure 3D). This suggests

that while the UPR is activated in endothelial cells it does not functionally

modulate IL-6 release. A future goal of this project is to interrogate how the UPR

is rapidly activated in both endothelial and cancer cells following DNA damage. It

is also unclear why the UPR is activated before it functionally restrains a

secretory phenotype.

The UPR represses senescence through the SASP

To more broadly measure whether the UPR represses the entire SASP,

conditioned media from FOCUS cells expressing a vector control or shATF6

were collected from untreated cells or cells treated with doxorubicin for 24 hours

or 5 days. Soluble factors present in these conditioned media were analyzed

using a quantitative bead-based ELISA assay. We see no major differences

between control and shATF6 FOCUS cells acutely following damage or at a

basal level. In contrast, we see that suppression of ATF6 results in increased

secretion of many factors upon senescence. This suggests that ATF6 and the

UPR repress the SASP (Figure 4A).

A.

6Kine
BCA-1
CD40L
CTAK
EGF
ENA-78
Eotaxin
Eotaxin-2
Eotaxin-3
FGF-2
Flt-3 ligand
Fractalkine
G-CSF
GM-CSF
GRO-α
I-309
IFN-α
IFN-γ
IL-1α
IL-1β
IL-1ra
IL-2
IL-3
IL-4
IL-5
IL-6
IL-7
IL-8
IL-9
IL-10
IL-12
IL-13
IL-15
IL-16
IL-17
IL-20
IL-21
IL-23
IL-28A
IL-33
IP-10
LIF
MCP-1
MCP-2
MCP-3
MCP-4
MDC
MIP-1α
MIP-1β
MIP-1δ
PDGF-A
PDGF-B
RANTES
SCF
SDF-1α + β
sIL-2Rα
TARC
TGFα
TNFα
TNFβ
TPO
TRAIL
TSLP
VEGF

Fold Change (log2)
-3
-2.25
-1.5
-0.75
0
0.75
1.5
2.25
3

Doxorubicin   −   +   +
24h 5d

FOCUS cells
sh-ATF6/Vector

Figure 4. The unfolded protein response restrains the SASP and senescence. (A) A heat map displaying the relative change in concentrations of 65 growth factors, cytokines and chemokines secreted by FOCUS cells expressing sh-ATF6 or a vector control, untreated or treated with doxorubicin. The data are displayed as log$_2$ of the fold change comparing sh-ATF6 FOCUS cells over vector control FOCUS cells (n=3). **(B)** β-galactosidase staining and quantification of β-galactosidase staining in FOCUS cells, expressing a vector control, sh-ATF6 or sh-XBP1. Cells were fixed untreated or at 6 days following doxorubicin-induced DNA damage. The data are represented as mean +/- SEM. **(C)** β-galactosidase staining of FOCUS cells expressing a vector control or sh-ATF6. Cells were fixed untreated or at 6 days following doxorubicin-induced DNA

98

damage. Representative fields are shown at 20x magnification. **(D)** A colony-formation assay showing FOCUS cells expressing a vector control, sh-ATF6 or sh-XBP1. FOCUS cells were treated with doxorubicin as indicated. Results are representative of 3 independent experiments.

Previous reports suggested that two SASP factors, IL-6 and IL-8, are autocrine tumor suppressors during oncogene-induced senescence. To test whether the SASP can promote DNA-damage-mediated senescence in cancer cells, we utilized the fact that suppression of ATF6 or XBP1 in FOCUS cells increases the SASP compared to vector control cells. We treated shATF6 and shXBP1 or vector control FOCUS cells with a low dose of doxorubicin and measured the amount of senescence 6 days later. Here, we see a significant increase in the percentage of β-galactosidase-positive cells following suppression of either ATF6 or XBP1 (Figure 4B). Escape from senescence was clearly increased in the vector controls where clonal populations of growing cells could be seen adjacent to senescent cells (Figure 4C and data not shown). Using a colony formation assay to measure escape from senescence, we see that suppression of ATF6 or XBP1 promotes the re-enforcement of senescence (Figure 4D). These data suggest that the UPR represses the SASP and functionally reduces senescence following DNA damage.

Discussion

DNA damage induces cell-intrinsic changes such as cell death, cell-cycle arrest, and senescence. Recently, it has also been shown that DNA damage can indirectly function as a paracrine effector. Here, DNA damage induces the activation of secretory phenotypes that have diverse effects on various cell types

99

including the induction of cell migration, activation of the immune system, and the induction of local pro-survival microenvironments. We see that depending on the cellular context DNA damage induces two distinct secretory phenotypes. These secretory phenotypes differ in their functions, their timing, and their molecular mechanism.

The acute secretory response in endothelial cells is dynamic. We see, both *in vitro* and *in vivo,* this response is rapidly activated and then shut off. The kinetics of such a response are consistent with normal inflammatory processes. This rapid activation is a key temporal requirement for survival factors. Survival factors must pre-exist or be induced rapidly following DNA damage as the DNA-damage-induced cellular life/death decision process generally occurs within 48 hours of damage. Here, we see induction of the ASAP in endothelial cells by 18 hours following the administration of doxorubicin. This suggests that kinetically the acute secretory phenotype could function as a survival process *in vivo*.

In contrast, the senescence-associated secretory phenotype is primarily a tumor suppressor mechanism. Senescence induces up-regulation of natural killer cell ligands and the SASP. Together this process recruits and activates the innate immune system resulting in the rapid clearance of damaged senescent cells (149,150). This process is suggested to be important in clearing pre-neoplastic cells. Importantly, the SASP begins at 6-8 days following the induction of senescence both *in vivo* and *in vitro*. The induction of the SASP is significantly

delayed relative to secretory processes with described roles in tissue repair (210-216). Here diverse models of tissue injury including excisional wounds, GI syndrome induced by radiation, chemical ablation of the bone marrow, ischemia, or surgical ablation of the liver or lung show induction of many factors including EPO, FGF2, GM-CSF, HGF, IL-6, MIP1α, MMP9, MMP14, SDF1α, sKitL, Wnt-2. The common feature in each of these models is that the induction of proteins involved in tissue repair occurs between 12 and 72 hours following injury and then decreases rapidly as repair occurs. In contrast, in senescent cells the SASP continues to increase in magnitude over time. Here the SASP doubles in magnitude between 6 and 10 days following the induction of senescence by DNA damage (144). In some settings it may be that the SASP is involved not in tissue repair but in the resolution of tissue-repair processes, as tissue repair can lead to fibrosis if unchecked. Here, in a model of liver injury, clearance of senescent hepatic stellate cells by natural killer cells reduces fibrosis (150). Thus the SASP and ASAP are distinct DNA-damage-induced secretory responses and their function as a damage response *in vivo* may be distinct.

The unfolded protein response is an ancient stress response pathway present in all eukaryotes. This pathway is activated by dysfunction in the endoplasmic reticulum, which can result from protein misfolding, toxic compounds, or improper post-translational processing. Here we see that DNA damage acutely activates XBP1 splicing and the UPR. How this occurs is an active area of research. We see that senescence does not activate the UPR but

the SASP does. Thus the UPR seems to be activated by both an acute process related to DNA damage and the SASP however this acute activation of the UPR does not seem to affect the ASAP. Whether the UPR is induced by DNA damage *in vivo* is also unclear. In *Caenorhabditis elegans* the UPR functions to balance the activation of an innate secretory immune response with basal ER homeostasis (217,218). This suggests there is a conserved role for the UPR in balancing metazoan secretory phenotypes induced by stress and ER homeostasis.

Experimental Procedures

Cell culture and chemicals

FOCUS cells were cultured in 45%DMEM/45% IMDM/10% FBS, supplemented with 2mM L-glutamine and 5µM β-mercaptoethanol. HUVEC cells were cultured in Endothelial Cell Growth Medium 2 (Lonza). Doxorubicin was purchased from Tocris Bioscience.

Conditioned media and drug treatments

Conditioned media was made from the thymus of individual mice 18 hours after doxorubicin treatment. All tissues were dissociated manually in FOCUS cell media. Soluble factors in the thymus were allowed to conditioned media for 6 hours at 37°C. All conditioned medias were cleared of tissue and cells by centrifugation. Conditioned medias for HUVEC and FOCUS cell experiments were made by collecting the secreted proteins for each time point for 24 hours

from 50,000 or 150,000 cells seeded into 24 well or 6 well plates respectively. Endothelial cells were untreated or treated with 200nM doxorubicin. FOCUS cells were untreated or treated with 200nM doxorubicin for 24 hour time points or 50-100nM for 5 day time points. The media was changed after 24 hours for the 5 day FOCUS cell experiments.

ELISA and Luminex Cytokine Measurements

All values shown for ELISAs and cytokine arrays are normalized to the weight of the dissected tissue or the number cells at the end of the assay. IL-6 ELISA kits were purchased from eBioscience. Multiplexed luminex assays for growth factor, chemokine and cytokine levels were preformed as described by the manufacturer by Eve Technologies.

β-galactosidase activity staining

Detection of SA-β-galactosidase activity was performed as described previously. Briefly, cells were fixed with 0.5% gluteraldehyde in PBS for 15 min, washed with PBS supplemented with 1mM $MgCl_2$, and stained for 5 hours in pH 5.5 PBS containing 1mM $MgCl_2$, 1mg/ml X-Gal, and 5mM each of potassium ferricyanide II and potassium ferrocyanide III. Images were collected on an Axioplan2 (Zeiss) microscope equipped with Openlab software from Improvision.

XBP1 splicing assay

Total mRNA was isolated from cells using Qiashredder and RNeasy kits from Qiagen. cDNA was made from 100ng or 1μg of RNA using random

hexamers and M-MLV reverse transcriptase from Invitrogen. The XBP1 PCR was preformed as previously described (207).

shRNA constructs

shRNA constructs were designed and cloned as previously described (86). The hairpin targeting sequence for shATF6 is AAGGAGTTGGATTTGTCTTCT. The hairpin targeting sequence for shXBP1 is CCAGCAAGTGGTAGATTTAGA.

Clonogenic survival assay

To address clonogenic survival, 100,000 Focus HCC cells were plated in a $10cm^2$ well plate. Cells were treated with 50-100nM doxorubicin. After 24 hours of treatment, the media was changed to remove the doxorubicin. After 8-10 days cells were fixed and surviving colonies were stained with 0.1% crystal violet (Sigma-Aldrich).

Statistical Analysis

Statistical analysis was performed using GraphPad Prism4 software. Two-tailed Student's t tests were used, as indicated. Error bars represent mean ± SEM or STDEV as noted.

Chapter 4:

BCL-2 family genetic profiling reveals microenvironment-specific determinants of chemotherapeutic response

Justin R. Pritchard*[1], Luke A. Gilbert*[1], Corbin E. Meacham[1], Jennifer L. Ricks[1], Hai Jiang[1] Douglas A. Lauffenburger[1,2], and Michael T. Hemann[1]

[1] The Koch Institute for Integrative Cancer Research at MIT, [2] Department of Biological Engineering, Massachusetts Institute of Technology, Cambridge, MA 02139

* these authors contributed equally to this work

Abstract

The Bcl-2 family represents a diverse set of pro and anti-apoptotic factors that are dynamically activated in response to a variety of cell-intrinsic and extrinsic stimuli. While *in vitro* experiments have identified growth factor-, cytokine-, and drug-dependent effects on utilization of BCL-2 family members, *in vivo* studies have typically focused on the role of one or two particular members in development and organ homeostasis. Thus, the ability of complex physiologically relevant contexts to modulate canonical dependencies has yet to be systematically investigated. Here, we have developed a pool-based shRNA measurement assay to systematically interrogate the functional dependence of

leukemia and lymphoma cells upon the various BCL-2 family members comprehensively across diverse *in vitro* and *in vivo* settings. Using this approach, we report the first *in vivo* loss-of-function screen for modifiers of response to a frontline chemotherapeutic. Notably, our data reveal an unexpected role for the extrinsic death pathway as a tissue-specific modifier of therapeutic response. Our findings demonstrate that particular sites of tumor dissemination can play critical roles in demarcating cancer-cell vulnerabilities and mechanisms of chemoresistance.

Introduction

Chemotherapy represents a major treatment modality for cancer, and numerous genetic screens have probed the mechanisms underlying cell-intrinsic resistance or sensitivity to front-line chemotherapy (180,219-223). However, these studies, while informative, have not been adapted to relevant tumor microenvironments, which may contain diverse stromal and/or immune cell types, are subject to immune surveillance, and harbor physical barriers to drug delivery (48). Additionally, the native tumor microenvironment comprises a diverse mixture of chemokines and cytokines that may impact responses to genotoxic agents (178,203). Thus, the central determinants of therapeutic outcome may be highly dependent upon paracrine survival or stress signals. Indeed, it is well documented that gene function and relevance can vary dramatically when compared *in vivo* versus *in vitro* (178,179). Consequently, studying the impact of defined genetic alterations on therapeutic response in native tumor

microenvironments is critical for effective drug development, personalized cancer regimens, and the rational design of combination therapies.

Recent advances in the development of tractable mouse models of cancer have, for the first time, enabled the examination of complex sets of defined alterations in individual mice. For example, retroviral infection of murine hematopoietic stem cells or primary embryonic hepatocytes with small pools of short hairpin RNAs (shRNAs), followed by adoptive transfer into lethally, irradiated, recipient mice, has been used to screen for suppressors of B cell lymphomagenesis or hepatocellular carcinoma (79,224). Additionally, *ex vivo* manipulation of lymphoma cells followed by transfer into syngeneic recipient mice has permitted the interrogation of thousands of shRNAs for modulators of tumor growth and dissemination (87). These screens provide powerful proofs of principle that diverse alterations can be introduced in chimeric tumor models *in vivo* and that these systems might permit the simultaneous examination of the relevance of a whole set of genes to therapeutic response in relevant physiological contexts.

Front-line cancer therapies generally exert their effects by modulating the proportion of pro- to anti- apoptotic death regulators, most notably members of the Bcl-2 family (225,226). Thus, we reasoned that interrogating Bcl-2 family functionality might provide a high-resolution focus on a crucial facet of cytotoxic cellular responses to chemotherapy in a variety of distinct settings. Notably,

previous studies using recombinant BH3 peptides in reconstituted mitochondrial suspensions have systematically identified cellular states associated with the loss of function of one of the BH3-only Bcl-2 family members, the loss of function of a multi-domain pro-apoptotic Bcl-2 family member, or the enhanced function of an anti-apoptotic family member; these states characterize the potential range of dysregulation that the Bcl-2 family can acquire during tumorigenesis and demarcate central cell-fate decisions that are susceptible to therapeutic intervention (227,228). However, this approach, while quite powerful, does not allow the comprehensive examination of the role and relevance of individual Bcl-2 family members to cell death following chemotherapy. Here we describe a complementary *in vivo* screening approach that provides a detailed assessment of the role of each Bcl-2 family member in the response to chemotherapy in heterogeneous tumor environments.

Results

A bead-based assay for the direct measurement of pooled shRNA representation

The Bcl-2 family consists of 16 pro- and 6 anti-apoptotic proteins that regulate programmed cell death in response to a diverse set of intrinsic and extrinsic death stimuli (229,230). To assess how these genes modulate chemotherapy-induced cell death across multiple *in vivo* contexts, as well as across diverse *in vitro* conditions in a multiplexed manner, we adapted a validated set of shRNAs targeting all 22 Bcl-2 family members to Luminex bead-

based analysis (Figure 1A and (231)). This technology has previously been used to quantify diverse sets of microRNAs in solution with improved accuracy relative to classic microarray approaches (232). Thus, we reasoned that this approach could be modified to perform reproducible quantification of sub-genome-sized shRNA pools.

Briefly, we covalently coupled an amino-modified oligonucleotide that is the reverse complement of the unique guide-strand section of each shRNA to fluorescently labeled Luminex beads. Our PCR strategy uses a forward primer complementary to the microRNA loop sequence present in all hairpins and a biotinylated reverse primer complementary to the flanking microRNA sequence (Figure 1B). Thus, all shRNA guide strands can be amplified using common primers, and the quantity of individual shRNAs can be visualized with streptavidin-PE after bead hybridization. Notably, this approach is distinct from barcoded shRNA libraries, in which shRNAs are identifiable by a flanking DNA sequence. In this case, we used the unique portion of the shRNA, itself, as the barcode. This allows for multiplexed shRNA quantification in any vector backbone.
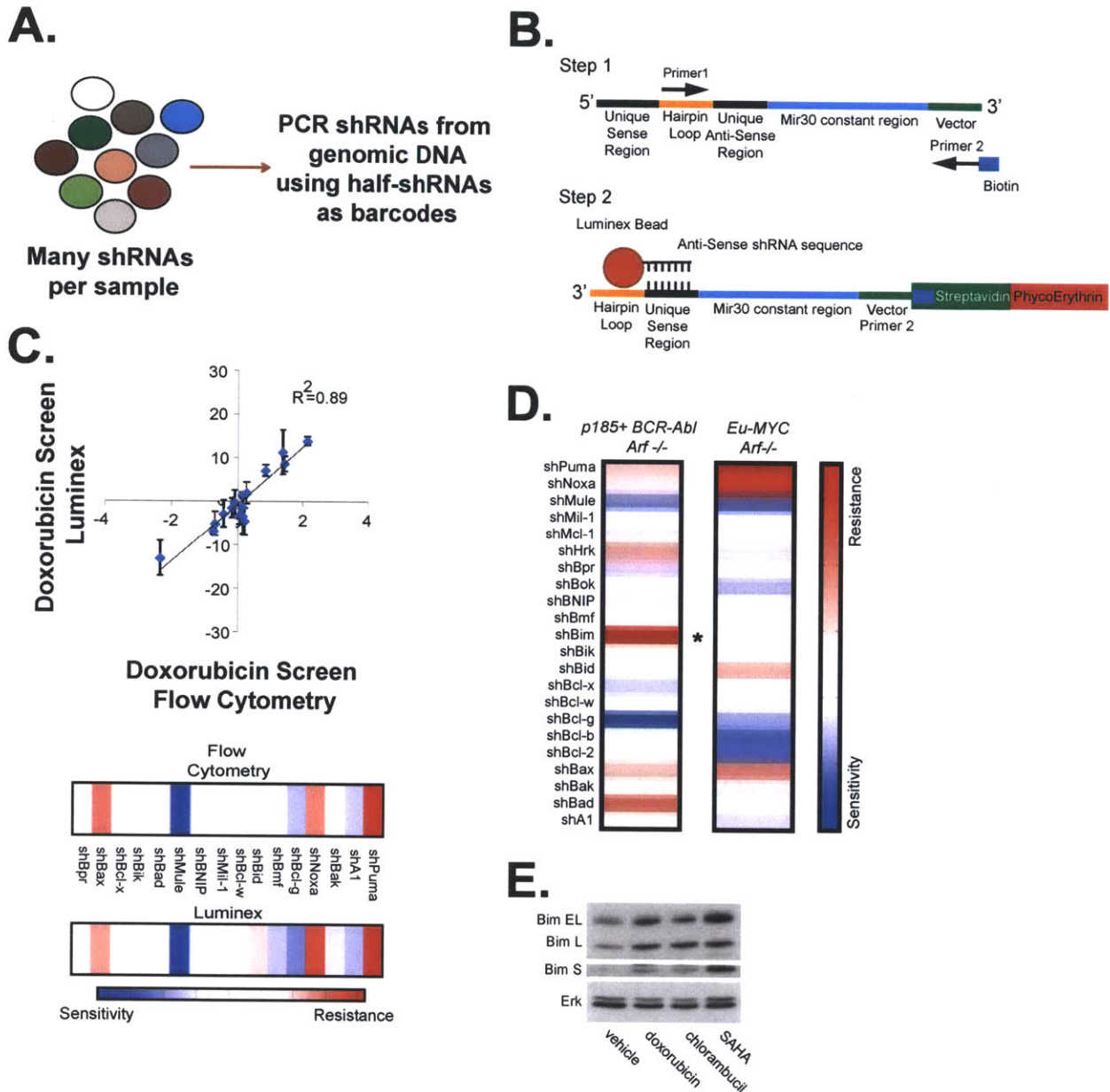
Figure 1. Examining the role of the entire Bcl-2 family in therapeutic response. (A) A schematic depicting the difference between single and pool-based evaluation of shRNA composition. **(B)** A diagram illustrating the Luminex-based shRNA PCR strategy. PCR primers were designed from constant regions flanking all hairpins. After PCR amplification, a biotinylated primer is used to measure hairpin abundance, and the unique fluorescence of the luminex bead distinguishes hairpin identity. **(C)** A comparison of the bead-based quantification of hairpin representation following doxorubicin treatment with single-cell flow cytometry measurements (231). (Left) Bead-based measurements are plotted against each corresponding single-hairpin measurement. (Right) Heat maps comparing shRNA enrichment and depletion using bead-based and flow cytometry approaches. **(D)** A heat map comparing the impact of depleting each

Bcl-2 family hairpin on the response to doxorubicin treatment in $E\mu$-myc $p19^{Arf-/-}$ lymphomas and $p185$ BCR-Abl+ $p19^{Arf-/-}$ B-ALLs. The asterisk demarcates the differential impact of suppressing the BH3-only protein Bim on doxorubicin sensitivity in these two cell types. **(E)** $p185$ BCR-Abl+ $p19^{Arf-/-}$ cells were treated for 12 hrs at an LD90 of the indicated compounds and analyzed for Bim levels by western blot.

As an initial proof-of-principle experiment, we confirmed that each Bcl-2 shRNA could be quantified by Luminex bead hybridization when starting with similar concentrations of dsPCR product (Supplemental Figure 1A). Importantly, while each PCR product with a cognate bead was readily detectable, a control probe exhibited no significant signal with any of the 22 shRNAs in the plasmid library. In fact, the average maximum signal for an shRNA present in the pool was approximately 100-fold higher than the control probe signal. While this negative control ruled out any large magnitude non-specific hybridization, we wanted to rule out smaller amounts of cross-hybridization as the source of the variation in the maximum fluorescence intensity of the various probes (Supplemental Figure 1B). To this end, we noted a strong relationship between probe GC content and maximum signal intensity. Oligonucleotides deviating from this relationship were analyzed for local sequence alignments across the entire shRNA library utilizing the dynamic programming method of Smith-Waterman (233). The variation in the average local alignment bit scores for all "outlier" probes was highly similar (Supplemental Figure 1C), indicating that cross-hybridization is an unlikely contributor to overall signal intensity. Thus, oligonucleotide sequences chosen for optimal siRNA performance are well suited for hybridization-based sequence identification.

We next performed mock enrichment experiments in which known concentrations of genomic DNA from single hairpin-infected $E\mu$-myc $p19^{Arf-/-}$ lymphoma cells were combined at distinct ratios (Supplemental Figure 1D). These lymphoma cells were derived from a well-established pre-clinical mouse model of Burkitt's lymphoma and represent a tractable setting to investigate the genetics of therapeutic response (70,97). Using these cells, we observed a linear and highly reproducible change in measured fluorescence intensity that tightly correlated with the known fold enrichment of the control sample across 8-fold changes in relative DNA abundance.

A.

B.

C.

D.
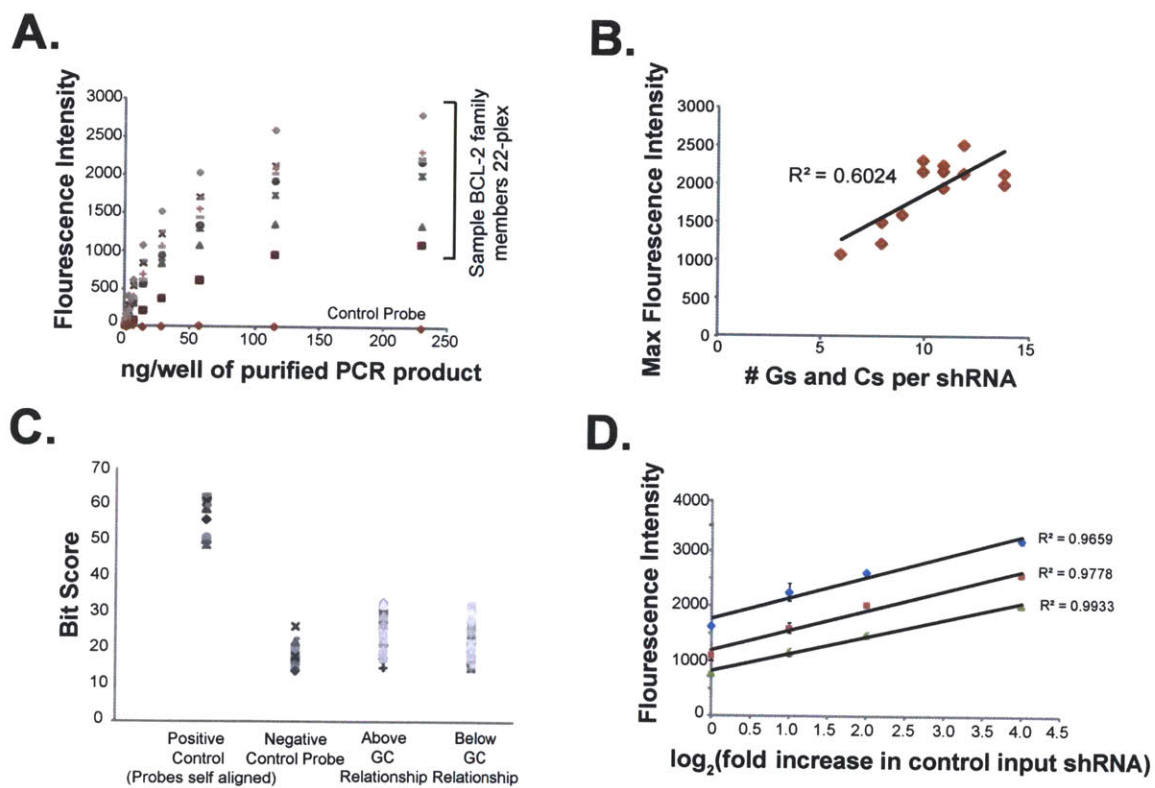
Supplemental Figure 1. Analysis of the variation in probe maximum fluorescence intensity. (A) Representative curves show the range of

measurement for shRNAs targeting multiple members of the BCL-2 family in a 22-plex experiment with pooled plasmid DNA. A control sequence that is not in the 22-plasmid mixture shows little signal. **(B)** A graph showing the relationship between GC content and the variation maximum fluorescence intensity for a given probe. **(C)** A graph in which outliers deviating significantly above and below the relationship depicted in (A) were analyzed for local sequence alignments with the entire shRNA library. These values were compared to values for probes with high local sequence alignments (self-aligned probes) and the negative control probe from Figure 1C. **(D)** Purified single hairpin DNA mixed at known ratios was used to examine the measurement resolution of single hairpins in a complex shRNA pool. shPuma DNA was introduced at 10-80% of the total pool composition. The fluorescence readings of hairpin abundance are plotted against the known fold enrichment. The different linear fits encompass analogous measurements across an 8-fold range of sample concentrations (increasing bottom to top).

The BCL-2 family differentially modulates therapeutic response in distinct B-cell tumors

The initial validation of our measurement technology led us to benchmark this approach against an established single shRNA flow cytometry based assay. In this assay, GFP was used as a surrogate marker for the presence of each of 16 distinct Bcl-2 family member shRNAs, and the impact of gene suppression was determined by the relative change in the percent of GFP-positive cells following treatment (231). In each case, we examined the effect of Bcl-2 family gene knockdown on the *in vitro* response of *Eμ-myc p19*$^{Arf-/-}$ lymphoma cells to the front-line chemotherapeutic doxorubicin (Figure 1C). A linear relationship (r^2=0.89) was observed between multiplexed bead-based measurements and single shRNA flow cytometry measurements of shRNA enrichment and depletion following doxorubicin treatment. Thus, a bead hybridization assay can rapidly and accurately measure shRNA pool composition following drug selection.

A key advantage of shRNA pool-based approaches lies in their inherent adaptability to diverse experimental systems and conditions. In order to test the flexibility of our system, we examined the effects of Bcl-2 family member suppression on doxorubicin response in a distinct cell line. In this case, we examined cells derived from a BCR-Abl-driven murine model of B cell acute lymphoblastic leukemia (B-ALL) (80). As observed in the Burkitt's lymphoma model, we could identify a robust Bcl-2 family shRNA drug resistance and sensitivity profile in these cells. However, the shRNA signatures were distinct between cell types. The most obvious feature differentiating the two cell lines was the critical role for the BH3-only member Bim in doxorubicin-induced cell death in B-ALL (Figure 1D). Since Bim levels are known to increase in response to environmental but not genotoxic stress, the involvement of Bim in the response to a DNA-damaging agent in this context was unexpected. In order to explore the mechanism of Bim-induced cell death, we examined Bim levels in p185+ BCR-Abl ALL cells treated with genotoxic agents (doxorubicin and chlorambucil) and a histone deacetylase inhibitor known to promote significant Bim induction (SAHA) in B cell malignancies (234). Notably, protein levels of Bim were induced acutely following treatment with DNA-damaging agents in B-ALL cells (Figure1E). These data highlight the potential of pool-based shRNA approaches to identify tumor cell-specific determinants of therapeutic response.

An *in vivo* screen for microenvironment-specific modifiers of therapeutic response

A central challenge in the development of effective anti-cancer approaches is to understand the impact of the tumor microenvironment on therapeutic response. To test whether our system could be used to examine cancer therapy *in vivo*, we performed a screen to identify Bcl-2 family members that modulate the response of lymphomas to doxorubicin. Here, all Bcl-2 family shRNAs were simultaneously co-transfected into viral packaging cells to produce a multi-construct viral pool (Figure 2A). The resulting pool was used to infect primary *Eμ-myc p19$^{Arf-/-}$* lymphoma cells *ex vivo*, and transduced cells were tail-vein injected into syngeneic recipient mice. A cohort of 8 mice was sacrificed following tumor onset, and a second cohort was treated with 8mg/kg doxorubicin. Following tumor relapse, lymphoma cells were harvested from lymph nodes and the thymus, two common sites of lymphoma manifestation in the *Eμ-myc* mouse (70), and the relative shRNA content was compared between untreated and treated tumors in these distinct tumor microenvironments.
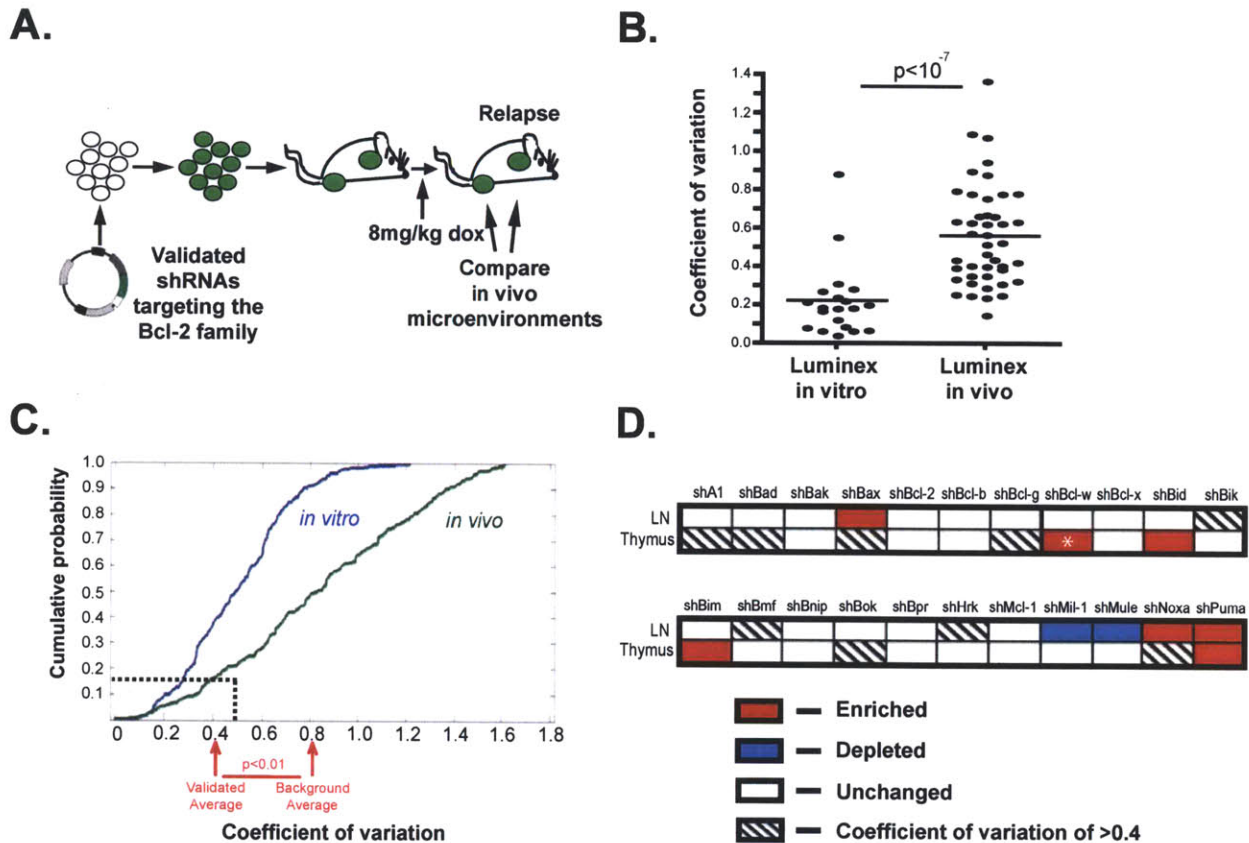
Figure 2. An *in vivo* shRNA screen for modulators of doxorubicin response. **(A)** A diagram depicting the *in vivo* screening strategy. Pooled shRNAs targeting Bcl-2 family members were retrovirally transduced into *Eμ-myc p19^{Arf-/-}* lymphomas. shRNA composition was measured either following the presentation of palpable tumor burden or following tumor relapse after treatment with 8mg/kg doxorubicin. **(B)** A comparison of the coefficient of variation (CV) for hairpins targeting the Bcl-2 family in cell culture versus *in vivo* screens using a Luminex measurement methodology. **(C)** An analysis of the distribution of shRNA CV values for a large *in vitro* versus *in vivo* screening data set generated by high-throughput sequencing. The vertical line represents the CV threshold used to filter *in vivo* data. The arrows denote averages for validated hairpins relative to all hairpins **(D)** Bcl-2 family "hits" following filtering for CV and enrichment criteria and separated by anatomical niche. The asterisk denotes a Bcl-w shRNA that scored as enriched in the thymus, but was excluded due to the lack of Bcl-w expression in this context.

A striking feature of the resulting data was the mouse-to-mouse variability in hairpin composition following drug treatment. This suggests that the complexity of the *in vivo* microenvironment can substantially influence the measured effect

116

of a relatively neutral shRNA. Further inspection of this variation suggested that

a subset of shRNAs exhibited a level of variation comparable to the *in vitro* data

while the remainder showed significantly higher fluctuation (Figure 2B). If

otherwise neutral hairpins exhibit larger variation in *in vivo* datasets, the size of

this variation may represent a meaningful discriminator to focus on hairpins

whose effects are large and reproducible enough to overcome this variability. To

determine whether such variation is a consistent feature of *in vivo* data sets, we

made use of a comprehensive *in vivo* versus *in vitro* shRNA screening data set

(87). Indeed, most shRNAs exhibited high mouse-to-mouse CVs *in vivo* (Figure

2C). However, when we focused on shRNAs shown to exert a biological effect in

subsequent validation experiments, we saw a significant decrease in shRNA CVs

(p<0.01). Thus, variation present in this established data set can be used to

generate a CV threshold that identifies shRNAs with a high probability of exerting

a relevant biological effect. This cutoff was then employed to filter data

generated using our Luminex approach (Figure 2D). As a test of the relevance of

this variation cutoff to other drug screens, we examined the stochastic variation

in the representation of *Eμ-myc* tumor cells infected with a vector control

following treatment with the microtubule poison vincristine *in vivo*. Here, we

transplanted tumor cells into recipient mice at a defined infection efficiency, as

monitored by GFP expression, and examined the variation in the percentage of

GFP-positive cells in distinct mice following treatment. Importantly, these

controls exhibited an *in vivo* CV that was greater than the doxorubicin variation

cutoff (Supplemental Figure 2), suggesting that the CV threshold established in this study may be broadly applicable to other data sets.

A.

B.
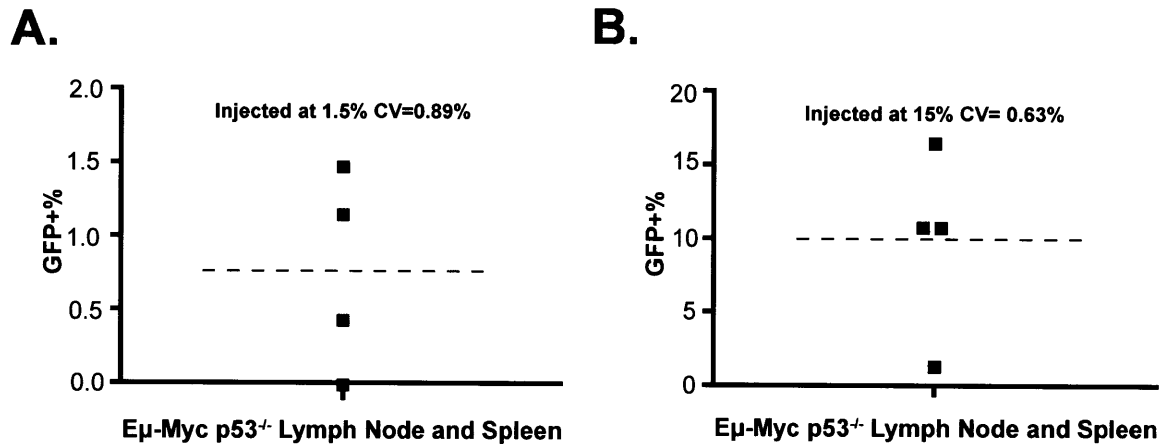
Supplemental Figure 2. An analysis of the variation in the population of cells expressing a control vector following vincristine treatment *in vivo* (A)
A graph showing the percentage of GFP-positive *Eμ-myc p53*^{-/-} lymphoma cells following treatment with 1.5mg/kg vincristine in vivo. The input population was infected to **(A)** 1.5% or **(B)** 15%. At the presentation of palpable disease, tumors were harvested and analyzed in triplicate. The CV is indicated above each graph and the mean is demarcated with a dashed line.

As additional criteria for examining *in vivo* screening data, we required that shRNA target mRNAs be present in un-transduced lymphoma cells and that the representation of a "scoring" shRNA be significantly enriched or depleted as a consequence of doxorubicin treatment (see methods). The resulting list of scoring shRNAs included Bcl-2 family members previously described to influence therapeutic response (228) (Figure 2D and Supplemental Table 1). For instance, we found that suppression of the BH3-only protein Puma promoted doxorubicin resistance in both the lymph node and thymus compartments, consistent with previous reports examining either B lymphoma cells or thymocytes (97,235).

Thus, this approach can readily identify important regulators of drug-induced cell death.

The extrinsic death pathway is a thymus-specific mediator of therapeutic response

Interestingly, in contrast with Puma and other general cell death regulators, we identified the pro-apoptotic Bcl-2 family member Bid as a specific mediator of doxorubicin cytotoxicity in the thymus but not in the lymph nodes. To validate and extend the genetic result in light of this finding, we performed an *in vivo* GFP competition assay in the spleen, bone marrow, peripheral lymph nodes and thymus. In this assay, GFP positivity is used as a surrogate marker for the presence of a Bid shRNA, and the impact of Bid suppression is determined by the relative change in the percent of GFP-positive tumor cells. Consistent with the initial screening data, Bid loss impaired lymphoma cell death in the thymic tumor microenvironment, but not other tumor microenvironments (Figure 3A and B). This tissue specificity was not due to the selective expression of these proteins in specific tumor microenvironments, as we observed similar levels of Bid and its upstream regulator Caspase 8 in the tumor-bearing lymph node and thymus (Supplemental Figure 3A and B). Notably, Bid is unique among Bcl-2 family members in that it translocates to the mitochondria following extrinsic activation of death receptors (236,237). Thus, these data are consistent with a mechanism whereby constitutively present Bid is activated following the release

119

of secreted factors or tumor-stromal cell interactions that are specific to the

treated thymic microenvironment.
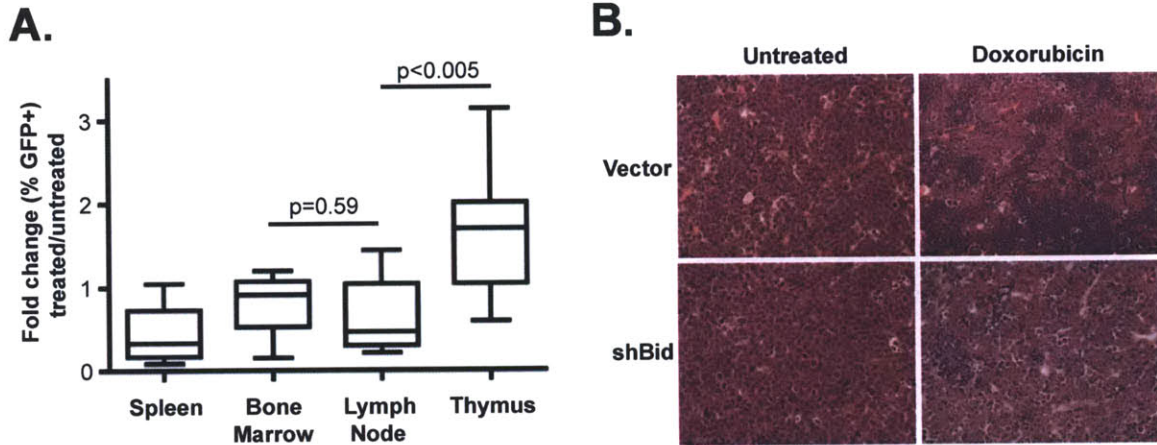
Figure 3. Bid potentiates doxorubicin efficacy in the thymus. **(A)** A graph depicting an *in vivo* GFP competition assay in *Eμ-myc p19*$^{Arf-/-}$ lymphoma cells partially transduced with shBid-1. Mice were injected with partially transduced lymphoma populations. At tumor onset all mice were treated with 10mg/kg doxorubicin. 72 hours after treatment, mice were sacrificed and surviving lymphoma populations were harvested. Fold change in GFP percentage was assessed 48 hours later (n≥4). **(B)** H&E stained sections from mice bearing vector control or shBid thymic lymphomas. Mice were treated with 10mg/kg doxorubicin and sacrificed 48 hours later. Representative fields from treated and untreated are shown at 25x magnification. Dark patches in treated vector control tumors indicate sites of normal lymphocyte infiltration.
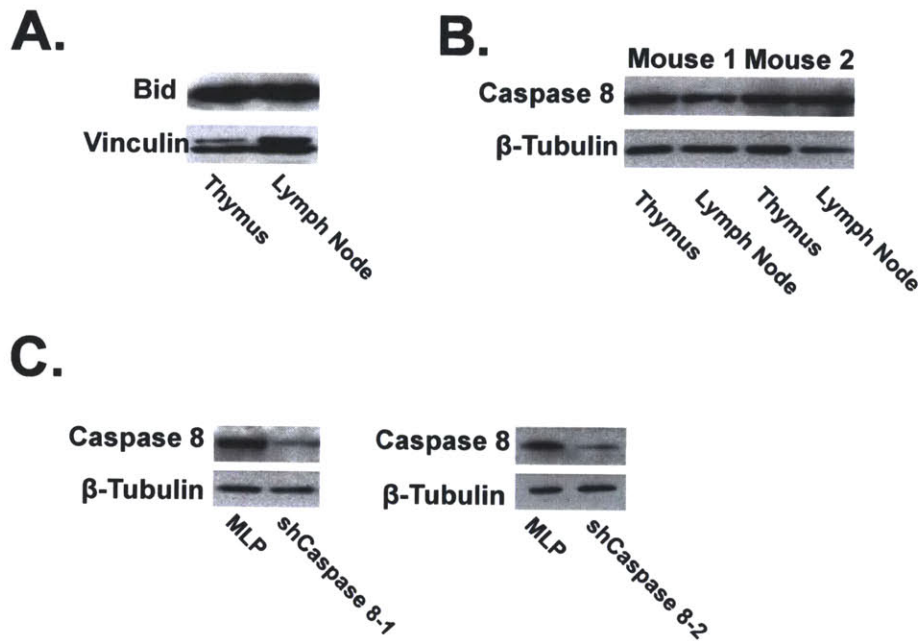
Supplemental Figure 3. Western blots showing protein levels in distinct tumor sites. (A) A western blot showing Bid levels in $E\mu$-myc $p19^{Arf-/-}$ lymphoma cells from tumor-bearing lymph node and thymus. **(B)** A western blot for Caspase 8 levels in $E\mu$-myc $p19^{Arf-/-}$ lymphoma cells from tumor-bearing lymph node and thymus. **(C)** Examination of the protein knockdown conferred by two shRNAs targeting Caspase 8 in $E\mu$-myc $p19^{Arf-/-}$ lymphoma cells.

The relevance of Bid to DNA-damage-induced death remains a subject of debate (238,239). To confirm the importance of Bid to doxorubicin-induced cell death *in vivo*, we injected three cohorts of syngeneic mice with Eu-myc $p19^{Arf-/-}$ lymphoma cells expressing one of two validated shRNAs targeting Bid or a vector control. At tumor onset, all mice were treated with 10mg/kg doxorubicin and monitored for tumor regression and relapse. Suppression of Bid resulted in decreased tumor-free survival and tumor-cell clearance compared to control tumors (Figure 4A). Furthermore, in mice bearing shBid-transduced lymphomas, 50% of the mice showed no tumor-free survival while 90% of control mice exhibited a period of tumor-free survival. Notably, in the case of the lymphoma cells used in this study, suppression of Bid *in vitro* had minimal effect on

lymphoma cell survival following doxorubicin treatment (Figure 4B). Thus,

treatment of these tumors in their native microenvironment reveals genetic

dependencies that are not present in cultured cells.
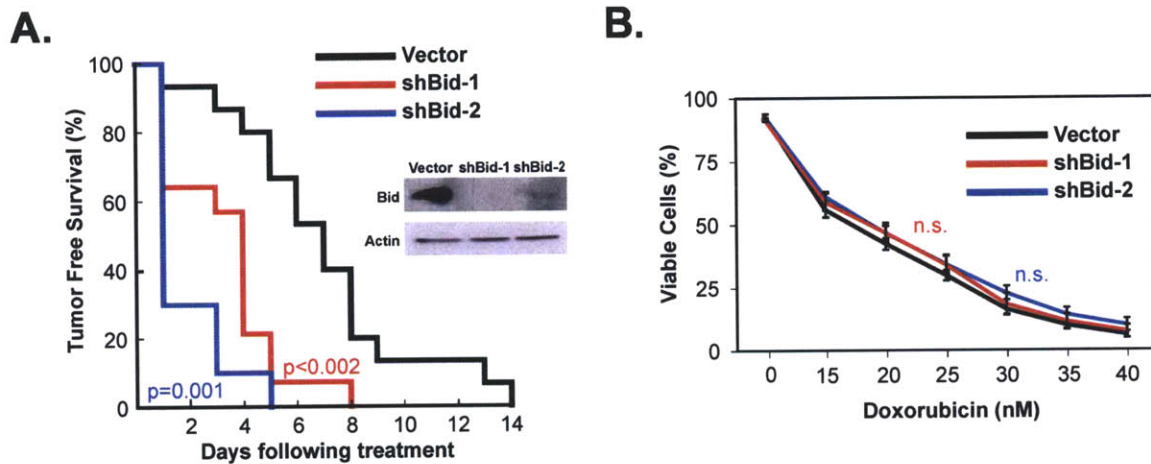
Figure 4. Bid status affects therapeutic outcome *in vivo*, but not *in vitro*.
(A) A Kaplan-Meier curve showing tumor-free survival in mice bearing vector or
shBid lymphomas. All mice were treated with a single dose of 10mg/kg
doxorubicin (n≥10). (Inset) A western blot showing Bid protein levels in the
presence of Bid shRNAs. **(B)** A dose-response curve showing the relative
viability of lymphoma cells treated with doxorubicin *in vitro* for 48 hours.
Lymphoma cells were transduced with either a vector control or an shRNA
targeting Bid.

These data suggest that activation of components of the extrinsic cell

death pathway potentiate chemotherapeutic efficacy in the thymus. To further

interrogate the role of death receptor signaling in therapeutic response in this

setting, we targeted Caspase 8, the direct activator of Bid by generating hairpins

targeting Caspase 8 (Supplemental Figure 3C). Suppression of Caspase 8 in

transplanted lymphomas phenocopied the effect of Bid silencing as measured by

tumor-free survival (Figure 5A), suggesting an upstream induction of death

receptor signaling in the thymus following doxorubicin treatment.
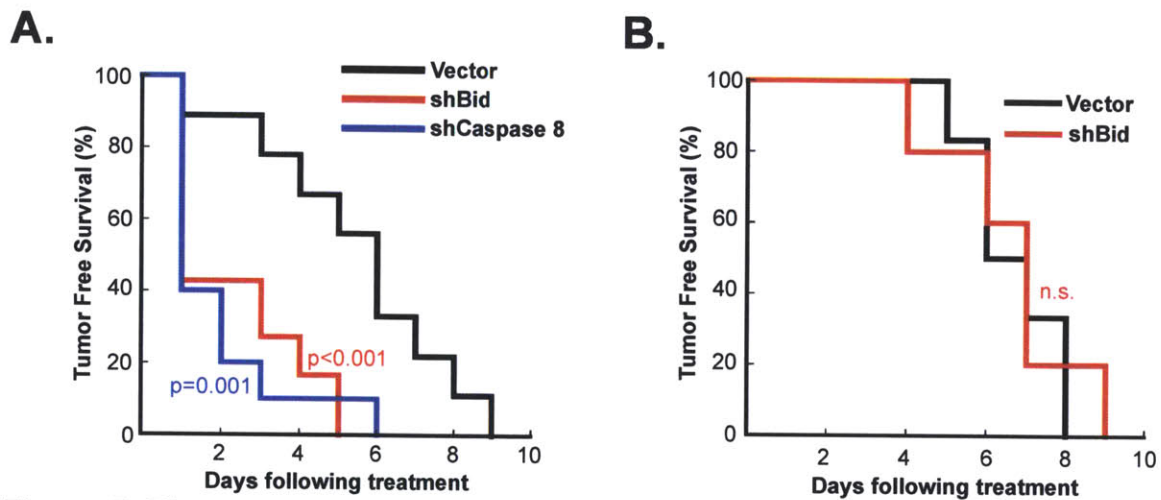
Figure 5. The extrinsic death pathway mediates doxorubicin response in the thymus. **(A)** A Kaplan-Meier curve showing tumor free survival of mice bearing vector, shBid or shCaspase 8 expressing lymphomas. All mice were treated with a single dose of 10mg/kg doxorubicin (n≥10). **(B)** A Kaplan-Meier curve showing the tumor-free survival of thymectomized mice transplanted with pure populations of lymphoma cells transduced with shBid or a vector control. All mice were treated with a single dose of 10mg/kg doxorubicin (n=6 for both cohorts).

Finally, to confirm the specificity of Bid-induced cell death in the thymus relative to whole organism chemotherapeutic response, we examined the effect of Bid suppression on tumor-free survival following doxorubicin treatment in athymic mice. Pure populations of either shBid or vector control transduced lymphoma cells were transplanted into surgically thymectomized recipient mice. Upon the presentation of a palpable disease burden, mice were dosed with 10mg/kg of doxorubicin and monitored for tumor-free and overall survival. In this context, chemotherapeutic response was indistinguishable in the presence or absence of Bid (Figure 5B).

Discussion

We have presented a tractable methodology for pooled shRNA screens that can be rapidly adapted to diverse vector systems and gene families. The value of this system is exemplified by the rapid manner in which drug function can be interrogated in multiple cell types *in vitro* and in diverse anatomical contexts *in vivo*. Importantly, while numerous cell-culture-based loss-of-function screens have been performed to identify modulators of therapeutic response, this is the first report to describe an *in vivo* loss-of-function therapy screen – the relevance of which is apparent in light of the discordant *in vitro* and *in vivo* phenotypes resulting from Bid suppression. While the set of shRNAs probed in this work is restricted to a particular aspect of cell biology, recent advances in bead-based DNA hybridization now permit the simultaneous resolution of as many as 500 distinct oligonucleotides so that multiple facets can be explored simultaneously. We have recently shown that as many as 1000 distinct shRNAs can be introduced into individual mice (87), suggesting that large shRNA libraries can be combined with this technology to probe the impact of myriad genetic lesions in diverse pathophysiological contexts.

In this study we systematically examined shRNAs targeting the entire Bcl-2 family in multiple *in vitro* and *in vivo* settings. In all therapeutic contexts, we identified a specific BH3 "activator" gene essential for mediating the effects of frontline chemotherapy. Biochemical studies have previously defined critical roles for the BH3 only family members Bid, Puma and Bim. Furthermore, the recent development of a Bid, Puma, and Bim triple knockout mouse confirmed

the essential role of these proteins in developmentally regulated apoptosis (240). Interestingly, our data suggest that the relevant "activator" protein can vary quite significantly in neoplastic cells. While an "activator" is always necessary for cell death, the cellular environment or driving oncogene can dramatically shift the precise BH3-only family member that is most relevant for therapy-induced apoptosis. This context-dependent relevance of apoptotic regulators may underlie the significant challenge in eradicating disseminated malignancies and highlights the need to understand the relationship between intrinsic and paracrine signals and Bcl-2 family regulation.

An unexpected finding from this work is that while Caspase 8 and Bid are expressed at similar levels in diverse tumor-bearing locations *in vivo*, they are specifically required for drug efficacy in the thymus. Examined in isolation, this result would suggest that the thymus is a pro-death microenvironment. However, previous studies in thymectomized mice have shown that the thymus can exert a net protective effect on tumor cells following doxorubicin treatment (203). This cytoprotective effect is mediated in a paracrine fashion by thymic endothelial cells that secrete multiple pro-survival cytokines in response to DNA damage. Cytokine induction subsequently upregulates BCL-xL and promotes the survival of target tumor cells. Thus, the unique role of death receptor activity in this context may function to counterbalance unchecked survival signaling following cellular stress in the thymic microenvironment. Notably, however, the precise mechanism of death receptor engagement in this context remains to be

determined. Addition of recombinant death receptor ligands, such as FASL, TNF, and TRAIL *in vitro* fails to induce lymphoma cell death. Consequently, the engagement of death receptor signaling, like survival signaling, may require a more complex concerted action of secreted factors and cell-cell or cell-stromal interactions.

Experimental Procedures

shRNA generation

shRNAs targeting the Bcl-2 family (231) were designed using Biopredsi from Novartis. shRNAs were cloned into the MLS (86) retroviral vector containing a Mir30 expression cassette under the transcriptional control of the MSCV LTR and coexpressing GFP. Plasmids were verified for mRNA target knockdown using standard qRT-PCR techniques. Western blots were performed to analyze total protein knock down for a subset of Bcl-2 family members. Bim, Bax, and Bak knockdown are shown in Supplemental Figure 4. The shRNA library was constructed by evenly pooling individual minipreps of each individual shRNA. This mixture was co-transfected into Phoenix retroviral packaging cells and pooled virus was collected.

Western Blots

SDS-PAGE was performed according to standard protocols, and gels were transferred to PVDF membranes. The antibodies used were as follows; Bid (polyclonal antisera from Honglin Li), BAX (Cell Signaling Technologies #2772),

BAK (Upstate #06-536), BIM (Cell Signaling Technologies #C34C5), Caspase 8 (Cell Signaling Technologies #D35G2), beta-Actin (Cell Signaling Technologies #4967L), and Tubulin (ECM Biosciences #TM1541).

Luminex bead-based assay

Carboxylated Luminex beads were purchased from Mirai biosystems. Probe oligonucleotides comprised of the shRNA anti-sense strand modified with C12-amine were conjugated to the beads using EDC in a pH 4.5 MES hydrate buffer. Coupling efficiency was validated with sense oligonucleotides. 3500 beads were added to a 50μl reaction volume in a 3M Tetra-methyl ammonium chloride (TMAC) buffer to reduce the differences in T_m that accompany differences in GC content. DNA loading concentrations are as indicated (2-200ng per well were added). Blocking oligos that corresponded to the biotinylated PCR product but lacked the sense portion of the shRNA were added at 100-fold molar excess to compete out the dsPCR product and reduce the preferential re-hybridization of the PCR product. Samples were denatured for 3 min at 95°C and hybridized for 30 minutes at 52°C. Streptavidin-PE (Invitrogen)/TMAC was then added to the wells and incubated for 5 minutes at 52°C. All samples were incubated at 52°C to ensure they stayed at equilibrium, and the PMT setting on the Luminex machine was approximately 520 volts (low calibration).

Polymerase Chain Reaction

Three individual 25μl PCR reactions were performed using a 5' primer

targeting the constant hairpin loop region and a 3' primer targeting the vector

backbone. The PCR buffer was 2x Failsafe Buffer B (Epicentre Biotechnologies)

and we ran 35 cycles with an extension time of 1 minute at 72°C and a

hybridization temperature of 52°C for 35 seconds. The 3' primer was biotinylated.

Pooled PCR product was column purified and resuspended in 36μl water prior to

serial dilution and subsequent measurement.

Cell culture

All lymphoma and leukemia cells were isolated directly from tumor-bearing

animals and cultured at 5% CO2 at 37°C. *Eμ-myc p19$^{ARF-/-}$* cells were isolated

and maintained as described (180). B-ALL cells were maintained as described

(123). All *in vitro* viral transduction was performed by co-infecting 1 million cells

per 10cm plate. Infection efficiency was quantified by flow cytometry for GFP+

cell populations. Infection efficiencies under 50% were utilized to ensure an MOI

of approximately one. Pool composition was measured at the beginning of the

experiment, as well as following recovery from an LD90 doxorubicin drug dose.

Untreated cells that had grown in culture for the duration of the experiment were

used as controls. Hairpin 97mer sequences in the Mir30 context were:

shBid-1-
TGCTGTTGACAGTGAGCGCCACAGAAGATTCCATATCAAATAGTGAAGCCA
CAGATGTATTTGATATGGAATCTTCTGTGATGCCTACTGCCTCGGA,
shBid-2-
TGCTGTTGACAGTGAGCGCCACAGAAGATTCCATATCAAATAGTGAAGCCA
CAGATGTATTTGATATGGAATCTTCTGTGATGCCTACTGCCTCGGA.

shCaspase 8-
TGCTGTTGACAGTGAGCGAAACTATGACGTGAGCAATAAATAGTGAAGCCA
CAGATGTATTTATTGCTCACGTCATAGTTCTGCCTACTGCCTCGGA

Background distribution analysis for *in vivo* screening data

454 sequencing data used to determine CV thresholds is available from

the GEO database (accession number GSE16090). Coefficients of variation

were calculated by dividing the standard deviation of the fold change in read

number (for any hairpin with >4 reads) by the mean of the fold change. To be

included in this analysis hairpins had to be present at high enough quantities to

have at least 4 reads. Previously validated hit CVs (87) included IL-6, Lyn,

Rac2, Twf, and CrkL and were compared to the background distribution by t-test.

Cumulative distributions were plotted in Matlab using the dfittool.

In vivo **screening**

6-week old C57BL/6J mice (Jackson Laboratories) were tail vein injected

with 2 million *Eμ-myc p19$^{ARF-/-}$* lymphoma cells expressing the 22 shRNAs

targeting the Bcl-2 family. Infection was optimized such that each tumor cell

expressed a single shRNA. We sampled pool composition before injection, upon

the development of a palpable tumor burden, and upon relapse following IP

injection of 8mg/kg of doxorubicin. For *in vivo* screen validation, pure populations

of cells expressing shRNAs were isolated by GFP sorting using a FACS ARIA

cell sorter. 2 million cells transduced with a vector control or specific shRNAs

were injected into syngeneic recipient mice. At the presentation of palpable

lymphomas, mice were treated with 10mg/kg doxorubicin and disease free survival/tumor free progression were monitored.

Screening analysis

Luminex intensities for serial dilutions of PCR samples from pooled hairpin libraries were compared by calculating a curve fit for a given sample using the equation $(Y=a*(1-exp(-b*x)))$. Sample integrals were then calculated, and these integral scores were compared after subtracting the initial from the final integral score. All independent Luminex runs were normalized to the maximum signal intensity and all runs performed on different days contained internal standards for day-to-day normalization. Scoring shRNAs were identified following a three-step process. First, in order to eliminate a systematic error for depleting hairpins, we transformed all the data by adding the hairpin mean to all *in vivo* measurements. We then applied two filters. The first filter was based upon a comparison of the distribution of a given shRNA with the variation of neutral hairpins. We required our "hits" to have a coefficient of variation that was equal to or less than 0.4. This allowed us to threshold out approximately 80% of neutral hairpins. The second filter was based upon a comparison of treated samples with untreated hairpin samples. To progress to further validation efforts, we required our treated sample to be different at the 0.10 significance level versus untreated controls.

Data analysis

Linear fits were calculated using a least squares algorithm. Sequences were compared for overlap using the local alignment method of Smith-Waterman in the Matlab function localalign.m. Heat maps were generated in Matlab. Kaplan Meier analyses were performed using Graph Pad Prism software.

Acknowledgements

Supplemental Figure 4 and Supplemental Table 1.
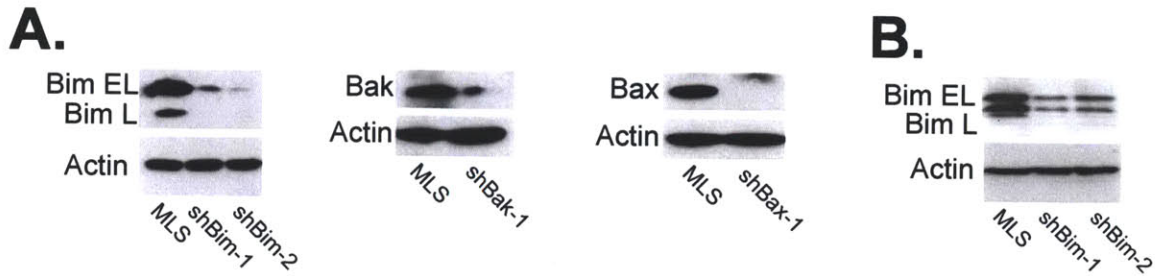
Supplemental Figure 4. Western blots showing shRNA-induced protein knockdown for three pro-apoptotic Bcl-2 family members. **(A)** Western blots of Eμ-myc lymphoma cells expressing the indicated shRNAs. **(B)** A western blot showing Bim suppression in B-ALL cells.

Lymph Node	Change vs. Untreated	Untreated Integral Score	Treated Integral Score	CV
shNoxa	8.3	32.7	41	0.2
shPuma	8	26.9	34.9	0.24
shBax	5.1	25.9	31	0.4
shMule	-3.5	16.5	13	0.3
shMil1	-4.3	24	19.7	0.25
Thymus				
shBid	11	13.1	24.1	0.4
shBim	10.3	18.7	29	0.25
shPuma	5.4	15.7	21.1	0.33

Supplemental Table 1. A list of top scoring shRNAs meeting the hit criteria separated by anatomical location. The change versus untreated represents the level of enrichment/depletion, and the coefficient of variation is the mean divided by the standard deviation for the doxorubicin treated cohort.

Chapter 5:

Developmentally specified roles for paracrine IL-6 in lymphomagenesis

Luke A. Gilbert[1] and Michael T. Hemann[1]*

[1] The Koch Institute for Integrative Cancer Research at MIT, Massachusetts Institute of Technology, Cambridge, MA 02139

Abstract

A basic requirement for the development of complex organ systems is that the cellular response to identical environmental cues can vary significantly between distinct cell types and developmental stages. While it is well established that paracrine signaling can similarly elicit diverse responses in distinct tumor types, the relevance of developmental stage-specific signaling responses to tumor development remains unclear. Here, we show that the same microenvironmental factor, IL-6, can both promote and prevent lymphoma development by acting on cells at distinct stages of hematopoietic development. Specifically, paracrine IL-6 signaling promotes the survival of transplanted hematopoietic stem cells following lethal irradiation, allowing the persistence and expansion of progenitor cells bearing a cancer-promoting alteration. Conversely,

133

IL-6 signaling also initiates a paracrine secretory program in the bone marrow that promotes B cell differentiation and inhibits the development of B cell malignancies. Thus, stage-specific responses to cytokines may promote progenitor cell expansion while also inhibiting neoplastic development within a single developmental lineage. Once transformed, the resulting B cell lymphomas again utilize paracrine IL-6 signaling as a survival signal, highlighting the ability of tumor cells to co-opt pathways utilized for stem cell protection. These data not only suggest a complex regulation of tumor development by the pre-neoplastic microenvironment, but also suggest that this regulation can decisively impact the outcome of well-established tumor modeling approaches.

Introduction

Maintaining tissue homeostasis requires the ability to replace damaged cells. In many organs, this regenerative potential is maintained by long-lived tissue-specific adult stem cells. These cells are largely quiescent, enabling more efficient DNA repair and suppression of apoptosis (241,242). In response to cellular stress, adult stem cells are induced to both proliferate and differentiate to reconstitute organ systems (243). However, the mechanisms promoting stem cell re-entry into the cell cycle following tissue injury are less understood. Recent evidence suggests that in some tissues paracrine survival factors promote normal stem cell homeostasis and also modulate stem cell survival and tissue repair in response to DNA damage (155,244,245).

The activation of adult stem cells to promote tissue homeostasis is particularly important in the hematopoietic system. All differentiated hematopoietic cells have a transient lifespan, thus each of these cell types needs to be regenerated on an ongoing basis. Additionally, exogenous stresses from insults like hemorrhage and chemotherapy require the stimulation of progenitor cells to reconstitute the hematopoietic compartment. This requirement for paracrine signaling is not specific to *bona fide* hematopoietic stem cells, as differentiated hematopoietic cell types also require ongoing paracrine signaling to complete terminal steps of differentiation (246). For example, in the B cell lineage, BAFF and IL-21 synergize to activate and differentiate memory B cells into plasma cells (247-249). Additionally, emerging evidence suggests that the requirement for specific paracrine growth factor signaling is highly context-specific during development. For example, mice that express constitutively active Stat5b, a central mediator of IL-7 receptor signaling, show a dramatic expansion of pro/pre-B cells and mature T cells but not mature B cells or pro-T cells (250). This suggests that during hematopoiesis, the activation of a given receptor may exert dramatically distinct effects depending on cell type or stage of differentiation.

Paracrine survival factors are also important in the growth and survival of transformed cells. For example, in multiple myeloma, multiple factors emanating from the bone marrow microenvironment are essential for tumor progression (178). Additionally, we have recently shown that survival signals important for

tissue homeostasis can be co-opted by hematopoietic malignancies to promote tumor cell survival and fuel tumor progression (203). Specifically, DNA damage induces the acute release of pro-survival cytokines, including IL-6, from tumor-associated endothelial cells, and these paracrine factors act to prevent lymphoma cell apoptosis and promote tumor relapse. Thus, survival signaling promotes normal tissue repair but can also promote tumor persistence in select microenvironments.

While stem and tumor cells are receptive to paracrine signaling, it remains unclear whether pre-neoplastic cells can utilize these same survival signals to bypass apoptotic barriers early in tumor development (251). Tumor development is a multi-step process in which normal growth and differentiation control is lost (44). This process, at its most basic level requires the activation of a proto-oncogene to drive proliferation. For example, deregulated expression of c-Myc as a result of aberrant VDJ recombination, resulting in the t(8; 14) translocation, provides the initiating lesion in Burkitt's lymphoma (89,252). Paradoxically, however, this initiating lesion also represents a crucial barrier to tumor development, as oncogenic signaling in pre-neoplastic cells can promote apoptosis or senescence (253-256). Thus, it remains unclear how rare pre-neoplastic cells survive during the period after oncogene activation but prior to the loss of a tumor suppressor.

Given the role of IL-6 in promoting lymphoma cell survival in a therapeutic

context, we wondered whether the pro-survival cytokine, IL-6, potentiates early

lymphoma development by promoting cellular survival following oncogene

activation. Surprisingly, we found that IL-6 could either promote or inhibit tumor

development, depending on the target pre-neoplastic cell type. While IL-6

facilitates the expansion of HSCs bearing oncogenic alterations – a tumor

promoting activity, it also stimulates the maturation of pro/pre- B cells to more

mature B cells. As pro/pre B cells are more susceptible than mature B cells to

oncogenic transformation, IL-6 supports a differentiation process that inhibits

lymphoma development (257-260). Thus, paracrine signaling can either support

or inhibit tumor progression within a given lineage, depending upon the

developmental stage of the target cell – a process that balances the beneficial

effects of tissue regeneration with the detrimental effects of neoplastic

development. Additionally, IL-6 promotes the survival of HSCs and B-lymphoma

cells, but not B cell precursors, suggesting that tumors cells re-acquire the ability

to respond to stem cell survival signals following transformation.

Results

Paradoxical roles for IL-6 in lymphoma development

To examine the role of paracrine IL-6 signaling in B-cell

lymphomagenesis, we utilized an adoptive transfer approach in which *Eµ-myc*

hematopoietic stem cells derived from fetal liver were transplanted into lethally

irradiated wild-type or *IL-6$^{-/-}$* recipient mice (Figure 1A). This approach is

frequently used to interrogate the role of cell-intrinsic alterations in normal or tumor development within the hematopoietic system. Following transplantation, all recipient mice developed B cell lymphomas as assessed by tumor pathology and immunophenotype (Supplemental Figure 1A-B). However, tumor latency varied considerably with recipient IL-6 status. Notably, $IL-6^{-/-}$ recipient mice showed significantly delayed tumor onset when compared with control recipient mice ($IL-6^{-/-}$ mean survival of 415 ± 49 days versus $IL-6^{+/+}$ mean survival of 182 ± 49 days p=0.0093) (Figure 1A). As IL-6 has previously been shown not to play a role in mature lymphoma cell proliferation, these data suggest that paracrine IL-6 may support the survival of tumor cell progenitors *in vivo* (203).
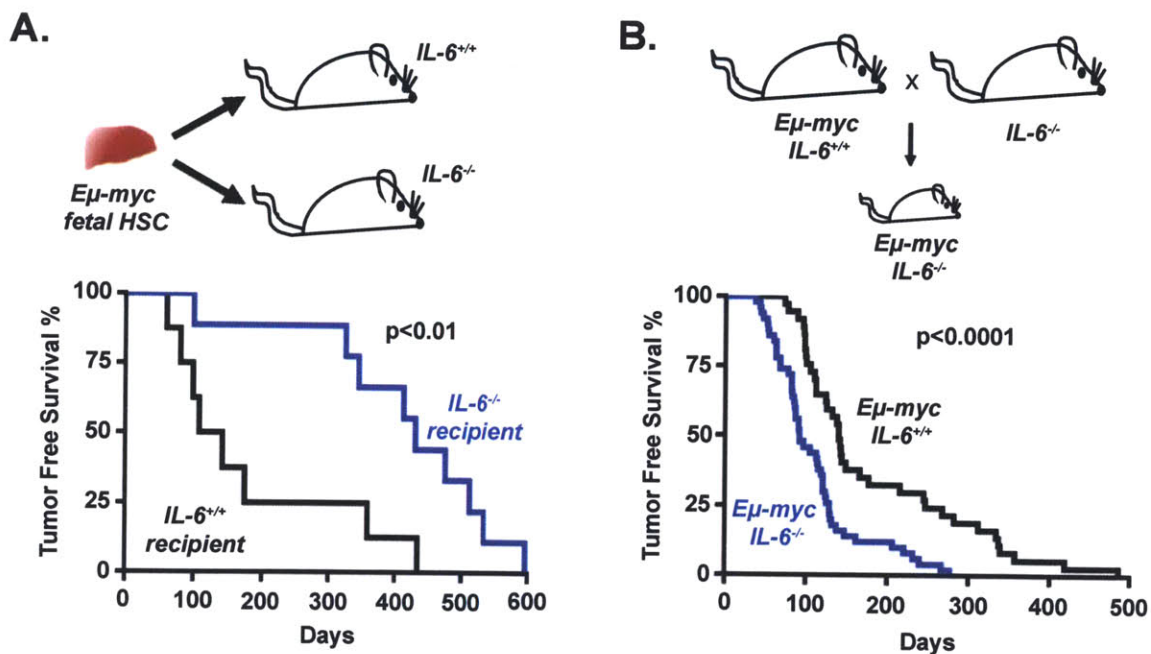
Figure 1. *IL-6* status modulates *Eμ-Myc* lymphomagenesis in a context-specific manner. (A) (above) A schematic diagram depicting the adoptive transfer approach for transplantation of *Eμ-Myc* fetal liver hematopoietic stem cells into $IL-6^{+/+}$ (n=8) or $IL-6^{-/-}$ (n=9). (below) A Kaplan-Meier curve displaying tumor free survival for both cohorts of mice. The p value was calculated using a log rank test. **(B)** (above) A schematic diagram depicting the generation of germ-

line *IL-6$^{-/-}$ Eμ-Myc* and *IL-6$^{+/+}$ Eμ-Myc* mice. (below) A Kaplan-Meier curve displaying tumor free survival for *IL-6$^{-/-}$ Eμ-Myc* (n=50) and *IL-6$^{+/+}$ Eμ-Myc* mice (n=37). The p value was calculated using a log rank test.

As a complementary strategy to examine the role of IL-6 in lymphoma development, *IL-6$^{-/-}$* mice were crossed with *Eμ-myc* mice to generate germ line *IL-6$^{-/-}$ Eμ-myc* mice (Figure 1B). Again, all *Eμ-myc* mice developed B cell lymphomas regardless of IL-6 status (Figure 2A and Supplemental Figure 1A). However, in this context, *IL-6$^{-/-}$ Eu-myc* mice developed B cell lymphomas *more* rapidly than control *Eu-myc* mice (*IL-6$^{-/-}$* mean survival of 110 ± 8 days versus *IL-6$^{+/+}$* mean survival of 184.5 ± 18 days p=0.0001). Thus, paradoxically, IL-6 loss can either accelerate or delay lymphomagenesis in *Eμ-myc* mice, depending on the specific construction of the mouse model.

A.

Eµ-myc IL-6⁺/⁺ Eµ-myc IL-6⁺/⁺ transplant Eµ-myc IL-6⁻/⁻ Eµ-myc IL-6⁻/⁻ transplant

B.

Eµ-myc IL-6⁺/⁺ n=2   Eµ-myc IL-6⁻/⁻ n=6

■ B220⁺IgM⁻   ▨ B220⁺IgM⁺

C.
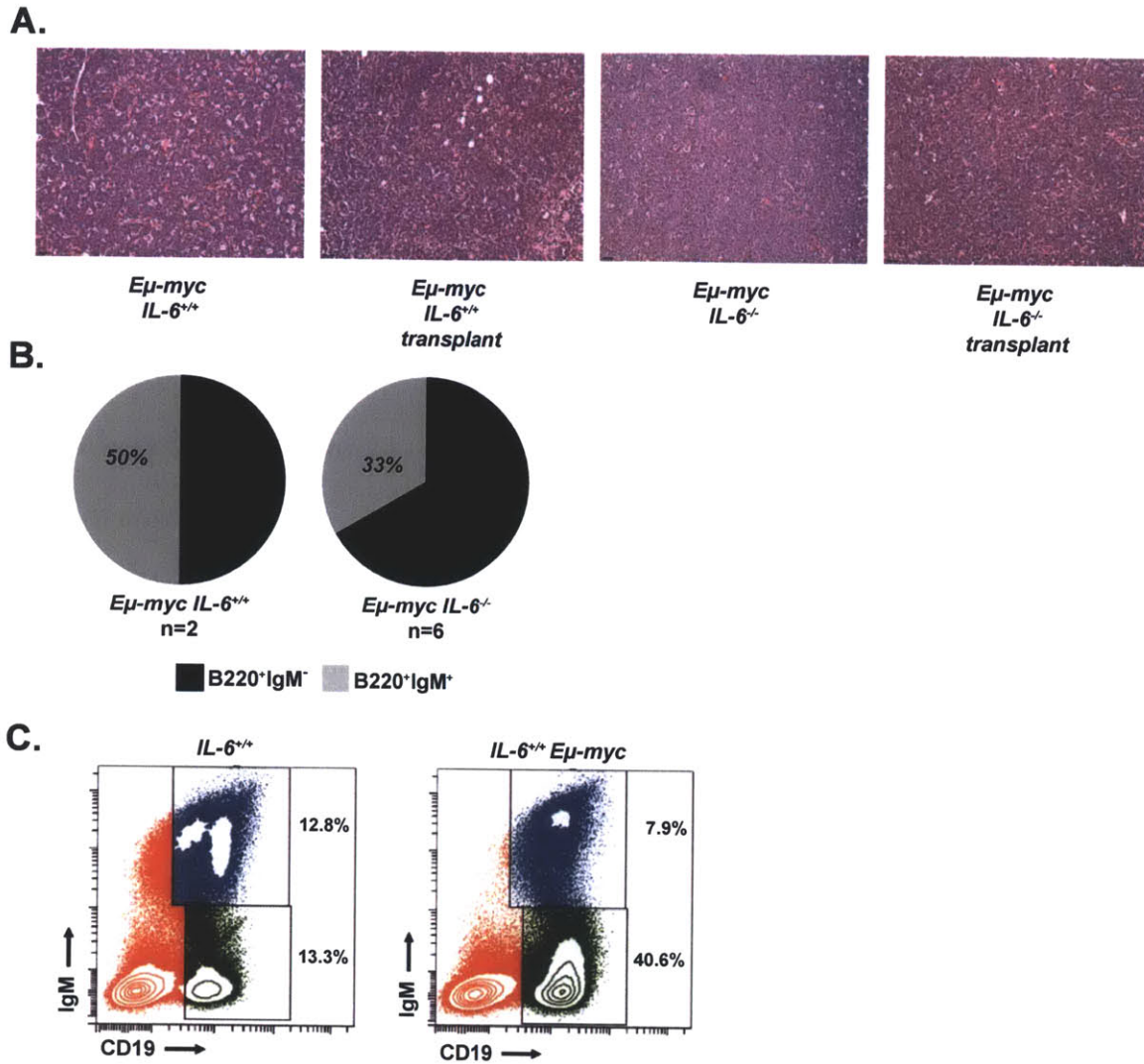
Supplemental Figure 1. *Eµ-Myc* **transplant and germline mouse models develop B cell lymphomas regardless of IL-6 status. (A)** Hematoxylin and Eosin (H&E) staining of tumors from mice of the indicated genotype. Tumors were harvested at an end stage of disease. Representative fields are shown at 20X. **(B)** A pie chart displaying the IgM status of *IL-6⁺/⁺ Eµ-Myc* transplant (n=2) and *IL-6⁻/⁻ Eµ-Myc* transplant (n=6) B cell lymphomas. **(C)** A representative flow cytometry plot from wild type and *Eµ-Myc* mice prior to tumor onset. This gating scheme was used to define IgM status for tumor immunophenotyping and B cell percentages throughout the paper.

IL-6 promotes B cell maturation

To begin to reconcile these opposing roles for IL-6 in tumor development,

we first examined lymphoma cell differentiation status in germ-line *Eµ-myc* mice

in the presence and absence of IL-6. Notably, *IL-6$^{-/-}$ Eμ-myc* tumors were more

immature and polyclonal, as assessed by surface IgM expression, than control

Eμ-myc tumors (Figure 2A and Supplemental Figure 1C). This observation

suggested that *IL-6* deficiency might result in aberrant B cell maturation. B cell

development is a complex process, during which B cells pass through a series of

developmental stages characterized by distinct patterns of surface markers. For

B cells to develop, they require multiple survival signals from the bone marrow

microenvironment, including IL-7, SCF, and adhesion-mediated survival signaling

(261). As it is well established that IL-6 is required for T cell development and

plasma cell maturation and to better understand the results of our

lymphomagenesis experiments, we examined whether IL-6 is involved in early B

cell development or growth (159,262). Here, we measured the percentage of

pro/pre- and immature B cells (defined here as CD19+/IgM- and CD19+/IgM+,

respectively) in the bone marrow of wild-type and *IL-6$^{-/-}$* mice. *IL-6$^{-/-}$* mice showed

a similar overall B cell number but the ratio of pro/pre- to immature B cells is

increased compared to wild-type bone marrow. Specifically, we observed

decreased numbers of immature B cells and increased numbers of pro/pre-B

cells in *IL-6$^{-/-}$* mice (Figure 2B and Supplemental Figure 2A). We also observed a

decreased relative percentage of mature B cells (Hardy Fraction F) in *IL-6$^{-/-}$ Eμ-*

myc compared to *Eμ-myc* mice (Supplemental Figure 2B) (263). To further

characterize this developmental defect, we measured surface IgM, CD24, CD43

and BP-1 expression, which are canonical cell surface markers associated with

the pro-pre B-cell transition, by flow cytometry in B cells from wild-type, *IL-6$^{-/-}$*,

Eµ-myc and *IL-6⁻/⁻ Eµ-myc* mice. Here we observed changes associated with the presence of the *Eµ-myc* transgene, but no significant differences associated with IL-6 status (Supplemental Figure 1C and data not shown). Together, these results suggest that IL-6 deficiency results in a block early in the transition from pre to immature B cells in wild-type and *Eµ-myc* mice.
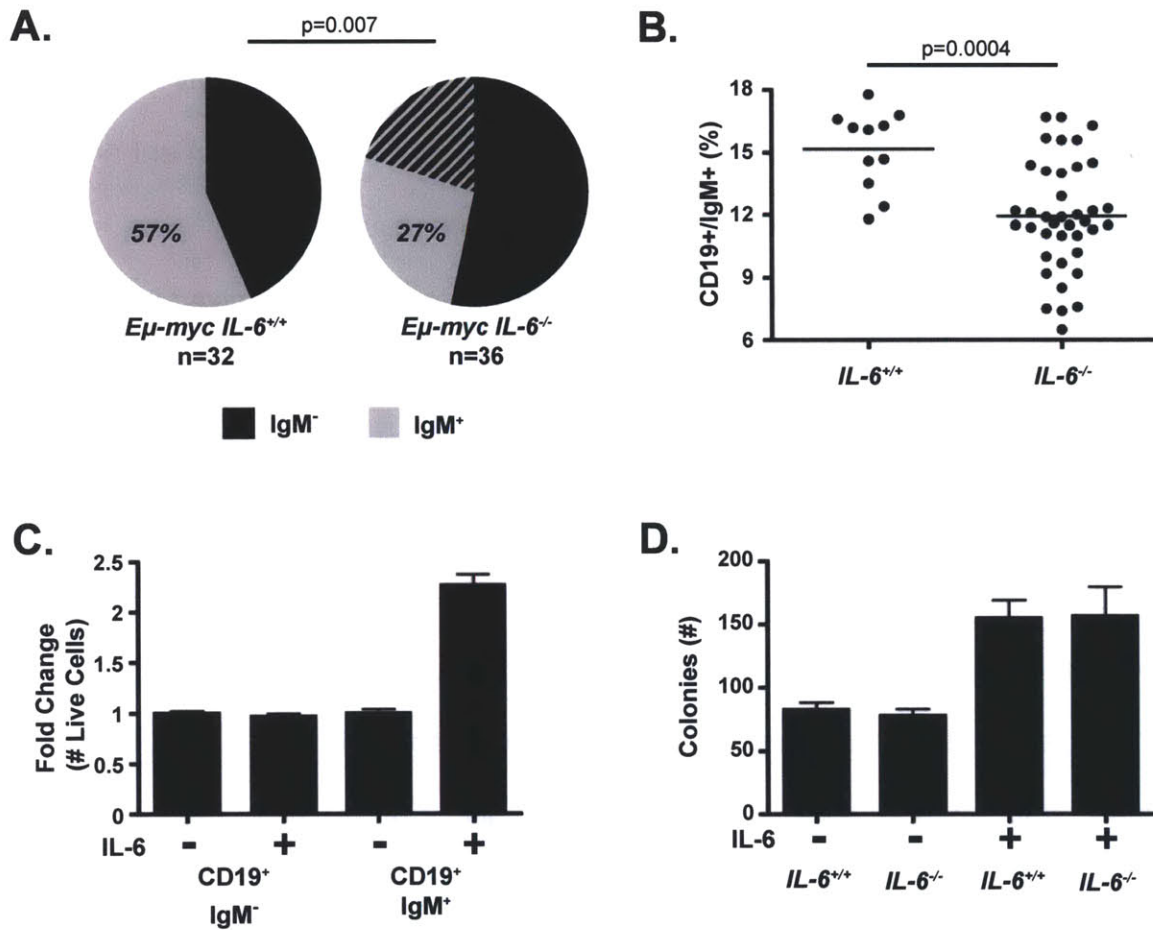
Figure 2. IL-6 promotes the differentiation of normal and neoplastic B cells.
(A) A pie chart displaying the IgM status of *IL-6⁺/⁺ Eµ-Myc* (n=32) and *IL-6⁻/⁻ Eµ-Myc* (n=36) B cell lymphomas. The hatched area represents multi-clonal tumors that were partially IgM positive and negative. **(B)** A graph showing the percentage of CD19⁺/IgM⁺ cells within the bone marrow of *IL-6⁺/⁺* (n=11) and *IL-6⁻/⁻* (n=39) mice. Each dot represents an individual mouse, with a line demarcating the mean for each cohort. **(C)** A graph showing the fold change in the number of live pro/pre or immature B cells after 72 hours in culture in the

presence or absence of 10ng/mL recombinant IL-6. The data are represented as mean ± SD (n≥6 for 2 independent experiments). **(D)** A bar graph displaying the number of B cell colonies in a methylcellulose colony formation assay for B cell progenitor number. Bone marrow from $IL-6^{+/+}$ and $IL-6^{-/-}$ mice was treated with IL-7 and SCF in the presence or absence of IL-6 for 7 days, at which point colonies were counted. The data are shown as mean ± SEM (n=6 for 2 independent experiments).

Many paracrine survival signals such as IL-7, SCF, Notch and TPO act at specific stages of hematopoietic development (264). To determine whether IL-6 directly promotes B cell maturation we isolated pro/pre and immature B cells from the bone marrow of wild-type mice. Pure populations of B cells were then plated *in vitro* in B cell medium containing IL-7 and SCF with or without IL-6. 72 hours later, we measured cell number and the percentage of pro/pre and immature B cells in all samples using flow cytometry. Here we see that IL-6 has no direct effect on pro/pre B cells *in vitro*, while it promoted the survival or proliferation of immature B cells. (Figure 2C).
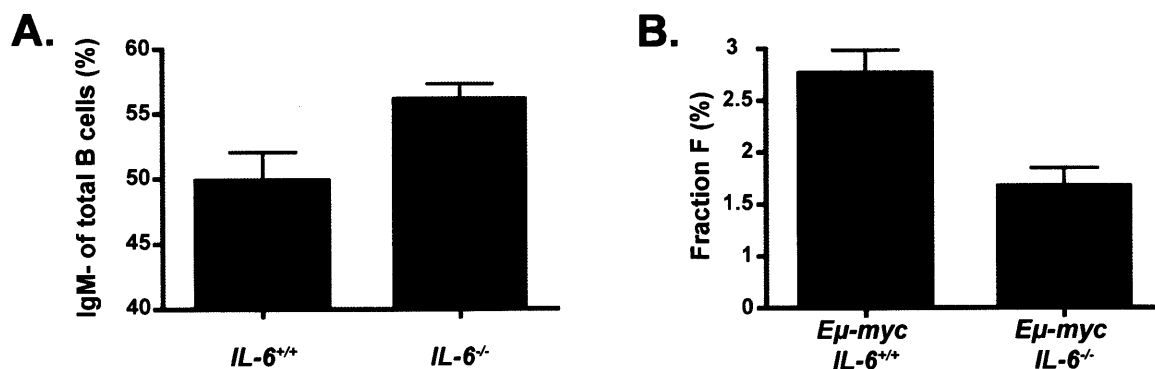
Supplemental Figure 2. IL-6 promotes specific B cell development transitions. (A) A bar graph representing the percentage of IgM- B cells as a fraction of the total B cell population in $IL-6^{+/+}$ (n=15) and $IL-6^{-/-}$ (n=44) mice. The data are represented as mean ± SEM. **(B)** A graph showing the percent of Hardy Fraction F (CD19+/B220^{Hi}) within the bone marrow of $IL-6^{+/+}$ Eμ-Myc (n=6) and

IL-6$^{-/-}$ Eµ-Myc (n=4) mice. The data are represented as mean ± SEM.

To more formally address the possibility that the B cell maturation defect we see in *IL-6$^{-/-}$* mice results from a defect in the B cell progenitor population, we performed a pre-B cell methylcellulose colony formation assay. In this assay, cells from *IL-6$^{-/-}$* or wild-type bone marrow are tested for their ability to form colonies of pre/pro-B cells in the presence or absence of recombinant IL-6. Here, we observed that bone marrow cells from *IL-6$^{-/-}$* and wild-type mice produced the same number of colonies, suggesting that there is no defect in B cell progenitor cell number or function in *IL-6$^{-/-}$* mice (Figure 2D). The addition of recombinant IL-6 to either *IL-6$^{-/-}$* or wild-type bone marrow resulted in a two-fold increase in colony number, demonstrating that paracrine IL-6 can directly promote a minor survival benefit to B cell progenitor cells *in vitro*. Together these data suggest that IL-6 promotes B cell differentiation and survival, and that the accelerated tumorigenesis seen in *IL-6$^{-/-}$ Eµ-myc* mice may occur due to defects in B cell development. These data are consistent with multiple reports showing that the predominant cell of origin in the *Eµ-myc* mouse is a committed B cell progenitor (257-260).

IL-6 loss results in systemic changes to the bone marrow microenvironment which indirectly block B cell development

The minimal survival benefit conferred by IL-6 on immature B cells *in vitro* suggested that perhaps other factors that promote B cell development in the bone marrow microenvironment were altered in *IL-6$^{-/-}$* mice. To determine

whether IL-6 deficiency could indirectly affect B cell development we measured

the levels of 32 cytokines, chemokines and growth factors within the bone

marrow of wild-type and $IL-6^{-/-}$ mice. Interestingly, $IL-6^{-/-}$ mice showed

significantly decreased levels of IL-1α, IL-1β, IL-10, IL-12, IL-13, IL-15, G-CSF

and GM-CSF when compared with control mice, while the levels of the remaining

24 factors were unchanged (Figure 3A and Supplemental Table S1). This

suggests that IL-6 acts as a key upstream regulator of the bone marrow

microenvironment and promotes expression of diverse molecules implicated in

many biological processes, including monocyte development, T and B cell

development or effector function, and the regulation of inflammation.
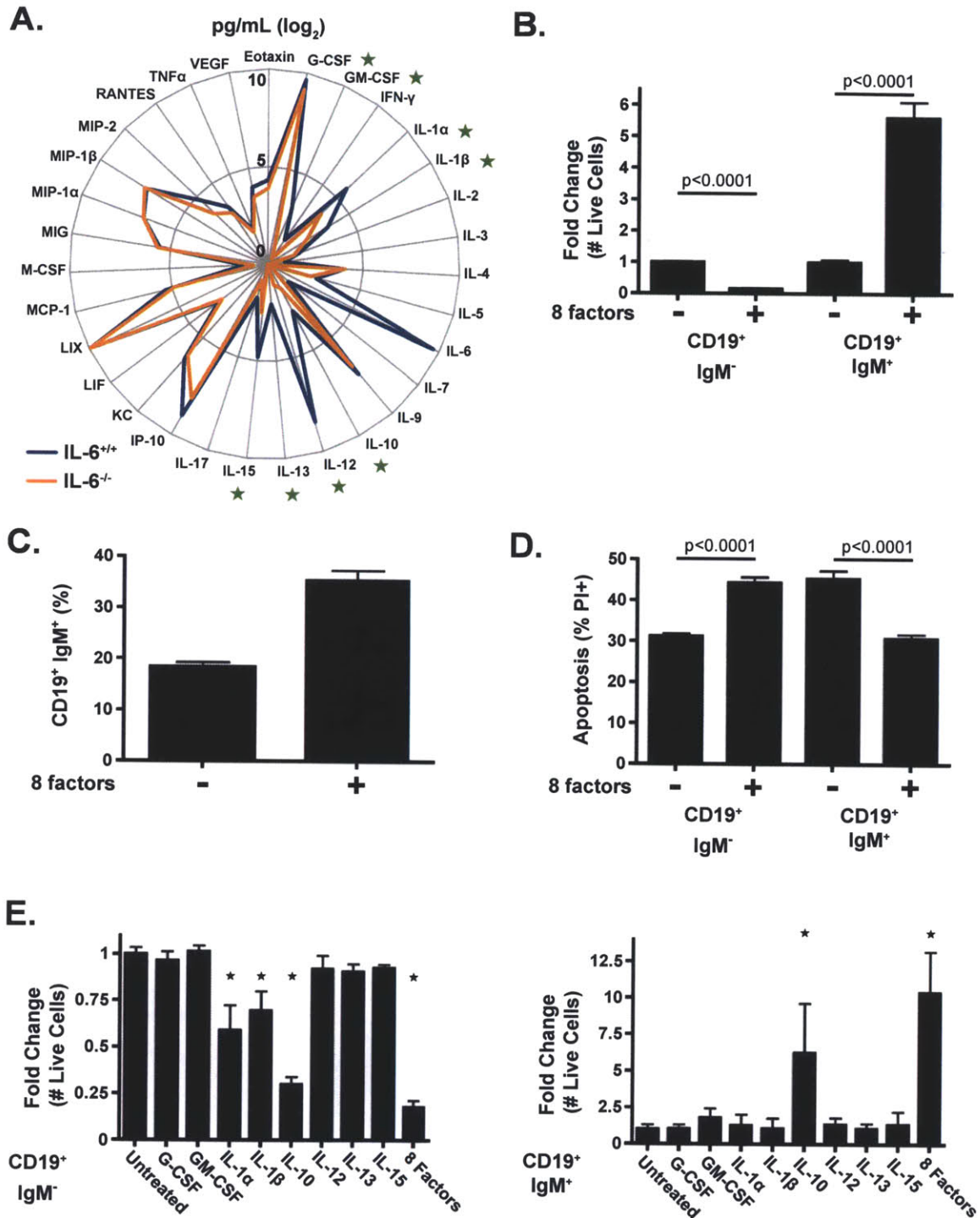
Figure 3. The absence of IL-6 alters the bone marrow microenvironment to indirectly reduce pre/pro to immature B cell maturation. (A) A radar chart displaying the concentrations of 32 cytokines and chemokines in the bone marrow of *IL-6*$^{+/+}$ (n=16) and *IL-6*$^{-/-}$ (n=18) mice. The concentrations are displayed as log$_2$ transformed pg/mL. Significant differences between *IL-6*$^{+/+}$ and *IL-6*$^{-/-}$ bone marrow concentrations are demarcated with stars (p<0.01). **(B)** A bar graph showing the fold change in live CD19$^+$/IgM$^-$ and CD19$^+$/IgM$^+$ B cells FACS

146

sorted and grown for 72 hours with IL-7 and SCF in the presence or absence of the 8-factor cocktail. The data are represented as mean ± SD (n=9 for 3 independent experiments). **(C)** A graph depicting the percentage of maturing CD19$^+$/IgM$^+$ B cells in a FACS sorted population of CD19$^+$/IgM$^-$ B cells after 72 hours *in vitro* with IL-7 and SCF, with or without the 8-factor cocktail. The data are represented as mean ± SEM (n =3 independent experiments). **(D)** A graph showing the percent of basal apoptosis in pure populations of CD19$^+$/IgM$^-$ and CD19$^+$/IgM$^+$ B cells, FACS sorted and grown for 72 hours with IL-7 and SCF in the presence or absence of the 8-factor cocktail. The data are represented as mean ± SEM (n =9 for 3 independent experiments). **(E)** Two bar graphs showing the fold change in cell number for pure populations of CD19$^+$/IgM$^-$ (left) and CD19$^+$/IgM$^+$ (right) B cells, FACS sorted and grown for 72 hours with IL-7 and SCF with the indicated recombinant proteins. The data are represented as mean ± SD (n ≥ 3 for 3 independent experiments ★ denotes p≤0.005).

Since several of the eight factors depleted in the absence of IL-6 are reported to regulate B cell biology, we next examined whether these factors affect B cell development or survival *in vitro*. Whole bone marrow from wild-type mice was harvested and plated with IL-7 and SCF on a bone marrow stromal cell feeder population (BMSC). Cells were then either left untreated or treated with recombinant IL-1α, IL-1β, IL-10, IL-12, IL-13, IL-15, G-CSF and GM-CSF, as an eight factor cocktail. 72 hours later, we measured both pro/pre- and immature B cell percentage within the culture, as well as the total cell number, to determine the absolute change in B cell representation. Notably, the eight-factor cocktail robustly reduced the number of pro/pre-B cells, while increasing the number of immature B cells (Supplemental Figure 3A). Thus, IL-6 deficiency results in profound changes in the bone marrow microenvironment that both directly and indirectly prevent B cell maturation.

To determine whether B cell maturation defects were due to a direct effect of these eight factors on B cells, we sorted pro/pre- or immature B cells from the bone marrow of wild type mice and plated cells with IL-7 and SCF either with or without a BMSC layer. Cells were then either left untreated or treated with the 8 factors in combination. Interestingly, in both assays, the eight-factor cocktail directly promoted both immature B cell survival and an increased immature to pro/pre B cell ratio (Figure 3B and Supplemental Figure 3B). As this phenotype could result either from changes in B cell survival or differentiation status we examined B cell maturation following addition of the eight-factor cocktail to pro/pre-B cells *in vitro*. In this context, the eight-factor cocktail directly promoted pro/pre-B cell maturation into immature B cells (Figure 3C). Notably, we also observed that addition of the eight-factor cocktail directly promoted pro/pre-B cell death, while reducing basal immature B-cell death (Figure 3D). Thus, the eight-factor cocktail promotes the survival of immature B cells, while it promotes cell death and differentiation of pro/pre-B cells.
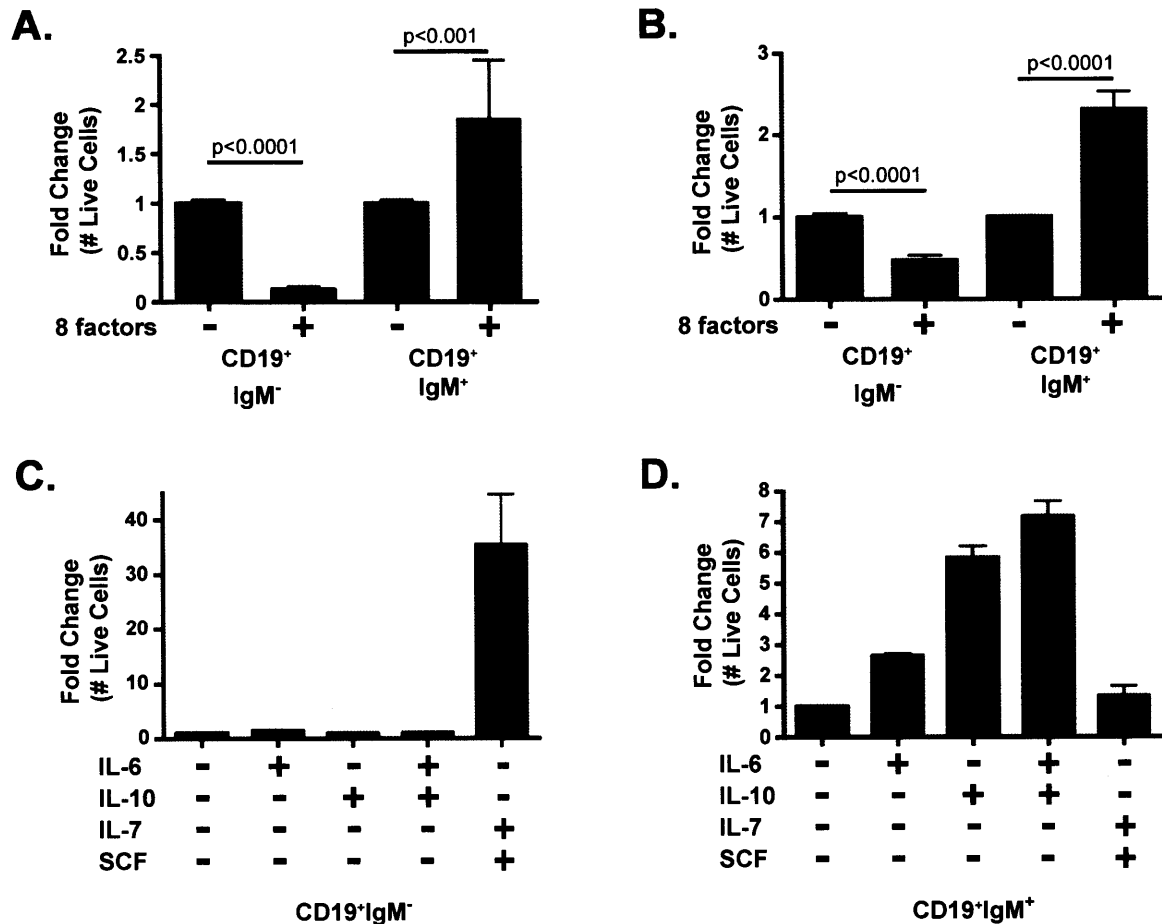
Supplemental Figure 3. B cells rely on distinct sets of survival factors at the pre/pro to immature B cell transition. (A) A bar graph showing the fold change in live $CD19^+/IgM^-$ and $CD19^+/IgM^+$ B cells in whole bone marrow from wild type mice harvested and grown for 72 hours with IL-7 and SCF in the presence or absence of the 8-factor cocktail on a BMSC feeder layer. The data are represented as mean $\pm$ SD (n=9 for 3 independent experiments). **(B)** A graph depicting the fold change in live $CD19^+/IgM^-$ and $CD19^+/IgM^+$ B cells FACS sorted and grown for 72 hours with IL-7 and SCF in the presence or absence of the 8-factor cocktail on a BMSC feeder layer. The data are represented as mean $\pm$ SD (n=12 for 4 independent experiments). **(C)** A graph showing the fold change in live cell number in $CD19^+/IgM^-$ B cells FACS sorted and grown for 72 hours with the indicated cytokines. The data are represented as mean $\pm$ SD (n$\geq$10 for 3 independent experiments). **(D)** A bar graph of the fold change in live cell number in $CD19^+/IgM^+$ B cells FACS sorted and grown for 72 hours with the indicated cytokines. The data are represented as mean $\pm$ SD (n$\geq$3).

To examine which of these eight factors was responsible for these B cell phenotypes, we again sorted pro/pre- or immature B cells and plated cells in

149

recombinant IL-7 and SCF. Cells were then treated with each component from the eight-factor cocktail as individual recombinant proteins. 72 hours later, we measured the effect of each protein on pro/pre- or immature B cell growth and survival. Here we observed that IL-1α, IL-1β and IL-10 decreased pre/pro-B cell survival, but, interestingly, IL-10 alone was able to phenocopy the effects of the eight-factor cocktail on both pre/pre- and immature B cells (Figure 3E). Thus, IL-10 exerts distinct effects on cells at different stages of B cell development, promoting pro/pre-B cell death and immature B cell survival. Further, we observed that IL-6 and IL-10 promote immature B cell survival but not pre/pro B cell survival *in vitro* in an additive manner, suggesting that these two proteins may activate distinct downstream survival pathways (Supplemental Figure 3C-D). Thus, IL-6 deficiency results in decreased levels of multiple factors, some of which promote B cell maturation and survival at the pre/pro- to immature B cell transition.

Impaired B cell development promotes the survival of premalignant B cells

Previous work in the *Eu-myc* model has shown that precursor B cells show enhanced resistance to Myc-induced apoptosis and are the cells of origin for many *Eu-myc* lymphomas (257-260). In the *Eu-myc* model, induction of *myc* transcription in pro/pre B cells following rearrangement of the heavy chain locus results in a drastic increase in the number of pro/pre B cells and large decrease in the number of immature B cells due to apoptosis. Thus, we reasoned that if the combination of IL-1α, IL-1β, IL-6 and IL-10 promotes pro/pre B-cell differentiation

into immature B cells, then *IL-6$^{-/-}$ Eu-myc* mice should have fewer apoptotic B

cells than *IL-6*-proficient *Eu-myc* mice. To test this hypothesis, we examined

basal cell death in the B cell compartment of pre-malignant mice. Using flow

cytometry, we observed that *IL-6$^{-/-}$ Eμ-myc* mice display, on average, two-fold

fewer apoptotic B cells than *IL-6*-proficient Eu-*myc* mice, while there was no

difference in the steady-state levels of B cell death between wild-type and *IL-6$^{-/-}$*

mice (Figure 4A). These data are consistent with a model by which impaired B

cell development, associated with the combined loss of IL-6 and a decrease in

IL-1α, IL-1β and IL-10 levels, leads to increased numbers and enhanced survival

of early B cells and accelerated lymphomagenesis.
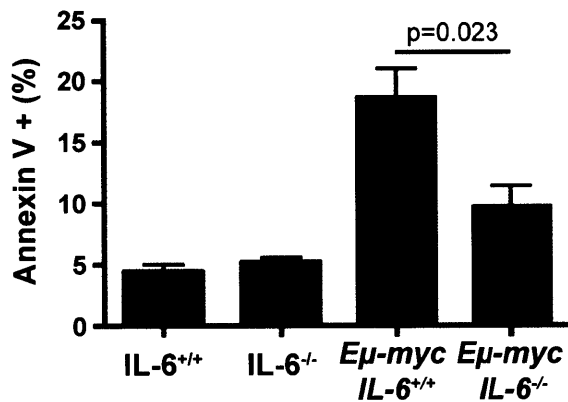
Figure 4. IL-6 induces B-cell apoptosis during *Eμ-Myc* lymphomagenesis. A graph depicting the percentage of Annexin V$^+$ B cells *in vivo* in the bone marrow of *IL-6$^{+/+}$* (n=18), *IL-6$^{-/-}$* (n=20), *IL-6$^{+/+}$ Eμ-Myc* (n=14) and *IL-6$^{-/-}$ Eμ-Myc* (n=7) mice. The data are represented as mean ± SEM.

IL-6 promotes hematopoietic stem cell survival *in vitro* and *in vivo*

Given a role for IL-6 in B cell differentiation and tumor suppression, we next sought to investigate the mechanism underlying *delayed* tumor development following adoptive transfer of *Eu-myc* stem cells into *IL-6$^{-/-}$* recipient mice. A major experimental difference between germ line and adoptive transfer models is the requirement for hematopoietic stem cells (HSC) to engraft and expand in the transplant model. Recent work has shown paracrine factors such as TNFα are important modulators of HSC reconstitution, although they have no effect on steady state HSCs (265). Since IL-6 has been shown to promote cell survival *in vivo* in multiple experimental models, we asked whether IL-6 promotes HSC survival under stress *in vitro*. (159,161,203,262,266). Whole bone marrow from wild type mice was plated in culture in the presence or absence of recombinant IL-6. Cells were then either left untreated or treated with four Gray irradiation. 24 hours following irradiation, all samples were analyzed by flow cytometry for hematopoietic stem and progenitor cell number (HSPC - here defined as Lin$^-$ Sca1$^+$c-kit$^+$). Here, IL-6 promoted the acute survival of HSPC in response to both culture stress and DNA damage associated with irradiation (Figure 5A-B).

To determine whether IL-6 similarly promotes HSC survival *in vivo*, we administered a sub-lethal dose of irradiation to wild type and *IL-6$^{-/-}$* mice. Mice were then monitored for signs of bone marrow failure. While wild type mice survived irradiation, 60% of *IL-6$^{-/-}$* mice developed terminal illness due to bone marrow failure (Figure 5C). Thus, IL-6 promotes HSPC survival *in vitro* and *in vivo*. Interestingly IL-6 also regulates basal HSPC homeostasis *in vivo*, as *IL-6$^{-/-}$*

152

mice displayed an expanded HSPC pool relative to wild type mice. This expansion is characteristic of HSPC dysfunction and eventual exhaustion (Figure 5D). Interestingly, it has previously been reported that $IL-6^{-/-}$ HSCs show impaired renewal capacity in a serial competitive HSC reconstitution assay (267). These data suggest that IL-6 deficiency results in impaired HSC engraftment and expansion – a defect that likely impairs the outgrowth of tumor-promoting stem cells following adoptive transfer.
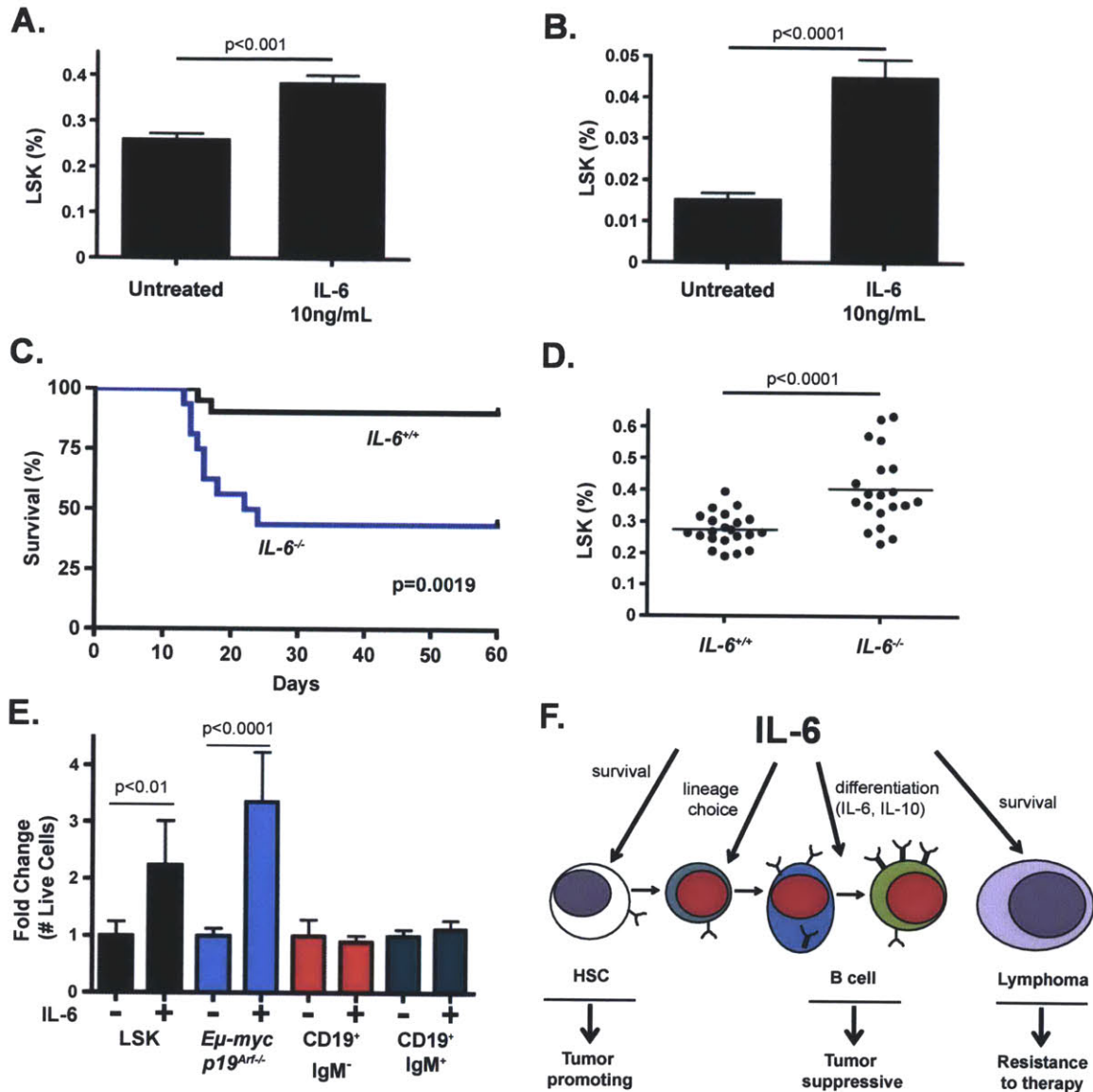
Figure 5. *IL-6* **status impacts hematopoietic stem cell survival** *in vitro* **and** *in vivo*. **(A)** A graph depicting the percent of Lineage⁻ Sca-1⁺ Kit⁺ (LSK) cells within a population of whole bone marrow cells treated with or without IL-6 for 24 hours. The data are represented as mean ± SEM (n=6 independent experiments). **(B)** A graph depicting the percent of LSK cells within a population of whole bone marrow cells irradiated with 4gy and treated with or without IL-6 for 24 hours. The data are represented as mean ± SEM (n=6 independent experiments). **(C)** A Kaplan-Meier curve showing post irradiation survival of *IL-6*⁺/⁺ (n=21) and *IL-6*⁻/⁻ (n=16) mice. All mice were treated with 7.2 Gray of irradiation in a single dose. The p value was calculated using a log rank test. **(D)** A dot plot showing the percent of LSK cells in the bone marrow of *IL-6*⁺/⁺ (n=22) and *IL-6*⁻/⁻ (n=20) mice. Each dot represents an individual mouse, with a line demarcating the mean for each cohort. **(E)** A graph showing the fold change in live LSK, *Eμ-Myc p19*^Arf-/-, CD19⁺/IgM⁻ and CD19⁺/IgM⁺ B cells at 48 hours following irradiation with or

154

without 10ng/mL IL-6. The data are represented as mean ± SEM (n ≥ 3 for 2 independent experiments). **(F)** A model for the stage-specific effects of IL-6 during normal and neoplastic B cell development. IL-6 promotes the survival of stem and tumor cells, the lineage commitment choice of bi-potential committed progenitor cells (268) and the differentiation of pre/pro B cells.

Cancer cells co-opt stem cell survival signals

Numerous studies have described similarities between adult stem cells and tumor-initiating cells. Factors such as Wnt, Hedgehog and Notch promote self-renewal in adult stem cells within adult stem cell niches and in tumor-initiating cells within certain tumor microenvironments. It is less well understood whether most cancer cells co-opt survival factors important for stem cell survival and tissue regeneration following damage. To more carefully examine contexts in which IL-6 functions as a survival factor, we sorted HSPC, pro/pre-B cells, immature B cells and *Eμ-Myc* lymphoma cells. Each cell type was plated in normal growth media with or without IL-6 and then left untreated or irradiated at a dose in which 95% of each cell type dies in the absence of IL-6. Notably, IL-6 promoted HSPC and lymphoma cell survival following irradiation, while normal B cells were equally sensitive to irradiation in the presence and absence of IL-6 (Figure 5E). Thus, transformed cells can gain responsiveness to survival signals used by stem cells, while this protective buffer is lost during normal B cell development. This suggests that a balance of tumor suppression and tissue regeneration occurs in which IL-6 promotes stem cell expansion, B cell differentiation and tumor cell survival.

Discussion

155

IL-6 is a pro-inflammatory cytokine critically required to orchestrate the immune response to viral and bacterial pathogens and for induction of the acute phase response (157,160,269,270). It is less well understood how IL-6 promotes normal tissue homeostasis and response to non-infectious tissue damage. IL-6 has been shown to promote T cell survival, both basally and in response to DNA damage (159,203). IL-6 is also a critical survival factor for plasma cell maturation and for the pathogenesis of plasma cell tumors (171,178,262,271,272). In non-hematopoietic tissues, IL-6 similarly promotes both cellular survival and tissue repair. For example, IL-6 plays a critical role in liver regeneration, fibrosis and hepatocellular carcinoma tumorigenesis and has recently been implicated in resistance to therapy in both hepatocellular carcinoma and non-small-cell lung cancer (73,150,161,168,169,273).

Here, we have uncovered a new role for IL-6 as a paracrine signal required for the survival and development of multiple hematopoietic cell types. IL-6 deficient mice are dramatically more sensitive to bone marrow failure following irradiation than their wild-type counterparts, and IL-6 acts to directly promote HSPC survival *in vitro*. IL-6 also promotes immature B cell and B cell progenitor cell survival, but not the survival of the intermediates between these two cell types. This suggests that cells within the same developmental lineage vary in their responsiveness to IL-6 as a pro-survival cue. Furthermore, in the bone marrow, IL-6-deficient mice show a dramatic decrease in key molecules that promote myeloid development, B cell maturation and inflammation. Our work and

recent work from others suggest that normal and malignant development within the myeloid and lymphoid lineages is dynamically controlled by IL-6 in a stage- and oncogene-specific manner (268,274). Thus, IL-6 signaling is significantly more complex than anticipated, with context-specific information dictating how this pleiotropic cytokine affects the survival and maturation of hematopoietic cells.

Proper differentiation and survival of developing hematopoietic cells within the bone marrow microenvironment requires the input of multiple paracrine signals. For example, during B cell development paracrine IL-7, SCF and Flt-3 ligand are required for pro-B cell differentiation (261). To ensure directional development, paracrine developmental factors often form positive feed-forward loops during differentiation. IL-7 induces the transcription of EBF1 and, indirectly, Pax5, and these transcription factors together induce and maintain their own expression and B cell lineage commitment (152,275). Here, we identify IL-10 as a key pro-differentiation factor critically important for the pro/pre to immature B cell transition and for survival of immature B cells *in vitro*. IL-6-deficient mice have a developmental block in the B cell lineage, in part due to loss of IL-6, but also due to dramatically decreased IL-10 levels. Thus, the absence of a pleiotropic extracellular ligand such as IL-6 causes widespread changes in the bone marrow, resulting in multiple direct and indirect survival and differentiation defects.

In all stages of B cell development, genetic alterations that inhibit

developmental progression can promote tumorigenesis. Deregulation of genes

encoding B cell transcription factors such as Ikaros, Ebf1, Pax5, Bcl-6 and

Blimp1 all inhibit B cell development and promote leukemia or lymphoma

development (276-280). Here, we show that cell non-autonomous alterations to

the tumor microenvironment that block B cell maturation can also promote

lymphoma development. Thus, normal B cell development requires integration of

multiple paracrine signals that promote feed-forward transcriptional commitment

to the B cell lineage, and alterations to this process accelerate tumor

development (281). Notably, while IL-6 does not directly affect B cell survival

during the developmental stage associated with transformation in this model, we

see that B lymphoma cells can evolve to co-opt tissue-specific stem cell survival

factors. Specifically, following transformation, IL-6 signaling can promote survival

in response to apoptotic stress. Thus, tumor cells can co-opt mechanisms of

stem cell survival. This result is consistent with previous work showing that

lymphomas readily adapt stem cell characteristics, including high engraftment

rates in transplant experiments (282).

Mouse models of hematopoietic malignancy have provided deep insight

into the biology of leukemias and lymphomas (283). These models are

experimentally tractable, as stem cells and tumors can be transplanted into large

cohorts of syngeneic recipient mice to study both tumor development and

response to therapy. Here we have used both autochthonous and transplant

experiments to interrogate whether IL-6 affects lymphomagenesis in *Eμ-myc* mice. Surprisingly, these two tumor approaches yielded apparently conflicting results – providing a unique example of a paracrine factor that can either promote or delay tumor onset in the same tumor model. These data support the idea that cell non-autonomous factors can have indirect and unexpected roles in shaping the tumor microenvironment, particularly if they act on multiple cell types or at multiple stages during development. Additionally, this work suggests that chimeric or transplant-based mouse models need to be viewed with particular caution in dissecting the role of paracrine factors during oncogenic transformation.

Acknowledgements

Experimental Procedures

Mice

C57BL/6 *Eμ-Myc* and C57BL/6 *IL-6*$^{-/-}$ mice were purchased from Jackson

Laboratories. *Eμ-Myc* and *IL-6⁻/⁻* mice were crossed to generate *Eμ-Myc IL-6⁻/⁻* mice. For the *Eμ-Myc* fetal HSC transplant model, C57BL/6 female mice were mated to C57BL/6 *Eμ-Myc* males. At E13.5 pregnant female mice were sacrificed and individual fetal livers were manually dissociated and frozen. 5 hours prior to transplantation, C57BL/6 *IL-6⁺/⁺* and C57BL/6 *IL-6⁻/⁻* recipient mice were irradiated with 8.5 Gray. All mice were then tail vein injected with 2 million freshly thawed *Eμ-Myc* fetal liver cells. All mice were monitored for tumor onset by palpation. For the bone marrow failure assay, 6-8 week old C57BL/6 *IL-6⁺/⁺* and C57BL/6 *IL-6⁻/⁻* mice were irradiated with 7.2 Gray using a 137^{Cs} irradiator (Gamma cell 40) at a dose rate of approximately 70 cGy/min. All mice were closely monitored for signs of bone marrow failure. The MIT Department of Comparative Medicine approved all procedures described in this work.

Cell culture and chemicals

B cells, *Eμ-Myc* and *Eμ-Myc;p19^Arf-/-* mouse B cell lymphomas were cultured in B cell medium (45%DMEM/45% IMDM/10% FBS, supplemented with 2mM L-glutamine and 5μM β-mercaptoethanol). B cell cultures also contained 10ng/mL of IL-7 and SCF (Peprotech). Bone marrow derived stromal cells were used as feeder cells for the B cells. HSPC's were cultured in X-VIVO 10/10% FBS (Lonza). IL-6 and all other recombinant proteins were used at 10ng/mL (Peprotech).

Hematopoietic Cell Sorting and Analysis by Flow Cytometry

Whole bone marrow (BM) from the tibia and femur of 6-8 week old C57BL/6 IL-$6^{+/+}$ or C57BL/6 IL-$6^{-/-}$ mice was flushed into B cell media or X-VIVO 10 media and manually dissociated. BM was filtered through a 35µM cell strainer and washed once in PBS/10% FBS. BM was then stained in PBS/10% FBS for 1 hour at room temperature. HSPCs were analyzed and sorted as the Sca1$^+$/cKit$^+$/Lineage$^-$ fraction of bone marrow. The lineage cocktail of antibodies included α-B220, α-CD3, α-CD4, α-CD8, α-CD11b, α-CD11c, α-CD19, α-GR-1, α-Ter119. To sort and analyze B cells, whole bone marrow was stained with α-CD19 and α-IgM. The CD19$^+$ fraction was used to define all B cells and then gated as IgM$^+$ or IgM$^-$ to separate immature B cells from pro/pre B cells. This same designation was used to define B cell lymphoma developmental status. All antibodies for flow cytometry were purchased from BD Bioscience or eBioscience and used at 0.05mg/mL. To analyze apoptosis rates *in vivo* annexin V staining (eBioscience) was performed on whole bone marrow from individual mice according to the manufacturers protocol. All flow cytometry cell sorting was performed using either a FACS Aria II or MoFlo II (BD Biosciences and Beckman Coulter). All flow cytometry analysis was performed using a FACS Scan or LSR II (BD Biosciences).

In Vitro Viability and Cell Growth Assays

For the pre-B cell methylcellulose colony formation assay, BM from 6-8 week old female C57BL/6 IL-$6^{+/+}$ or C57BL/6 IL-$6^{-/-}$ mice was isolated, and the colony formation assay was performed as described by the manufacturer

(Stemcell Technologies). For all *in vitro* cell growth and survival assays, BM from 6-8 week old female C57BL/6 *IL-6$^{+/+}$* or C57BL/6 *IL-6$^{-/-}$* mice was isolated and FACS sorted as described above. For all B cell assays, 250,000 FACS sorted CD19$^+$/IgM$^-$ or CD19$^+$/IgM$^-$ cells were plated and treated *in vitro* as described and analyzed 72 hours later for cell number and developmental status. For the comparative irradiation experiment HSPC, pro/pre and immature B cells were sorted from the BM of wild type mice as described above. 10,000 of each of the 4 cell types were plated in a 96 well plate and irradiated with 2.5 (HSPC and B cells) or 3.5 Gray(*Eμ-Myc;p19$^{Arf-/-}$*). Live cell number was measured by FACS analysis 48 hours following irradiation.

Luminex Cytokine Measurements

Bone marrow from individual mice was flushed from a single femur and tibia into B cell media. Bone marrow was manually dissociated and allowed to condition media for 3 hours at 37°C. Samples were concentrated using Amicon Ultracel 3k centrifugal filters. All sample values were normalized by weight and concentration factor. Multiplexed luminex assays for chemokine and cytokine levels were preformed as described by the manufacturer by Eve Technologies.

Statistical Analysis

Statistical analysis was performed using GraphPad Prism4 software. Two-tailed Student's t tests were used, as indicated. Error bars represent mean ± SEM or STDEV as noted. For comparison of Kaplan-Meier survival curves, a log-

rank test was used. A Chi-squared test was used to evaluate *Eμ-Myc* and *IL-6*^{-/-}

Eμ-Myc differentiation status.

	IL-6+/+		IL-6-/-	
	Average (pg/mL)	Standard Deviation	Average (pg/mL)	Standard Deviation
Eotaxin	21.36	7.77	15.60	6.36
G-CSF	883.83	380.25	600.60	183.97
GM-CSF	9.42	4.25	2.10	3.38
IFN-γ	n.d.		n.d.	
IL-1α	59.94	31.41	21.15	12.89
IL-1β	13.68	4.34	6.09	2.71
IL-2	3.72	1.36	2.97	1.57
IL-3	n.d.		n.d.	
IL-4	17.64	7.34	18.30	9.35
IL-5	8.58	5.26	6.09	2.08
IL-6	927.57	595.29	n.d.	
IL-7	n.d.		n.d.	
IL-9	198.24	150.21	134.82	82.04
IL-10	7.02	2.27	3.21	2.19
IL-12 (p40)	n.d.		n.d.	
IL-12 (p70)	65.37	19.09	2.85	5.03
IL-13	6.78	7.94	n.d.	0
IL-15	30.69	15.41	11.58	12.56
IL-17	n.d.		n.d.	
IP-10	667.83	681.44	558.27	385.23
KC	103.44	61.24	84.45	42.98
LIF	9.9	4.46	9.48	6.72
LIX	1161.6	595.09	1079.91	549.41
MCP-1	42.57	13.864	32.76	13.89
M-CSF	3.15	2.38	2.19	2.318
MIG	50.94	23.41	53.76	28.45
MIP-1alpha	107.28	35.81	104.58	21.76
MIP-1beta	161.67	59.61	167.07	41.18
MIP-2	34.50	19.88	20.28	18.05
RANTES	12.06	3.99	9.45	2.40
TNF-alpha	4.50	2.37	3.87	1.38
VEGF	17.49	7.84	12.51	5.78

Supplemental Table S1. A table showing the average concentration and standard deviation (in pg/mL) for each protein measured by luminex in conditioned media derived from the bone marrow of $IL-6^{+/+}$ (n=16) and $IL-6^{-/-}$ (n=18) mice. n.d. indicates not detectable.

Chapter 6:

Discussion

Most cancers are clonal in origin with the primary tumor originating in a single organ (44). At later stages this primary tumor often disseminates to other organs where these cancer cells can form macro or micro metastases. In leukemia and lymphoma, cancer cells are detected in both hematopoietic and non-hematopoietic organs (284). This results in a clinical reality in which cancer patients can present with not one but many tumor microenvironments, each with an organ-specific tumor microenvironment comprised of a unique composition of immune, stromal and endothelial cells (285). It is well established that the presence of detectable metastases correlates with poor prognosis. Yet, how the initial presentation of tumor cells in many tumor microenvironments can so adversely affect the ultimate response to conventional chemotherapies is poorly understood. This thesis has attempted to use the $E\mu$-Myc mouse as a mouse model of disseminated disease to model drug resistance to the conventional chemotherapeutic agent doxorubicin. We see that the tumor microenvironment can promote drug resistance in unexpected ways. Here endothelial cells are activated by DNA damage to induce a cytoprotective secretory phenotype.

Stress-Induced Secretory Phenotypes

In settings where chemotherapies show efficacy, drug-induced antitumor activity occurs rapidly following therapeutic administration. Thus, for a secretory response to affect therapeutic response, it must occur acutely. This is particularly true for hematopoietic malignancies, where tumor clearance frequently occurs within 24 to 48 hours of treatment. In this thesis I have presented our work on an acute secretory phenotype that is induced following DNA damage. In the thymus, doxorubicin induces the acute release of at least 10 cytokines and chemokines. We chose to focus on two proteins, IL-6 and Timp-1, which promote lymphoma cell drug resistance both *in vitro* and *in vivo*. Here we see that both human and mouse endothelial cells secrete IL-6 and Timp-1 within 24 hours of treatment, suggesting that this secretory response is engaged rapidly enough to influence tumor response to therapy. As a proof of this concept, I have shown that IL-6 release induced by doxorubicin promotes the survival of *Eµ-Myc* lymphoma cells in the thymus. We do not fully understand the specificity of IL-6 induction in the thymus. We do see IL-6 induction in other organs such as the kidney and blood but not the spleen or liver. Why organ specific endothelial cells might respond to DNA damage and release IL-6 in some contexts but not others is unclear. The field of vascular biology is just now beginning to understand the functional diversity in vascular and lymphatic endothelial cells. As a conceptual advance in cancer therapy, we would place less emphasis on the *Eµ-Myc* lymphoma model, the thymus and IL-6 or Timp-1, but instead emphasize that our work is only one example of the idea that normal cells respond to damage associated with systemic chemotherapy to remodel normal and tumor microenvironments.

Mechanistically, in all conditions tested, induction of DNA double-strand breaks causes acute IL-6 release from endothelial cells, suggesting this process is not specific to doxorubicin. However, it is unclear which DNA-damage-responsive kinases activate p38α and induce IL-6 release. We see that activation of ATM, the canonical DNA-damage kinase activated by double-strand breaks, is dispensable for this process, suggesting that signaling downstream of DNA-PK, ATR or ATX must be required. Not all cytotoxic compounds induce IL-6 release from endothelial cells, suggesting this is not a general stress or apoptotic response. Here we see that spindle poisons, which do not induce DNA double-stranded breaks, do not induce IL-6 release. Accordingly, if we treat the *Eμ-Myc* lymphoma model with vincristine we do not see surviving lymphoma cells in the thymus. Thus, endothelial cells sense DNA double-strand breaks and induce a secretory response.

We also provide evidence that this acute secretory response is a physiologic stress response to damage. Here we see that the induction of IL-6 promotes the survival of both T cells in the thymus and hematopoietic stem cells in the bone marrow. The process of T cell recovery following induction of thymocyte cell death has been named thymic rebound. To our knowledge, IL-6 is the first factor identified to promote thymic survival and rebound following irradiation. Two other reports have shown that Flt-3 ligand and IL-22 are induced in the thymus following irradiation and promote the proliferation of newly

167

immigrated thymic progenitor cells, but the kinetics of this process are much slower than the survival phenotype we see for IL-6 (286, 287). This suggests that in the thymus there may be two temporally distinct processes that promote survival and regeneration, respectively. While many factors have been shown to be required for adult stem cell maintenance, few have been identified that promote adult stem cell survival following tissue damage. Here we identify IL-6 as one such factor, which directly promotes hematopoietic stem cell survival following DNA damage both *in vitro* and *in vivo*.

The acute-stress–associated phenotype (ASAP) is distinct from reported secretory phenotypes that are more indirectly engaged in response to DNA damage, such as the senescence-associated secretory phenotype (SASP). Diverse forms of stress induce senescence in untransformed cells, including oncogene activation, telomere erosion and DNA damage. Senescence is best defined functionally as a permanent cell-cycle arrest (288). Processes resembling senescence have been observed in many settings *in vivo* and senescence occurs during the aging process, tumorigenesis and chemotherapy (78,253,289). Recently, several groups have identified a secretory process associated with both oncogene and DNA-damage-induced senescence (140-143). Here IL-6 and IL-8 function as autocrine tumor suppressors, as they are required to maintain senescence. The SASP develops gradually over the course of 5 to 8 days and occurs only after established markers of senescence are detected. However, because apoptosis in treated hematopoietic cancers occurs

within 72 hours of treatment, a more rapid release of pro-survival factors would likely be essential to affect therapeutic outcome. This does not preclude a SASP from influencing therapeutic efficacy, but its relevance may be restricted to settings such as metronomic chemotherapy or fractional radiotherapy, in which therapy is applied in an ongoing manner over a period of days (290, 291).

Thus, the ASAP represents a microenvironment-specific stress response in which endothelial cells sense DNA damage and acutely activate a cytoprotective secretory program, protecting both normal and tumor cells in the thymus from apoptosis. Of note, distinct chemotherapeutics have been shown to engage in acute pro-tumorigenic processes in other settings. For example, treatment with paclitaxel, but not gemcitabine, can promote tumor angiogenesis through the mobilization and recruitment of bone marrow–derived endothelial cells to tumors (125,126). This process is mediated by an acute drug-mediated release of systemic SDF-1α. Thus, tumor cells can co-opt general stress-induced secretory responses that presumably have evolved to promote normal tissue repair and regeneration, to survive and progress after administration of frontline chemotherapy.

Our understanding of how the ASAP is regulated in endothelial cells is incomplete. This process is dynamic, suggesting negative regulation of IL-6 release and possibly the repression of a SASP-like process following the onset of senescence in endothelial cells. To better understand these processes we are

performing a chemical screen and a genetic screen in an arrayed format, which will measure IL-6 levels and cell death in endothelial cells untreated or treated with doxorubicin. Here we will use a 40,000 compound chemical library and a validated 2500 shRNA lentiviral library. We are also performing the same screens in the FOCUS cells to better understand the SASP. We hope this approach will allow us to integrate new genetic and chemical data with our existing data and that of others to better understand both the ASAP and SASP. The end goal of this work is to provide candidate genes for the development of novel therapeutic agents targeting pro-survival signaling within the tumor microenvironment.

The relevance of thymic tumor persistence in the *Eµ-Myc* model to therapeutic response in human tumors remains unclear. Of note, a subset of lymphoma patients do present with primary BCLs in the thymus. Mediastinal (thymic) diffuse large BCL (Med-DLBCL) is a highly aggressive disease that accounts for 5% to 10% of all DLBCLs (284). Med-DLBCL is treated with conventional chemotherapeutic regimens, all of which include anthracyclines such as doxorubicin. Although the question of how Med-DLBCLs respond to frontline chemotherapy relative to other DLBCLs remains somewhat controversial, our data suggest that counteracting IL-6 function may improve Med-DLBCL patient outcome (292). Below I will discuss our hypotheses on how our work understanding pro-survival signaling in the *Eµ-Myc* model can be applied to other types of cancer.

Enhancing Chemotherapeutic Efficacy by Targeting Pro-survival Signaling

The idea that tissue damage associated with chemotherapy can activate paracrine pro-survival secretory programs suggests that inhibition of local pro-survival signaling pathways might potentiate the therapeutic efficacy of conventional anticancer agents. In the Eμ-Myc model, we tested whether chemical inhibition of Jak kinase activity, a downstream mediator of both IL-6 and Timp-1 signaling, could potentiate the action of doxorubicin. Mice treated with a pan-JAK inhibitor and doxorubicin showed significantly longer tumor-free and overall survival than mice treated with doxorubicin alone. Of importance, mice subjected to IL-6 pathway inhibition alone showed no tumor regression or difference in overall survival when compared with vehicle control. Thus, simply blocking a pro-survival signal may not be an effective therapy in the absence of DNA damage. Consequently, determining whether a microenvironment-specific cytokine functions as a mitogen or a survival factor is critical for determining whether a targeted agent should be used as a mono-therapy or applied in combination with conventional chemotherapies.

Such combination therapies may be particularly important in cancers such as multiple myeloma (178). IL-6 is a tonic pro-survival factor for cultured multiple myeloma cells, such that IL-6 inhibition leads to cell death. However, clinical trials that used IL-6–neutralizing antibodies alone showed no survival benefit (293). In this malignancy, exogenous stress (culture stress or DNA damage) may be

required to reveal a dependency on pro-survival signaling. Thus, although IL-6 neutralizing antibodies are not effective as single agents, combining them with high-dose chemotherapeutic regimens could improve tumor clearance in a variety of tumor types. The value of such combination regimens may hold true for both conventional chemotherapeutics and emerging targeted therapies. For example, recent work showed improved antitumor activity when IL-6 inhibition was combined with the administration of targeted therapy for the treatment of a mouse model of lung cancer (273). Here, TGF-β-mediated IL-6 release promotes resistance to erlotinib. Additionally, inhibition of pro-survival cytokine signaling was shown to improve the efficacy of the Bcr-Abl inhibitor imatinib in the treatment of B-cell acute lymphoblastic leukemia (123). This suggests that in the future, increased mechanistic insight into local resistance could provide rational combinations of targeted medicines with increased clinical efficacy.

Clues to additional tumor types that may similarly co-opt IL-6 signaling following systemic DNA damage may come from an examination of non-transformed tissues that respond to IL-6 signaling. The IL-6 receptor is only expressed on hematopoietic cells and hepatocytes, and it is these two cell types that activate the majority of physiologic responses to IL-6 induction during inflammation (294). Furthermore, IL-6 promotes the pathogenesis of hepatocellular carcinoma (HCC) in response to chemical carcinogenesis in mice and underlies the gender disparity observed in HCC in humans (168). It has been observed that male humans and mice have a higher incidence of HCC. It was recently shown that in female mice but not males, estrogen signaling suppresses

MyD88-dependent activation of IL-6 release following administration of carbon tetrachloride. This same group also demonstrated that in male mice IL-6 promotes tumorigenesis. Here, IL-6 deficient male mice develop HCC at the same rate as female mice following administration of carbon tetrachloride. Of note in both mice and humans, HCCs are highly treatment-refractory, yet until recently doxorubicin treatment was the major treatment modality in unresectable disease. Additionally, a poor prognosis in HCC is strongly associated with a paracrine stromal IL-6 signature (295). These data suggest that perhaps, as in the *Eμ-myc* model, inhibition of IL-6 signaling could promote drug sensitivity in this tumor type.

Interestingly, the new standard of care for advanced hepatocellular carcinoma is twice daily treatment with sorafenib, a multi-kinase inhibitor that has been shown, amongst other things, to effectively inhibit IL-6 signaling (20,296). Additionally, sorafenib was suggested to work in part by inhibiting VEGF and tumor angiogenesis. In a conceptual extension of our work on damage-mediated induction of IL-6/Timp-1 in the thymus, we see that doxorubicin treatment rapidly induces an 8-fold increase in VEGF levels in the liver. This suggests that treating patients with both sorafenib and doxorubicin could have synergistic effects by inducing apoptotic stress while at the same time inhibiting both IL-6 and VEGF signaling. We intend to test this hypothesis using an orthotopic transplantable model of liver cancer. Here, using an intra-splenic injection, we can derive either *k-Ras*$^{G12D/+}$ *p53*$^{-/-}$, *c-myc p53*$^{-/-}$ and *c-myc sh-p16/p19* hepatocellular carcinoma tumors in *IL-6*$^{+/+}$ and *IL-6*$^{-/-}$ recipient mice. We intend to treat mice with

doxorubicin at tumor onset and interrogate whether paracrine IL-6 promotes resistance to doxorubicin *in vivo*. Additionally, we intend to carry out similar experiments to test therapeutic efficacy by treating this model with a combination of doxorubicin and sorafenib or doxorubicin and a VEGF blocking antibody in *IL-6$^{+/+}$* and *IL-6$^{-/-}$* recipient mice.

Thus, it remains to be tested whether inhibition of acute pro-survival secretory phenotypes can promote the cytotoxic activity of conventional chemotherapeutic agents in a variety of cancers in humans. In the future, a central component of investigating this process will be rapid examination of post-treatment tumor microenvironments. Most studies that examine cytokine and chemokine levels in tumor biopsies report on steady-state concentrations in the absence of treatment, an environment that may be drastically altered in the presence of chemotherapy. Here, the analysis of tumor samples subjected to neoadjuvant treatment prior to surgery may provide key information regarding the impact of chemotherapy on the tumor microenvironment. Additionally, the application of frontline therapies to a range of existing genetically engineered mouse models of cancer would allow a temporal analysis of dynamic changes in the tumor microenvironment that accompany drug treatment.

Conclusions

Tumors can relapse despite months to years of sustained remission following therapy. Thus, understanding how subsets of cancer cells survive treatment and where they persist during this period of remission are fundamental

174

questions in cancer biology. It has long been appreciated that tumor initiation and progression involve a complex set of interactions between tumor cells and their associated stroma. The work described in this thesis suggests that the tumor microenvironment also plays an integral role in overall therapeutic response and tumorigenesis. This is perhaps not surprising given the striking difficulties of treating tumors in their native setting versus treating tumor cells in culture. Nevertheless, this work highlights the emerging relevance of developmental biology and tissue homeostasis to the response to anticancer therapies. Understanding how cancers co-opt developmental survival cues will be essential for the development of combination therapies that can achieve effective and durable treatment outcomes.

References:

1.   Egeblad, M., Nakasone, E.S., and Werb, Z. (2010). Tumors as organs: complex tissues that interface with the entire organism. Dev Cell *18*, 884-901.

2.   Provenzano, P.P., Cuevas, C., Chang, A.E., Goel, V.K., Von Hoff, D.D., and Hingorani, S.R. (2012). Enzymatic targeting of the stroma ablates physical barriers to treatment of pancreatic ductal adenocarcinoma. Cancer Cell *21*, 418-429.

3.   Kuppers, R. (2009). The biology of Hodgkin's lymphoma. Nature reviews Cancer *9*, 15-27.

4.   Strebhardt, K., and Ullrich, A. (2008). Paul Ehrlich's magic bullet concept: 100 years of progress. Nature reviews Cancer *8*, 473-480.

5.   Krumbhaar, E.B., and Krumbhaar, H.D. (1919). The Blood and Bone Marrow in Yelloe Cross Gas (Mustard Gas) Poisoning: Changes produced in the Bone Marrow of Fatal Cases. J Med Res *40*, 497-508 493.

6.   Goodman, L.S., Wintrobe, M.M., and et al. (1946). Nitrogen mustard therapy; use of methyl-bis (beta-chloroethyl) amine hydrochloride and tris (beta-chloroethyl) amine hydrochloride for Hodgkin's disease, lymphosarcoma, leukemia and certain allied and miscellaneous disorders. J Am Med Assoc *132*, 126-132.

7.   Gilman, A. (1946). Therapeutic applications of chemical warfare agents. Fed Proc *5*, 285-292.

8.   Goodman, L.S., Wintrobe, M.M., Dameshek, W., Goodman, M.J., Gilman, A., and McLennan, M.T. (1984). Landmark article Sept. 21, 1946: Nitrogen mustard therapy. Use of methyl-bis(beta-chloroethyl)amine hydrochloride and tris(beta-chloroethyl)amine hydrochloride for Hodgkin's disease, lymphosarcoma, leukemia and certain allied and miscellaneous disorders. By Louis S. Goodman, Maxwell M. Wintrobe, William Dameshek, Morton J. Goodman, Alfred Gilman and Margaret T. McLennan. Jama *251*, 2255-2261.

9.   Farber, S., and Diamond, L.K. (1948). Temporary remissions in acute leukemia in children produced by folic acid antagonist, 4-aminopteroyl-glutamic acid. The New England journal of medicine *238*, 787-793.

10.   DeVita, V.T., Jr. (1978). The evolution of therapeutic research in cancer. The New England journal of medicine *298*, 907-910.

11.   DeVita, V.T., Jr., and Chu, E. (2008). A history of cancer chemotherapy. Cancer research *68*, 8643-8653.

12.   Frei, E., 3rd (1972). Combination cancer therapy: Presidential address. Cancer research *32*, 2593-2607.

13.   DeVita, V.T., Jr., Young, R.C., and Canellos, G.P. (1975). Combination versus single agent chemotherapy: a review of the basis for selection of drug treatment of cancer. Cancer *35*, 98-110.

14.   Kath, R., Blumenstengel, K., Fricke, H.J., and Hoffken, K. (2001). Bendamustine monotherapy in advanced and refractory chronic lymphocytic leukemia. J Cancer Res Clin Oncol *127*, 48-54.

15.   Conroy, T., Desseigne, F., Ychou, M., Bouche, O., Guimbaud, R., Becouarn, Y., Adenis, A., Raoul, J.L., Gourgou-Bourgade, S., de la Fouchardiere, C., *et al.* (2011). FOLFIRINOX versus gemcitabine for metastatic pancreatic cancer. The New England journal of medicine *364*, 1817-1825.

16.   Druker, B.J., Tamura, S., Buchdunger, E., Ohno, S., Segal, G.M., Fanning, S., Zimmermann, J., and Lydon, N.B. (1996). Effects of a selective inhibitor of the Abl tyrosine kinase on the growth of Bcr-Abl positive cells. Nat Med *2*, 561-566.

17.   Lynch, T.J., Bell, D.W., Sordella, R., Gurubhagavatula, S., Okimoto, R.A., Brannigan, B.W., Harris, P.L., Haserlat, S.M., Supko, J.G., Haluska, F.G., *et al.* (2004). Activating mutations in the epidermal growth factor receptor underlying responsiveness of non-small-cell lung cancer to gefitinib. The New England journal of medicine *350*, 2129-2139.

18.   Sosman, J.A., Kim, K.B., Schuchter, L., Gonzalez, R., Pavlick, A.C., Weber, J.S., McArthur, G.A., Hutson, T.E., Moschos, S.J., Flaherty, K.T., *et al.* (2012). Survival in BRAF V600-mutant advanced melanoma treated with vemurafenib. The New England journal of medicine *366*, 707-714.

19.   Kwak, E.L., Bang, Y.J., Camidge, D.R., Shaw, A.T., Solomon, B., Maki, R.G., Ou, S.H., Dezube, B.J., Janne, P.A., Costa, D.B., *et al.* (2010). Anaplastic lymphoma kinase inhibition in non-small-cell lung cancer. The New England journal of medicine *363*, 1693-1703.

20.   Llovet, J.M., Ricci, S., Mazzaferro, V., Hilgard, P., Gane, E., Blanc, J.F., de Oliveira, A.C., Santoro, A., Raoul, J.L., Forner, A., *et al.* (2008). Sorafenib in advanced hepatocellular carcinoma. The New England journal of medicine *359*, 378-390.

21.   Keime-Guibert, F., Chinot, O., Taillandier, L., Cartalat-Carel, S., Frenay, M., Kantor, G., Guillamo, J.S., Jadaud, E., Colin, P., Bondiau, P.Y., *et al.* (2007). Radiotherapy for glioblastoma in the elderly. The New England journal of medicine *356*, 1527-1535.

22.   Ni Chonghaile, T., Sarosiek, K.A., Vo, T.T., Ryan, J.A., Tammareddi, A., Moore Vdel, G., Deng, J., Anderson, K.C., Richardson, P., Tai, Y.T., *et al.* (2011). Pretreatment mitochondrial priming correlates with clinical response to cytotoxic chemotherapy. Science *334*, 1129-1133.

23.   Zhu, A.X., Duda, D.G., Sahani, D.V., and Jain, R.K. (2011). HCC and angiogenesis: possible targets and future directions. Nature reviews Clinical oncology *8*, 292-301.

24.   Deeken, J.F., and Loscher, W. (2007). The blood-brain barrier and cancer: transporters, treatment, and Trojan horses. Clinical cancer research : an official journal of the American Association for Cancer Research *13*, 1663-1674.

25.   Olive, K.P., Jacobetz, M.A., Davidson, C.J., Gopinathan, A., McIntyre, D., Honess, D., Madhu, B., Goldgraben, M.A., Caldwell, M.E., Allard, D., *et al.* (2009). Inhibition of Hedgehog signaling enhances delivery of chemotherapy in a mouse model of pancreatic cancer. Science *324*, 1457-1461.

26.   Kim, H.K., Choi, I.J., Kim, C.G., Kim, H.S., Oshima, A., Michalowski, A., and Green, J.E. (2011). A gene expression signature of acquired chemoresistance to cisplatin and fluorouracil combination chemotherapy in gastric cancer patients. PLoS One *6*, e16694.

27.   Wang, W., and Figg, W.D. (2008). Secondary BRCA1 and BRCA2 alterations and acquired chemoresistance. Cancer biology & therapy *7*, 1004-1005.

28.   Oliver, T.G., Mercer, K.L., Sayles, L.C., Burke, J.R., Mendus, D., Lovejoy, K.S., Cheng, M.H., Subramanian, A., Mu, D., Powers, S., *et al.* (2010). Chronic cisplatin treatment promotes

enhanced damage repair and tumor progression in a mouse model of lung cancer. Genes & development *24*, 837-852.

29.   Ding, L., Ley, T.J., Larson, D.E., Miller, C.A., Koboldt, D.C., Welch, J.S., Ritchey, J.K., Young, M.A., Lamprecht, T., McLellan, M.D., *et al.* (2012). Clonal evolution in relapsed acute myeloid leukaemia revealed by whole-genome sequencing. Nature *481*, 506-510.

30.   Mullighan, C.G., Zhang, J., Kasper, L.H., Lerach, S., Payne-Turner, D., Phillips, L.A., Heatley, S.L., Holmfeldt, L., Collins-Underwood, J.R., Ma, J., *et al.* (2011). CREBBP mutations in relapsed acute lymphoblastic leukaemia. Nature *471*, 235-239.

31.   Mullighan, C.G., Phillips, L.A., Su, X., Ma, J., Miller, C.B., Shurtleff, S.A., and Downing, J.R. (2008). Genomic analysis of the clonal origins of relapsed acute lymphoblastic leukemia. Science *322*, 1377-1380.

32.   Wagle, N., Emery, C., Berger, M.F., Davis, M.J., Sawyer, A., Pochanard, P., Kehoe, S.M., Johannessen, C.M., Macconaill, L.E., Hahn, W.C., *et al.* (2011). Dissecting therapeutic resistance to RAF inhibition in melanoma by tumor genomic profiling. Journal of clinical oncology : official journal of the American Society of Clinical Oncology *29*, 3085-3096.

33.   O'Hare, T., Shakespeare, W.C., Zhu, X., Eide, C.A., Rivera, V.M., Wang, F., Adrian, L.T., Zhou, T., Huang, W.S., Xu, Q., *et al.* (2009). AP24534, a pan-BCR-ABL inhibitor for chronic myeloid leukemia, potently inhibits the T315I mutant and overcomes mutation-based resistance. Cancer Cell *16*, 401-412.

34.   Kobayashi, S., Boggon, T.J., Dayaram, T., Janne, P.A., Kocher, O., Meyerson, M., Johnson, B.E., Eck, M.J., Tenen, D.G., and Halmos, B. (2005). EGFR mutation and resistance of non-small-cell lung cancer to gefitinib. The New England journal of medicine *352*, 786-792.

35.   Goss, P.E., and Chambers, A.F. (2010). Does tumour dormancy offer a therapeutic target? Nature reviews Cancer *10*, 871-877.

36.   Brisco, M.J., Condon, J., Hughes, E., Neoh, S.H., Sykes, P.J., Seshadri, R., Toogood, I., Waters, K., Tauro, G., Ekert, H., *et al.* (1994). Outcome prediction in childhood acute lymphoblastic leukaemia by molecular quantification of residual disease at the end of induction. Lancet *343*, 196-200.

37.   Skipper, H.E., Schabel, F.M., Jr., and Wilcox, W.S. (1964). Experimental Evaluation of Potential Anticancer Agents. Xiii. On the Criteria and Kinetics Associated with "Curability" of Experimental Leukemia. Cancer Chemother Rep *35*, 1-111.

38.   Cave, H., van der Werff ten Bosch, J., Suciu, S., Guidal, C., Waterkeyn, C., Otten, J., Bakkus, M., Thielemans, K., Grandchamp, B., and Vilmer, E. (1998). Clinical significance of minimal residual disease in childhood acute lymphoblastic leukemia. European Organization for Research and Treatment of Cancer--Childhood Leukemia Cooperative Group. N Engl J Med *339*, 591-598.

39.   Aguirre-Ghiso, J.A. (2007). Models, mechanisms and clinical evidence for cancer dormancy. Nat Rev Cancer *7*, 834-846.

40.   Gillet, J.P., and Gottesman, M.M. (2010). Mechanisms of multidrug resistance in cancer. Methods Mol Biol *596*, 47-76.

41.   Gottesman, M.M. (2002). Mechanisms of cancer drug resistance. Annu Rev Med *53*, 615-627.

178

42.   Jiang, H., Reinhardt, H.C., Bartkova, J., Tommiska, J., Blomqvist, C., Nevanlinna, H., Bartek, J., Yaffe, M.B., and Hemann, M.T. (2009). The combined status of ATM and p53 link tumor development with therapeutic response. Genes & development *23*, 1895-1909.

43.   Minchinton, A.I., and Tannock, I.F. (2006). Drug penetration in solid tumours. Nature reviews Cancer *6*, 583-592.

44.   Hanahan, D., and Weinberg, R.A. (2000). The hallmarks of cancer. Cell *100*, 57-70.

45.   Berghmans, S., Jette, C., Langenau, D., Hsu, K., Stewart, R., Look, T., and Kanki, J.P. (2005). Making waves in cancer research: new models in the zebrafish. Biotechniques *39*, 227-237.

46.   Rudrapatna, V.A., Cagan, R.L., and Das, T.K. (2012). Drosophila cancer models. Dev Dyn *241*, 107-118.

47.   Dow, L.E., and Lowe, S.W. (2012). Life in the fast lane: Mammalian disease models in the genomics era. Cell *148*, 1099-1109.

48.   Sharpless, N.E., and Depinho, R.A. (2006). The mighty mouse: genetically engineered mouse models in cancer drug development. Nat Rev Drug Discov *5*, 741-754.

49.   Gutmann, D.H., Hunter-Schaedle, K., and Shannon, K.M. (2006). Harnessing preclinical mouse models to inform human clinical cancer trials. The Journal of clinical investigation *116*, 847-852.

50.   Shorthouse, A.J., Smyth, J.F., Steel, G.G., Ellison, M., Mills, J., and Peckham, M.J. (1980). The human tumour xenograft--a valid model in experimental chemotherapy? Br J Surg *67*, 715-722.

51.   Scholz, C.C., Berger, D.P., Winterhalter, B.R., Henss, H., and Fiebig, H.H. (1990). Correlation of drug response in patients and in the clonogenic assay with solid human tumour xenografts. European journal of cancer *26*, 901-905.

52.   Johnson, J.I., Decker, S., Zaharevitz, D., Rubinstein, L.V., Venditti, J.M., Schepartz, S., Kalyandrug, S., Christian, M., Arbuck, S., Hollingshead, M., *et al.* (2001). Relationships between drug activity in NCI preclinical in vitro and in vivo models and early clinical trials. Br J Cancer *84*, 1424-1431.

53.   Meyer, L.H., Eckhoff, S.M., Queudeville, M., Kraus, J.M., Giordan, M., Stursberg, J., Zangrando, A., Vendramini, E., Moricke, A., Zimmermann, M., *et al.* (2011). Early relapse in ALL is identified by time to leukemia in NOD/SCID mice and is characterized by a gene signature involving survival pathways. Cancer Cell *19*, 206-217.

54.   Kerbel, R.S. (2003). Human tumor xenografts as predictive preclinical models for anticancer drug activity in humans: better than commonly perceived-but they can be improved. Cancer Biol Ther *2*, S134-139.

55.   Richmond, A., and Su, Y. (2008). Mouse xenograft models vs GEM models for human cancer therapeutics. Dis Model Mech *1*, 78-82.

56.   Sarraf, P., Mueller, E., Jones, D., King, F.J., DeAngelo, D.J., Partridge, J.B., Holden, S.A., Chen, L.B., Singer, S., Fletcher, C., *et al.* (1998). Differentiation and reversal of malignant changes in colon cancer through PPARgamma. Nat Med *4*, 1046-1052.

57.   Saez, E., Tontonoz, P., Nelson, M.C., Alvarez, J.G., Ming, U.T., Baird, S.M., Thomazy, V.A., and Evans, R.M. (1998). Activators of the nuclear receptor PPARgamma enhance colon polyp formation. Nature medicine 4, 1058-1061.

58.   Kulke, M.H., Demetri, G.D., Sharpless, N.E., Ryan, D.P., Shivdasani, R., Clark, J.S., Spiegelman, B.M., Kim, H., Mayer, R.J., and Fuchs, C.S. (2002). A phase II study of troglitazone, an activator of the PPARgamma receptor, in patients with chemotherapy-resistant metastatic colorectal cancer. Cancer J 8, 395-399.

59.   Omer, C.A., Chen, Z., Diehl, R.E., Conner, M.W., Chen, H.Y., Trumbauer, M.E., Gopal-Truter, S., Seeburger, G., Bhimnathwala, H., Abrams, M.T., et al. (2000). Mouse mammary tumor virus-Ki-rasB transgenic mice develop mammary carcinomas that can be growth-inhibited by a farnesyl:protein transferase inhibitor. Cancer research 60, 2680-2688.

60.   Johnson, B.E., and Heymach, J.V. (2004). Farnesyl transferase inhibitors for patients with lung cancer. Clinical cancer research : an official journal of the American Association for Cancer Research 10, 4254s-4257s.

61.   Blyth, K., Morton, J.P., and Sansom, O.J. (2012). The right time, the right place: will targeting human cancer-associated mutations to the mouse provide the perfect preclinical model? Curr Opin Genet Dev 22, 28-35.

62.   Becher, O.J., and Holland, E.C. (2006). Genetically engineered models have advantages over xenografts for preclinical studies. Cancer Res 66, 3355-3358, discussion 3358-3359.

63.   Trimboli, A.J., Cantemir-Stone, C.Z., Li, F., Wallace, J.A., Merchant, A., Creasap, N., Thompson, J.C., Caserta, E., Wang, H., Chong, J.L., et al. (2009). Pten in stromal fibroblasts suppresses mammary epithelial tumours. Nature 461, 1084-1091.

64.   Tan, W., Zhang, W., Strasner, A., Grivennikov, S., Cheng, J.Q., Hoffman, R.M., and Karin, M. (2011). Tumour-infiltrating regulatory T cells stimulate mammary cancer metastasis through RANKL-RANK signalling. Nature 470, 548-553.

65.   DeNardo, D.G., Barreto, J.B., Andreu, P., Vasquez, L., Tawfik, D., Kolhatkar, N., and Coussens, L.M. (2009). CD4(+) T cells regulate pulmonary metastasis of mammary carcinomas by enhancing protumor properties of macrophages. Cancer Cell 16, 91-102.

66.   Cheon, D.J., and Orsulic, S. (2011). Mouse models of cancer. Annu Rev Pathol 6, 95-119.

67.   Brinster, R.L., Chen, H.Y., Messing, A., van Dyke, T., Levine, A.J., and Palmiter, R.D. (1984). Transgenic mice harboring SV40 T-antigen genes develop characteristic brain tumors. Cell 37, 367-379.

68.   Stewart, T.A., Pattengale, P.K., and Leder, P. (1984). Spontaneous mammary adenocarcinomas in transgenic mice that carry and express MTV/myc fusion genes. Cell 38, 627-637.

69.   Hanahan, D. (1985). Heritable formation of pancreatic beta-cell tumours in transgenic mice expressing recombinant insulin/simian virus 40 oncogenes. Nature 315, 115-122.

70.   Adams, J.M., Harris, A.W., Pinkert, C.A., Corcoran, L.M., Alexander, W.S., Cory, S., Palmiter, R.D., and Brinster, R.L. (1985). The c-myc oncogene driven by immunoglobulin enhancers induces lymphoid malignancy in transgenic mice. Nature 318, 533-538.

71.   DuPage, M., Dooley, A.L., and Jacks, T. (2009). Conditional mouse lung cancer models using adenoviral or lentiviral delivery of Cre recombinase. Nat Protoc 4, 1064-1072.

72.   Frese, K.K., and Tuveson, D.A. (2007). Maximizing mouse cancer models. Nature reviews Cancer 7, 645-658.

73.   Hoshida, Y., Villanueva, A., Kobayashi, M., Peix, J., Chiang, D.Y., Camargo, A., Gupta, S., Moore, J., Wrobel, M.J., Lerner, J., et al. (2008). Gene expression in fixed tissues and outcome in hepatocellular carcinoma. N Engl J Med 359, 1995-2004.

74.   Lowe, S.W., Ruley, H.E., Jacks, T., and Housman, D.E. (1993). p53-dependent apoptosis modulates the cytotoxicity of anticancer agents. Cell 74, 957-967.

75.   Boulos, N., Mulder, H.L., Calabrese, C.R., Morrison, J.B., Rehg, J.E., Relling, M.V., Sherr, C.J., and Williams, R.T. (2011). Chemotherapeutic agents circumvent emergence of dasatinib-resistant BCR-ABL kinase mutations in a precise mouse model of Philadelphia chromosome-positive acute lymphoblastic leukemia. Blood 117, 3585-3595.

76.   Wendel, H.G., de Stanchina, E., Cepero, E., Ray, S., Emig, M., Fridman, J.S., Veach, D.R., Bornmann, W.G., Clarkson, B., McCombie, W.R., et al. (2006). Loss of p53 impedes the antileukemic response to BCR-ABL inhibition. Proc Natl Acad Sci U S A 103, 7444-7449.

77.   Zuber, J., Radtke, I., Pardee, T.S., Zhao, Z., Rappaport, A.R., Luo, W., McCurrach, M.E., Yang, M.M., Dolan, M.E., Kogan, S.C., et al. (2009). Mouse models of human AML accurately predict chemotherapy response. Genes Dev 23, 877-889.

78.   Schmitt, C.A., Fridman, J.S., Yang, M., Lee, S., Baranov, E., Hoffman, R.M., and Lowe, S.W. (2002). A senescence program controlled by p53 and p16INK4a contributes to the outcome of cancer therapy. Cell 109, 335-346.

79.   Bric, A., Miething, C., Bialucha, C.U., Scuoppo, C., Zender, L., Krasnitz, A., Xuan, Z., Zuber, J., Wigler, M., Hicks, J., et al. (2009). Functional identification of tumor-suppressor genes through an in vivo RNA interference screen in a mouse lymphoma model. Cancer Cell 16, 324-335.

80.   Williams, R.T., Roussel, M.F., and Sherr, C.J. (2006). Arf gene loss enhances oncogenicity and limits imatinib response in mouse models of Bcr-Abl-induced acute lymphoblastic leukemia. Proc Natl Acad Sci U S A 103, 6688-6693.

81.   Zhang, X.H., Wang, Q., Gerald, W., Hudis, C.A., Norton, L., Smid, M., Foekens, J.A., and Massague, J. (2009). Latent bone metastasis in breast cancer tied to Src-dependent survival signals. Cancer Cell 16, 67-78.

82.   Zuber, J., Rappaport, A.R., Luo, W., Wang, E., Chen, C., Vaseva, A.V., Shi, J., Weissmueller, S., Fellmann, C., Taylor, M.J., et al. (2011). An integrated approach to dissecting oncogene addiction implicates a Myb-coordinated self-renewal program as essential for leukemia maintenance. Genes & development 25, 1628-1640.

83.   Sawey, E.T., Chanrion, M., Cai, C., Wu, G., Zhang, J., Zender, L., Zhao, A., Busuttil, R.W., Yee, H., Stein, L., et al. (2011). Identification of a therapeutic strategy targeting amplified FGF19 in liver cancer by Oncogenomic screening. Cancer Cell 19, 347-358.

84.   Doles, J., Oliver, T.G., Cameron, E.R., Hsu, G., Jacks, T., Walker, G.C., and Hemann, M.T. (2010). Suppression of Rev3, the catalytic subunit of Pol{zeta}, sensitizes drug-resistant lung tumors to chemotherapy. Proceedings of the National Academy of Sciences of the United States of America 107, 20786-20791.

85.   Chien, Y., Scuoppo, C., Wang, X., Fang, X., Balgley, B., Bolden, J.E., Premsrirut, P., Luo, W., Chicas, A., Lee, C.S., *et al.* (2011). Control of the senescence-associated secretory phenotype by NF-kappaB promotes senescence and enhances chemosensitivity. Genes & development *25*, 2125-2136.

86.   Dickins, R.A., Hemann, M.T., Zilfou, J.T., Simpson, D.R., Ibarra, I., Hannon, G.J., and Lowe, S.W. (2005). Probing tumor phenotypes using stable and regulated synthetic microRNA precursors. Nat Genet *37*, 1289-1295.

87.   Meacham, C.E., Ho, E.E., Dubrovsky, E., Gertler, F.B., and Hemann, M.T. (2009). In vivo RNAi screening identifies regulators of actin dynamics as key determinants of lymphoma progression. Nat Genet *41*, 1133-1137.

88.   Pritchard, J.R., Gilbert, L.A., Meacham, C.E., Ricks, J.L., Jiang, H., Lauffenburger, D.A., and Hemann, M.T. (2011). Bcl-2 family genetic profiling reveals microenvironment-specific determinants of chemotherapeutic response. Cancer research *71*, 5850-5858.

89.   Harris, A.W., Pinkert, C.A., Crawford, M., Langdon, W.Y., Brinster, R.L., and Adams, J.M. (1988). The E mu-myc transgenic mouse. A model for high-incidence spontaneous lymphoma and leukemia of early B cells. The Journal of experimental medicine *167*, 353-371.

90.   Schmitt, C.A., McCurrach, M.E., de Stanchina, E., Wallace-Brodeur, R.R., and Lowe, S.W. (1999). INK4a/ARF mutations accelerate lymphomagenesis and promote chemoresistance by disabling p53. Genes Dev *13*, 2670-2677.

91.   Schmitt, C.A., Fridman, J.S., Yang, M., Baranov, E., Hoffman, R.M., and Lowe, S.W. (2002). Dissecting p53 tumor suppressor functions in vivo. Cancer Cell *1*, 289-298.

92.   Schmitt, C.A., Rosenthal, C.T., and Lowe, S.W. (2000). Genetic analysis of chemoresistance in primary murine lymphomas. Nat Med *6*, 1029-1035.

93.   Wendel, H.G., De Stanchina, E., Fridman, J.S., Malina, A., Ray, S., Kogan, S., Cordon-Cardo, C., Pelletier, J., and Lowe, S.W. (2004). Survival signalling by Akt and eIF4E in oncogenesis and cancer therapy. Nature *428*, 332-337.

94.   Bordeleau, M.E., Robert, F., Gerard, B., Lindqvist, L., Chen, S.M., Wendel, H.G., Brem, B., Greger, H., Lowe, S.W., Porco, J.A., Jr., *et al.* (2008). Therapeutic suppression of translation initiation modulates chemosensitivity in a mouse lymphoma model. The Journal of clinical investigation *118*, 2651-2660.

95.   Lindemann, R.K., Newbold, A., Whitecross, K.F., Cluse, L.A., Frew, A.J., Ellis, L., Williams, S., Wiegmans, A.P., Dear, A.E., Scott, C.L., *et al.* (2007). Analysis of the apoptotic and therapeutic activities of histone deacetylase inhibitors by using a mouse model of B cell lymphoma. Proc Natl Acad Sci U S A *104*, 8071-8076.

96.   Helmrich, A., Lee, S., O'Brien, P., Dorken, B., Lowe, S.W., Schrock, E., and Schmitt, C.A. (2005). Recurrent chromosomal aberrations in INK4a/ARF defective primary lymphomas predict drug responses in vivo. Oncogene *24*, 4174-4182.

97.   Jiang, H., Reinhardt, H.C., Bartkova, J., Tommiska, J., Blomqvist, C., Nevanlinna, H., Bartek, J., Yaffe, M.B., and Hemann, M.T. (2009). The combined status of ATM and p53 link tumor development with therapeutic response. Genes Dev *23*, 1895-1909.

98. Johnson, L., Mercer, K., Greenbaum, D., Bronson, R.T., Crowley, D., Tuveson, D.A., and Jacks, T. (2001). Somatic activation of the K-ras oncogene causes early onset lung cancer in mice. Nature *410*, 1111-1116.

99. Xue, W., Meylan, E., Oliver, T.G., Feldser, D.M., Winslow, M.M., Bronson, R., and Jacks, T. (2011). Response and resistance to NF-kappaB inhibitors in mouse models of lung adenocarcinoma. Cancer Discov *1*, 236-247.

100. Xie, K., Doles, J., Hemann, M.T., and Walker, G.C. (2010). Error-prone translesion synthesis mediates acquired chemoresistance. Proceedings of the National Academy of Sciences of the United States of America *107*, 20792-20797.

101. De Raedt, T., Walton, Z., Yecies, J.L., Li, D., Chen, Y., Malone, C.F., Maertens, O., Jeong, S.M., Bronson, R.T., Lebleu, V., *et al.* (2011). Exploiting cancer cell vulnerabilities to develop a combination therapy for ras-driven tumors. Cancer Cell *20*, 400-413.

102. Chen, Z., Cheng, K., Walton, Z., Wang, Y., Ebi, H., Shimamura, T., Liu, Y., Tupper, T., Ouyang, J., Li, J., *et al.* (2012). A murine lung cancer co-clinical trial identifies genetic modifiers of therapeutic response. Nature *483*, 613-617.

103. Paget, S. (1989). The distribution of secondary growths in cancer of the breast. 1889. Cancer Metastasis Rev *8*, 98-101.

104. Kinsey, D.L. (1960). An experimental study of preferential metastasis. Cancer *13*, 674-676.

105. Hart, I.R., and Fidler, I.J. (1980). Role of organ selectivity in the determination of metastatic patterns of B16 melanoma. Cancer research *40*, 2281-2287.

106. Fidler, I.J., and Kripke, M.L. (1977). Metastasis results from preexisting variant cells within a malignant tumor. Science *197*, 893-895.

107. Langley, R.R., and Fidler, I.J. (2007). Tumor cell-organ microenvironment interactions in the pathogenesis of cancer metastasis. Endocr Rev *28*, 297-321.

108. Phung, T.L., Ziv, K., Dabydeen, D., Eyiah-Mensah, G., Riveros, M., Perruzzi, C., Sun, J., Monahan-Earley, R.A., Shiojima, I., Nagy, J.A., *et al.* (2006). Pathological angiogenesis is induced by sustained Akt signaling and inhibited by rapamycin. Cancer Cell *10*, 159-170.

109. Elgert, K.D., Alleva, D.G., and Mullins, D.W. (1998). Tumor-induced immune dysfunction: the macrophage connection. J Leukoc Biol *64*, 275-290.

110. Mueller, M.M., and Fusenig, N.E. (2004). Friends or foes - bipolar effects of the tumour stroma in cancer. Nature reviews Cancer *4*, 839-849.

111. Ham, R.G. (1965). Clonal Growth of Mammalian Cells in a Chemically Defined, Synthetic Medium. Proceedings of the National Academy of Sciences of the United States of America *53*, 288-293.

112. Sanford, K.K., Earle, W.R., and Likely, G.D. (1948). The growth in vitro of single isolated tissue cells. Journal of the National Cancer Institute *9*, 229-246.

113. Cohen, S., Levi-Montalcini, R., and Hamburger, V. (1954). A Nerve Growth-Stimulating Factor Isolated from Sarcom as 37 and 180. Proceedings of the National Academy of Sciences of the United States of America *40*, 1014-1018.

114.   Swain, S.L., and Dutton, R.W. (1982). Production of a B cell growth-promoting activity, (DL)BCGF, from a cloned T cell line and its assay on the BCL1 B cell tumor. The Journal of experimental medicine *156*, 1821-1834.

115.   Yoshizaki, K., Nakagawa, T., Kaieda, T., Muraguchi, A., Yamamura, Y., and Kishimoto, T. (1982). Induction of proliferation and Ig production in human B leukemic cells by anti-immunoglobulins and T cell factors. Journal of immunology *128*, 1296-1301.

116.   Smith, K.A., Gilbride, K.J., and Favata, M.F. (1980). Lymphocyte activating factor promotes T-cell growth factor production by cloned murine lymphoma cells. Nature *287*, 853-855.

117.   Nordan, R.P., and Potter, M. (1986). A macrophage-derived factor required by plasmacytomas for survival and proliferation in vitro. Science *233*, 566-569.

118.   Kishimoto, T. (2005). Interleukin-6: from basic science to medicine--40 years in immunology. Annu Rev Immunol *23*, 1-21.

119.   Yonish-Rouach, E., Resnitzky, D., Lotem, J., Sachs, L., Kimchi, A., and Oren, M. (1991). Wild-type p53 induces apoptosis of myeloid leukaemic cells that is inhibited by interleukin-6. Nature *352*, 345-347.

120.   Falschlehner, C., Schaefer, U., and Walczak, H. (2009). Following TRAIL's path in the immune system. Immunology *127*, 145-154.

121.   Fulciniti, M., Hideshima, T., Vermot-Desroches, C., Pozzi, S., Nanjappa, P., Shen, Z., Patel, N., Smith, E.S., Wang, W., Prabhala, R., *et al.* (2009). A high-affinity fully human anti-IL-6 mAb, 1339, for the treatment of multiple myeloma. Clinical cancer research : an official journal of the American Association for Cancer Research *15*, 7144-7152.

122.   Mitsiades, C.S., Mitsiades, N., Poulaki, V., Schlossman, R., Akiyama, M., Chauhan, D., Hideshima, T., Treon, S.P., Munshi, N.C., Richardson, P.G., *et al.* (2002). Activation of NF-kappaB and upregulation of intracellular anti-apoptotic proteins via the IGF-1/Akt signaling in human multiple myeloma cells: therapeutic implications. Oncogene *21*, 5673-5683.

123.   Williams, R.T., den Besten, W., and Sherr, C.J. (2007). Cytokine-dependent imatinib resistance in mouse BCR-ABL+, Arf-null lymphoblastic leukemia. Genes Dev *21*, 2283-2287.

124.   Denardo, D.G., Brennan, D.J., Rexhepaj, E., Ruffell, B., Shiao, S.L., Madden, S.F., Gallagher, W.M., Wadhwani, N., Keil, S.D., Junaid, S.A., *et al.* (2011). Leukocyte Complexity Predicts Breast Cancer Survival and Functionally Regulates Response to Chemotherapy. Cancer Discov *1*, 54-67.

125.   Shaked, Y., Ciarrocchi, A., Franco, M., Lee, C.R., Man, S., Cheung, A.M., Hicklin, D.J., Chaplin, D., Foster, F.S., Benezra, R., *et al.* (2006). Therapy-induced acute recruitment of circulating endothelial progenitor cells to tumors. Science *313*, 1785-1787.

126.   Shaked, Y., Henke, E., Roodhart, J.M., Mancuso, P., Langenberg, M.H., Colleoni, M., Daenen, L.G., Man, S., Xu, P., Emmenegger, U., *et al.* (2008). Rapid chemotherapy-induced acute endothelial progenitor cell mobilization: implications for antiangiogenic drugs as chemosensitizing agents. Cancer Cell *14*, 263-273.

127.   Gingis-Velitski, S., Loven, D., Benayoun, L., Munster, M., Bril, R., Voloshin, T., Alishekevitz, D., Bertolini, F., and Shaked, Y. (2011). Host response to short-term, single-agent chemotherapy induces matrix metalloproteinase-9 expression and accelerates metastasis in mice. Cancer research *71*, 6986-6996.

184

128.	Roodhart, J.M., Daenen, L.G., Stigter, E.C., Prins, H.J., Gerrits, J., Houthuijzen, J.M., Gerritsen, M.G., Schipper, H.S., Backer, M.J., van Amersfoort, M., *et al.* (2011). Mesenchymal stem cells induce resistance to chemotherapy through the release of platinum-induced fatty acids. Cancer Cell *20*, 370-383.

129.	Meads, M.B., Hazlehurst, L.A., and Dalton, W.S. (2008). The bone marrow microenvironment as a tumor sanctuary and contributor to drug resistance. Clinical cancer research : an official journal of the American Association for Cancer Research *14*, 2519-2526.

130.	Kessenbrock, K., Plaks, V., and Werb, Z. (2010). Matrix metalloproteinases: regulators of the tumor microenvironment. Cell *141*, 52-67.

131.	Meads, M.B., Gatenby, R.A., and Dalton, W.S. (2009). Environment-mediated drug resistance: a major contributor to minimal residual disease. Nature reviews Cancer *9*, 665-674.

132.	Quintana, E., Shackleton, M., Sabel, M.S., Fullen, D.R., Johnson, T.M., and Morrison, S.J. (2008). Efficient tumour formation by single human melanoma cells. Nature *456*, 593-598.

133.	Cook, N., Frese, K.K., Bapiro, T.E., Jacobetz, M.A., Gopinathan, A., Miller, J.L., Rao, S.S., Demuth, T., Howat, W.J., Jodrell, D.I., *et al.* (2012). Gamma secretase inhibition promotes hypoxic necrosis in mouse pancreatic ductal adenocarcinoma. The Journal of experimental medicine *209*, 437-444.

134.	Liu, H., Chi, A.W., Arnett, K.L., Chiang, M.Y., Xu, L., Shestova, O., Wang, H., Li, Y.M., Bhandoola, A., Aster, J.C., *et al.* (2010). Notch dimerization is required for leukemogenesis and T-cell development. Genes & development *24*, 2395-2407.

135.	Nefedova, Y., Sullivan, D.M., Bolick, S.C., Dalton, W.S., and Gabrilovich, D.I. (2008). Inhibition of Notch signaling induces apoptosis of myeloma cells and enhances sensitivity to chemotherapy. Blood *111*, 2220-2229.

136.	Tian, H., Callahan, C.A., DuPree, K.J., Darbonne, W.C., Ahn, C.P., Scales, S.J., and de Sauvage, F.J. (2009). Hedgehog signaling is restricted to the stromal compartment during pancreatic carcinogenesis. Proceedings of the National Academy of Sciences of the United States of America *106*, 4254-4259.

137.	Chen, G.Y., and Nunez, G. (2010). Sterile inflammation: sensing and reacting to damage. Nature reviews Immunology *10*, 826-837.

138.	Senger, D.R., Wirth, D.F., and Hynes, R.O. (1979). Transformed mammalian cells secrete specific proteins and phosphoproteins. Cell *16*, 885-893.

139.	Pazolli, E., Luo, X., Brehm, S., Carbery, K., Chung, J.J., Prior, J.L., Doherty, J., Demehri, S., Salavaggione, L., Piwnica-Worms, D., *et al.* (2009). Senescent stromal-derived osteopontin promotes preneoplastic cell growth. Cancer research *69*, 1230-1239.

140.	Acosta, J.C., O'Loghlen, A., Banito, A., Guijarro, M.V., Augert, A., Raguz, S., Fumagalli, M., Da Costa, M., Brown, C., Popov, N., *et al.* (2008). Chemokine signaling via the CXCR2 receptor reinforces senescence. Cell *133*, 1006-1018.

141.	Kuilman, T., Michaloglou, C., Vredeveld, L.C., Douma, S., van Doorn, R., Desmet, C.J., Aarden, L.A., Mooi, W.J., and Peeper, D.S. (2008). Oncogene-induced senescence relayed by an interleukin-dependent inflammatory network. Cell *133*, 1019-1031.

142.	Coppe, J.P., Patil, C.K., Rodier, F., Sun, Y., Munoz, D.P., Goldstein, J., Nelson, P.S., Desprez, P.Y., and Campisi, J. (2008). Senescence-associated secretory phenotypes reveal cell-

nonautonomous functions of oncogenic RAS and the p53 tumor suppressor. PLoS Biol *6*, 2853-2868.

143.   Wajapeyee, N., Serra, R.W., Zhu, X., Mahalingam, M., and Green, M.R. (2008). Oncogenic BRAF induces senescence and apoptosis through pathways mediated by the secreted protein IGFBP7. Cell *132*, 363-374.

144.   Rodier, F., Coppe, J.P., Patil, C.K., Hoeijmakers, W.A., Munoz, D.P., Raza, S.R., Freund, A., Campeau, E., Davalos, A.R., and Campisi, J. (2009). Persistent DNA damage signalling triggers senescence-associated inflammatory cytokine secretion. Nat Cell Biol *11*, 973-979.

145.   Ancrile, B., Lim, K.H., and Counter, C.M. (2007). Oncogenic Ras-induced secretion of IL6 is required for tumorigenesis. Genes & development *21*, 1714-1719.

146.   Sparmann, A., and Bar-Sagi, D. (2004). Ras-induced interleukin-8 expression plays a critical role in tumor growth and angiogenesis. Cancer Cell *6*, 447-458.

147.   Rak, J., Filmus, J., and Kerbel, R.S. (1996). Reciprocal paracrine interactions between tumour cells and endothelial cells: the 'angiogenesis progression' hypothesis. European journal of cancer *32A*, 2438-2450.

148.   Kang, T.W., Yevsa, T., Woller, N., Hoenicke, L., Wuestefeld, T., Dauch, D., Hohmeyer, A., Gereke, M., Rudalska, R., Potapova, A., *et al.* (2011). Senescence surveillance of pre-malignant hepatocytes limits liver cancer development. Nature *479*, 547-551.

149.   Xue, W., Zender, L., Miething, C., Dickins, R.A., Hernando, E., Krizhanovsky, V., Cordon-Cardo, C., and Lowe, S.W. (2007). Senescence and tumour clearance is triggered by p53 restoration in murine liver carcinomas. Nature *445*, 656-660.

150.   Krizhanovsky, V., Yon, M., Dickins, R.A., Hearn, S., Simon, J., Miething, C., Yee, H., Zender, L., and Lowe, S.W. (2008). Senescence of activated stellate cells limits liver fibrosis. Cell *134*, 657-667.

151.   Kikuchi, K., Lai, A.Y., Hsu, C.L., and Kondo, M. (2005). IL-7 receptor signaling is necessary for stage transition in adult B cell development through up-regulation of EBF. J Exp Med *201*, 1197-1203.

152.   Kikuchi, K., Kasai, H., Watanabe, A., Lai, A.Y., and Kondo, M. (2008). IL-7 specifies B cell fate at the common lymphoid progenitor to pre-proB transition stage by maintaining early B cell factor expression. Journal of immunology *181*, 383-392.

153.   Beachy, P.A., Karhadkar, S.S., and Berman, D.M. (2004). Tissue repair and stem cell renewal in carcinogenesis. Nature *432*, 324-331.

154.   McDonald, B., Pittman, K., Menezes, G.B., Hirota, S.A., Slaba, I., Waterhouse, C.C., Beck, P.L., Muruve, D.A., and Kubes, P. Intravascular danger signals guide neutrophils to sites of sterile inflammation. Science *330*, 362-366.

155.   Butler, J.M., Nolan, D.J., Vertes, E.L., Varnum-Finney, B., Kobayashi, H., Hooper, A.T., Seandel, M., Shido, K., White, I.A., Kobayashi, M., *et al.* (2010). Endothelial cells are essential for the self-renewal and repopulation of Notch-dependent hematopoietic stem cells. Cell Stem Cell *6*, 251-264.

156.   Grivennikov, S.I., Greten, F.R., and Karin, M. Immunity, inflammation, and cancer. Cell *140*, 883-899.

157.   Teijaro, J.R., Walsh, K.B., Cahalan, S., Fremgen, D.M., Roberts, E., Scott, F., Martinborough, E., Peach, R., Oldstone, M.B., and Rosen, H. (2011). Endothelial cells are central orchestrators of cytokine amplification during influenza virus infection. Cell *146*, 980-991.

158.   Chatterjee, M., Osborne, J., Bestetti, G., Chang, Y., and Moore, P.S. (2002). Viral IL-6-induced cell proliferation and immune evasion of interferon activity. Science *298*, 1432-1435.

159.   Kopf, M., Baumann, H., Freer, G., Freudenberg, M., Lamers, M., Kishimoto, T., Zinkernagel, R., Bluethmann, H., and Kohler, G. (1994). Impaired immune and acute-phase responses in interleukin-6-deficient mice. Nature *368*, 339-342.

160.   Harker, J.A., Lewis, G.M., Mack, L., and Zuniga, E.I. (2011). Late interleukin-6 escalates T follicular helper cell responses and controls a chronic viral infection. Science *334*, 825-829.

161.   Cressman, D.E., Greenbaum, L.E., DeAngelis, R.A., Ciliberto, G., Furth, E.E., Poli, V., and Taub, R. (1996). Liver failure and defective hepatocyte regeneration in interleukin-6-deficient mice. Science *274*, 1379-1383.

162.   Grivennikov, S., Karin, E., Terzic, J., Mucida, D., Yu, G.Y., Vallabhapurapu, S., Scheller, J., Rose-John, S., Cheroutre, H., Eckmann, L., *et al.* (2009). IL-6 and Stat3 are required for survival of intestinal epithelial cells and development of colitis-associated cancer. Cancer Cell *15*, 103-113.

163.   Rebouissou, S., Amessou, M., Couchy, G., Poussin, K., Imbeaud, S., Pilati, C., Izard, T., Balabaud, C., Bioulac-Sage, P., and Zucman-Rossi, J. (2009). Frequent in-frame somatic deletions activate gp130 in inflammatory hepatocellular tumours. Nature *457*, 200-204.

164.   Ngo, V.N., Young, R.M., Schmitz, R., Jhavar, S., Xiao, W., Lim, K.H., Kohlhammer, H., Xu, W., Yang, Y., Zhao, H., *et al.* Oncogenically active MYD88 mutations in human lymphoma. Nature.

165.   Baxter, E.J., Scott, L.M., Campbell, P.J., East, C., Fourouclas, N., Swanton, S., Vassiliou, G.S., Bench, A.J., Boyd, E.M., Curtin, N., *et al.* (2005). Acquired mutation of the tyrosine kinase JAK2 in human myeloproliferative disorders. Lancet *365*, 1054-1061.

166.   Bromberg, J.F., Wrzeszczynska, M.H., Devgan, G., Zhao, Y., Pestell, R.G., Albanese, C., and Darnell, J.E., Jr. (1999). Stat3 as an oncogene. Cell *98*, 295-303.

167.   Lesina, M., Kurkowski, M.U., Ludes, K., Rose-John, S., Treiber, M., Kloppel, G., Yoshimura, A., Reindl, W., Sipos, B., Akira, S., *et al.* (2011). Stat3/Socs3 activation by IL-6 transsignaling promotes progression of pancreatic intraepithelial neoplasia and development of pancreatic cancer. Cancer Cell *19*, 456-469.

168.   Naugler, W.E., Sakurai, T., Kim, S., Maeda, S., Kim, K., Elsharkawy, A.M., and Karin, M. (2007). Gender disparity in liver cancer due to sex differences in MyD88-dependent IL-6 production. Science *317*, 121-124.

169.   Park, E.J., Lee, J.H., Yu, G.Y., He, G., Ali, S.R., Holzer, R.G., Osterreicher, C.H., Takahashi, H., and Karin, M. (2010). Dietary and genetic obesity promote liver inflammation and tumorigenesis by enhancing IL-6 and TNF expression. Cell *140*, 197-208.

170.   Weissenberger, J., Loeffler, S., Kappeler, A., Kopf, M., Lukes, A., Afanasieva, T.A., Aguzzi, A., and Weis, J. (2004). IL-6 is required for glioma development in a mouse model. Oncogene *23*, 3308-3316.

171.   Rutsch, S., Neppalli, V.T., Shin, D.M., DuBois, W., Morse, H.C., 3rd, Goldschmidt, H., and Janz, S. (2010). IL-6 and MYC collaborate in plasma cell tumor formation in mice. Blood *115*, 1746-1754.

172.   Holen, K.D., and Saltz, L.B. (2001). New therapies, new directions: advances in the systemic treatment of metastatic colorectal cancer. Lancet Oncol *2*, 290-297.

173.   Bleau, A.M., Hambardzumyan, D., Ozawa, T., Fomchenko, E.I., Huse, J.T., Brennan, C.W., and Holland, E.C. (2009). PTEN/PI3K/Akt pathway regulates the side population phenotype and ABCG2 activity in glioma tumor stem-like cells. Cell Stem Cell *4*, 226-235.

174.   Eckstein, N., Servan, K., Hildebrandt, B., Politz, A., von Jonquieres, G., Wolf-Kummeth, S., Napierski, I., Hamacher, A., Kassack, M.U., Budczies, J., *et al.* (2009). Hyperactivation of the insulin-like growth factor receptor I signaling pathway is an essential event for cisplatin resistance of ovarian cancer cells. Cancer Res *69*, 2996-3003.

175.   Visvader, J.E., and Lindeman, G.J. (2008). Cancer stem cells in solid tumours: accumulating evidence and unresolved questions. Nat Rev Cancer *8*, 755-768.

176.   Corradini, P., Ladetto, M., Pileri, A., and Tarella, C. (1999). Clinical relevance of minimal residual disease monitoring in non-Hodgkin's lymphomas: a critical reappraisal of molecular strategies. Leukemia *13*, 1691-1695.

177.   Ignatiadis, M., Georgoulias, V., and Mavroudis, D. (2008). Micrometastatic disease in breast cancer: clinical implications. Eur J Cancer *44*, 2726-2736.

178.   Hideshima, T., Mitsiades, C., Tonon, G., Richardson, P.G., and Anderson, K.C. (2007). Understanding multiple myeloma pathogenesis in the bone marrow to identify new therapeutic targets. Nat Rev Cancer *7*, 585-598.

179.   Nguyen, D.X., Bos, P.D., and Massague, J. (2009). Metastasis: from dissemination to organ-specific colonization. Nat Rev Cancer *9*, 274-284.

180.   Burgess, D.J., Doles, J., Zender, L., Xue, W., Ma, B., McCombie, W.R., Hannon, G.J., Lowe, S.W., and Hemann, M.T. (2008). Topoisomerase levels determine chemotherapy response in vitro and in vivo. Proc Natl Acad Sci U S A *105*, 9053-9058.

181.   Morrison, A.J., and Shen, X. (2005). DNA repair in the context of chromatin. Cell Cycle *4*, 568-571.

182.   Heinrich, P.C., Behrmann, I., Muller-Newen, G., Schaper, F., and Graeve, L. (1998). Interleukin-6-type cytokine signalling through the gp130/Jak/STAT pathway. Biochem J *334 (Pt 2)*, 297-314.

183.   Lambert, E., Boudot, C., Kadri, Z., Soula-Rothhut, M., Sowa, M.L., Mayeux, P., Hornebeck, W., Haye, B., and Petitfrere, E. (2003). Tissue inhibitor of metalloproteinases-1 signalling pathway leading to erythroid cell survival. Biochem J *372*, 767-774.

184.   Gu, L., Zhuang, H., Safina, B., Xiao, X.Y., Bradford, W.W., and Rich, B.E. (2005). Combinatorial approach to identification of tyrphostin inhibitors of cytokine signaling. Bioorg Med Chem *13*, 4269-4278.

185.   Jourdan, M., De Vos, J., Mechti, N., and Klein, B. (2000). Regulation of Bcl-2-family proteins in myeloma cells by three myeloma survival factors: interleukin-6, interferon-alpha and insulin-like growth factor 1. Cell Death Differ *7*, 1244-1252.

186.   Medzhitov, R., and Horng, T. (2009). Transcriptional control of the inflammatory response. Nat Rev Immunol 9, 692-703.

187.   Dimri, G.P., Lee, X., Basile, G., Acosta, M., Scott, G., Roskelley, C., Medrano, E.E., Linskens, M., Rubelj, I., Pereira-Smith, O., et al. (1995). A biomarker that identifies senescent human cells in culture and in aging skin in vivo. Proc Natl Acad Sci U S A 92, 9363-9367.

188.   Delrez, M., Ikeh, V., Maisin, J.R., Mattelin, G., Haot, J., and Betz, E.H. (1978). Influence of a mixture of chemical protectors on the lymphoid regeneration of bone marrow and thymus in irradiated mice. Experientia 34, 1221-1222.

189.   Wong, V.W., Yu, J., Cheng, A.S., Wong, G.L., Chan, H.Y., Chu, E.S., Ng, E.K., Chan, F.K., Sung, J.J., and Chan, H.L. (2009). High serum interleukin-6 level predicts future hepatocellular carcinoma development in patients with chronic hepatitis B. Int J Cancer 124, 2766-2770.

190.   Xenidis, N., Ignatiadis, M., Apostolaki, S., Perraki, M., Kalbakis, K., Agelaki, S., Stathopoulos, E.N., Chlouverakis, G., Lianidou, E., Kakolyris, S., et al. (2009). Cytokeratin-19 mRNA-positive circulating tumor cells after adjuvant chemotherapy in patients with early breast cancer. J Clin Oncol 27, 2177-2184.

191.   Muller-Hermelink, H.K., Sale, G.E., Borisch, B., and Storb, R. (1987). Pathology of the thymus after allogeneic bone marrow transplantation in man. A histologic immunohistochemical study of 36 patients. Am J Pathol 129, 242-256.

192.   Sfikakis, P.P., Gourgoulis, G.M., Moulopoulos, L.A., Kouvatseas, G., Theofilopoulos, A.N., and Dimopoulos, M.A. (2005). Age-related thymic activity in adults following chemotherapy-induced lymphopenia. Eur J Clin Invest 35, 380-387.

193.   Trikha, M., Corringham, R., Klein, B., and Rossi, J.F. (2003). Targeted anti-interleukin-6 monoclonal antibody therapy for cancer: a review of the rationale and clinical evidence. Clin Cancer Res 9, 4653-4665.

194.   Seymour, J.F., Talpaz, M., Cabanillas, F., Wetzler, M., and Kurzrock, R. (1995). Serum interleukin-6 levels correlate with prognosis in diffuse large-cell lymphoma. J Clin Oncol 13, 575-582.

195.   Salgado, R., Junius, S., Benoy, I., Van Dam, P., Vermeulen, P., Van Marck, E., Huget, P., and Dirix, L.Y. (2003). Circulating interleukin-6 predicts survival in patients with metastatic breast cancer. Int J Cancer 103, 642-646.

196.   Malhotra, V., and Perry, M.C. (2003). Classical chemotherapy: mechanisms, toxicities and the therapeutic window. Cancer biology & therapy 2, S2-4.

197.   Abratt, R.P., Bezwoda, W.R., Goedhals, L., and Hacking, D.J. (1997). Weekly gemcitabine with monthly cisplatin: effective chemotherapy for advanced non-small-cell lung cancer. Journal of clinical oncology : official journal of the American Society of Clinical Oncology 15, 744-749.

198.   Werner, S., and Alzheimer, C. (2006). Roles of activin in tissue repair, fibrosis, and inflammatory disease. Cytokine Growth Factor Rev 17, 157-171.

199.   Coussens, L.M., and Werb, Z. (2002). Inflammation and cancer. Nature 420, 860-867.

200.   Mutsaers, S.E., Bishop, J.E., McGrouther, G., and Laurent, G.J. (1997). Mechanisms of tissue repair: from wound healing to fibrosis. Int J Biochem Cell Biol 29, 5-17.

201.   Stramer, B.M., Mori, R., and Martin, P. (2007). The inflammation-fibrosis link? A Jekyll and Hyde role for blood cells during wound repair. J Invest Dermatol *127*, 1009-1017.

202.   Garrett, W.S., Punit, S., Gallini, C.A., Michaud, M., Zhang, D., Sigrist, K.S., Lord, G.M., Glickman, J.N., and Glimcher, L.H. (2009). Colitis-associated colorectal cancer driven by T-bet deficiency in dendritic cells. Cancer Cell *16*, 208-219.

203.   Gilbert, L.A., and Hemann, M.T. (2010). DNA damage-mediated induction of a chemoresistant niche. Cell *143*, 355-366.

204.   Freund, A., Patil, C.K., and Campisi, J. (2011). p38MAPK is a novel DNA damage response-independent regulator of the senescence-associated secretory phenotype. The EMBO journal *30*, 1536-1548.

205.   Krtolica, A., Parrinello, S., Lockett, S., Desprez, P.Y., and Campisi, J. (2001). Senescent fibroblasts promote epithelial cell growth and tumorigenesis: a link between cancer and aging. Proceedings of the National Academy of Sciences of the United States of America *98*, 12072-12077.

206.   Bauernfeind, F.G., Horvath, G., Stutz, A., Alnemri, E.S., MacDonald, K., Speert, D., Fernandes-Alnemri, T., Wu, J., Monks, B.G., Fitzgerald, K.A., *et al.* (2009). Cutting edge: NF-kappaB activating pattern recognition and cytokine receptors license NLRP3 inflammasome activation by regulating NLRP3 expression. Journal of immunology *183*, 787-791.

207.   Calfon, M., Zeng, H., Urano, F., Till, J.H., Hubbard, S.R., Harding, H.P., Clark, S.G., and Ron, D. (2002). IRE1 couples endoplasmic reticulum load to secretory capacity by processing the XBP-1 mRNA. Nature *415*, 92-96.

208.   Shaffer, A.L., Shapiro-Shelef, M., Iwakoshi, N.N., Lee, A.H., Qian, S.B., Zhao, H., Yu, X., Yang, L., Tan, B.K., Rosenwald, A., *et al.* (2004). XBP1, downstream of Blimp-1, expands the secretory apparatus and other organelles, and increases protein synthesis in plasma cell differentiation. Immunity *21*, 81-93.

209.   Lee, A.H., Heidtman, K., Hotamisligil, G.S., and Glimcher, L.H. (2011). Dual and opposing roles of the unfolded protein response regulated by IRE1alpha and XBP1 in proinsulin processing and insulin secretion. Proceedings of the National Academy of Sciences of the United States of America *108*, 8885-8890.

210.   Paris, F., Fuks, Z., Kang, A., Capodieci, P., Juan, G., Ehleiter, D., Haimovitz-Friedman, A., Cordon-Cardo, C., and Kolesnick, R. (2001). Endothelial apoptosis as the primary lesion initiating intestinal radiation damage in mice. Science *293*, 293-297.

211.   Jin, D.K., Shido, K., Kopp, H.G., Petit, I., Shmelkov, S.V., Young, L.M., Hooper, A.T., Amano, H., Avecilla, S.T., Heissig, B., *et al.* (2006). Cytokine-mediated deployment of SDF-1 induces revascularization through recruitment of CXCR4+ hemangiocytes. Nature medicine *12*, 557-567.

212.   Madlambayan, G.J., Butler, J.M., Hosaka, K., Jorgensen, M., Fu, D., Guthrie, S.M., Shenoy, A.K., Brank, A., Russell, K.J., Otero, J., *et al.* (2009). Bone marrow stem and progenitor cell contribution to neovasculogenesis is dependent on model system with SDF-1 as a permissive trigger. Blood *114*, 4310-4319.

213.   Heissig, B., Hattori, K., Dias, S., Friedrich, M., Ferris, B., Hackett, N.R., Crystal, R.G., Besmer, P., Lyden, D., Moore, M.A., *et al.* (2002). Recruitment of stem and progenitor cells from the bone marrow niche requires MMP-9 mediated release of kit-ligand. Cell *109*, 625-637.

214.   Ding, B.S., Nolan, D.J., Butler, J.M., James, D., Babazadeh, A.O., Rosenwaks, Z., Mittal, V., Kobayashi, H., Shido, K., Lyden, D., *et al.* (2010). Inductive angiocrine signals from sinusoidal endothelium are required for liver regeneration. Nature *468*, 310-315.

215.   DiPietro, L.A., Burdick, M., Low, Q.E., Kunkel, S.L., and Strieter, R.M. (1998). MIP-1alpha as a critical macrophage chemoattractant in murine wound repair. The Journal of clinical investigation *101*, 1693-1698.

216.   Ding, B.S., Nolan, D.J., Guo, P., Babazadeh, A.O., Cao, Z., Rosenwaks, Z., Crystal, R.G., Simons, M., Sato, T.N., Worgall, S., *et al.* (2011). Endothelial-derived angiocrine signals induce and sustain regenerative lung alveolarization. Cell *147*, 539-553.

217.   Richardson, C.E., Kooistra, T., and Kim, D.H. (2010). An essential role for XBP-1 in host protection against immune activation in C. elegans. Nature *463*, 1092-1095.

218.   Richardson, C.E., Kinkel, S., and Kim, D.H. (2011). Physiological IRE-1-XBP-1 and PEK-1 signaling in Caenorhabditis elegans larval development and immunity. PLoS Genet *7*, e1002391.

219.   Bartz, S.R., Zhang, Z., Burchard, J., Imakura, M., Martin, M., Palmieri, A., Needham, R., Guo, J., Gordon, M., Chung, N., *et al.* (2006). Small interfering RNA screens reveal enhanced cisplatin cytotoxicity in tumor cells having both BRCA network and TP53 disruptions. Mol Cell Biol *26*, 9377-9386.

220.   Berns, K., Horlings, H.M., Hennessy, B.T., Madiredjo, M., Hijmans, E.M., Beelen, K., Linn, S.C., Gonzalez-Angulo, A.M., Stemke-Hale, K., Hauptmann, M., *et al.* (2007). A functional genetic approach identifies the PI3K pathway as a major determinant of trastuzumab resistance in breast cancer. Cancer Cell *12*, 395-402.

221.   Huang, S., Laoukili, J., Epping, M.T., Koster, J., Holzel, M., Westerman, B.A., Nijkamp, W., Hata, A., Asgharzadeh, S., Seeger, R.C., *et al.* (2009). ZNF423 is critically required for retinoic acid-induced differentiation and is a marker of neuroblastoma outcome. Cancer Cell *15*, 328-340.

222.   Doles, J., and Hemann, M.T. Nek4 status differentially alters sensitivity to distinct microtubule poisons. Cancer Res *70*, 1033-1041.

223.   Smogorzewska, A., Desetty, R., Saito, T.T., Schlabach, M., Lach, F.P., Sowa, M.E., Clark, A.B., Kunkel, T.A., Harper, J.W., Colaiacovo, M.P., *et al.* A genetic screen identifies FAN1, a Fanconi anemia-associated nuclease necessary for DNA interstrand crosslink repair. Mol Cell *39*, 36-47.

224.   Zender, L., Xue, W., Zuber, J., Semighini, C.P., Krasnitz, A., Ma, B., Zender, P., Kubicka, S., Luk, J.M., Schirmacher, P., *et al.* (2008). An oncogenomics-based in vivo RNAi screen identifies tumor suppressors in liver cancer. Cell *135*, 852-864.

225.   Adams, J.M., and Cory, S. (2007). Bcl-2-regulated apoptosis: mechanism and therapeutic potential. Curr Opin Immunol *19*, 488-496.

226.   Cotter, T.G. (2009). Apoptosis and cancer: the genesis of a research field. Nat Rev Cancer *9*, 501-507.

227.   Certo, M., Del Gaizo Moore, V., Nishino, M., Wei, G., Korsmeyer, S., Armstrong, S.A., and Letai, A. (2006). Mitochondria primed by death signals determine cellular addiction to antiapoptotic BCL-2 family members. Cancer Cell *9*, 351-365.

228.   Deng, J., Carlson, N., Takeyama, K., Dal Cin, P., Shipp, M., and Letai, A. (2007). BH3 profiling identifies three distinct classes of apoptotic blocks to predict response to ABT-737 and conventional chemotherapeutic agents. Cancer Cell 12, 171-185.

229.   Letai, A.G. (2008). Diagnosing and exploiting cancer's addiction to blocks in apoptosis. Nat Rev Cancer 8, 121-132.

230.   Youle, R.J., and Strasser, A. (2008). The BCL-2 protein family: opposing activities that mediate cell death. Nat Rev Mol Cell Biol 9, 47-59.

231.   Jiang, H., Pritchard, J.R., Williams, R.T., Lauffenburger, D.A., and Hemann, M.T. (2011). A mammalian functional-genetic approach to characterizing cancer therapeutics. Nature chemical biology 7, 92-100.

232.   Lu, J., Getz, G., Miska, E.A., Alvarez-Saavedra, E., Lamb, J., Peck, D., Sweet-Cordero, A., Ebert, B.L., Mak, R.H., Ferrando, A.A., et al. (2005). MicroRNA expression profiles classify human cancers. Nature 435, 834-838.

233.   Smith, T.F., and Waterman, M.S. (1981). Identification of common molecular subsequences. J Mol Biol 147, 195-197.

234.   Lindemann, R.K., Newbold, A., Whitecross, K.F., Cluse, L.A., Frew, A.J., Ellis, L., Williams, S., Wiegmans, A.P., Dear, A.E., Scott, C.L., et al. (2007). Analysis of the apoptotic and therapeutic activities of histone deacetylase inhibitors by using a mouse model of B cell lymphoma. Proceedings of the National Academy of Sciences of the United States of America 104, 8071-8076.

235.   Villunger, A., Michalak, E.M., Coultas, L., Mullauer, F., Bock, G., Ausserlechner, M.J., Adams, J.M., and Strasser, A. (2003). p53- and drug-induced apoptotic responses mediated by BH3-only proteins puma and noxa. Science 302, 1036-1038.

236.   Wang, K., Yin, X.M., Chao, D.T., Milliman, C.L., and Korsmeyer, S.J. (1996). BID: a novel BH3 domain-only death agonist. Genes Dev 10, 2859-2869.

237.   Li, H., Zhu, H., Xu, C.J., and Yuan, J. (1998). Cleavage of BID by caspase 8 mediates the mitochondrial damage in the Fas pathway of apoptosis. Cell 94, 491-501.

238.   Zinkel, S.S., Hurov, K.E., Ong, C., Abtahi, F.M., Gross, A., and Korsmeyer, S.J. (2005). A role for proapoptotic BID in the DNA-damage response. Cell 122, 579-591.

239.   Kaufmann, T., Tai, L., Ekert, P.G., Huang, D.C., Norris, F., Lindemann, R.K., Johnstone, R.W., Dixit, V.M., and Strasser, A. (2007). The BH3-only protein bid is dispensable for DNA damage- and replicative stress-induced apoptosis or cell-cycle arrest. Cell 129, 423-433.

240.   Ren, D., Tu, H.C., Kim, H., Wang, G.X., Bean, G.R., Takeuchi, O., Jeffers, J.R., Zambetti, G.P., Hsieh, J.J., and Cheng, E.H. (2010). BID, BIM, and PUMA are essential for activation of the BAX- and BAK-dependent cell death program. Science 330, 1390-1393.

241.   Mandal, P.K., Blanpain, C., and Rossi, D.J. (2011). DNA damage response in adult stem cells: pathways and consequences. Nature reviews Molecular cell biology 12, 198-202.

242.   Mohrin, M., Bourke, E., Alexander, D., Warr, M.R., Barry-Holson, K., Le Beau, M.M., Morrison, C.G., and Passegue, E. (2010). Hematopoietic stem cell quiescence promotes error-prone DNA repair and mutagenesis. Cell Stem Cell 7, 174-185.

243.   Beltrami, A.P., Barlucchi, L., Torella, D., Baker, M., Limana, F., Chimenti, S., Kasahara, H., Rota, M., Musso, E., Urbanek, K., *et al.* (2003). Adult cardiac stem cells are multipotent and support myocardial regeneration. Cell *114*, 763-776.

244.   Ashton, G.H., Morton, J.P., Myant, K., Phesse, T.J., Ridgway, R.A., Marsh, V., Wilkins, J.A., Athineos, D., Muncan, V., Kemp, R., *et al.* (2010). Focal adhesion kinase is required for intestinal regeneration and tumorigenesis downstream of Wnt/c-Myc signaling. Dev Cell *19*, 259-269.

245.   Blanpain, C., Mohrin, M., Sotiropoulou, P.A., and Passegue, E. (2011). DNA-damage response in tissue-specific and cancer stem cells. Cell Stem Cell *8*, 16-29.

246.   Rothenberg, E.V., Moore, J.E., and Yui, M.A. (2008). Launching the T-cell-lineage developmental programme. Nature reviews Immunology *8*, 9-21.

247.   Kuchen, S., Robbins, R., Sims, G.P., Sheng, C., Phillips, T.M., Lipsky, P.E., and Ettinger, R. (2007). Essential role of IL-21 in B cell activation, expansion, and plasma cell generation during CD4+ T cell-B cell collaboration. Journal of immunology *179*, 5886-5896.

248.   Ettinger, R., Sims, G.P., Robbins, R., Withers, D., Fischer, R.T., Grammer, A.C., Kuchen, S., and Lipsky, P.E. (2007). IL-21 and BAFF/BLyS synergize in stimulating plasma cell differentiation from a unique population of human splenic memory B cells. Journal of immunology *178*, 2872-2882.

249.   Ettinger, R., Sims, G.P., Fairhurst, A.M., Robbins, R., da Silva, Y.S., Spolski, R., Leonard, W.J., and Lipsky, P.E. (2005). IL-21 induces differentiation of human naive and memory B cells into antibody-secreting plasma cells. Journal of immunology *175*, 7867-7879.

250.   Burchill, M.A., Goetz, C.A., Prlic, M., O'Neil, J.J., Harmon, I.R., Bensinger, S.J., Turka, L.A., Brennan, P., Jameson, S.C., and Farrar, M.A. (2003). Distinct effects of STAT5 activation on CD4+ and CD8+ T cell homeostasis: development of CD4+CD25+ regulatory T cells versus CD8+ memory T cells. Journal of immunology *171*, 5853-5864.

251.   Hanahan, D., and Weinberg, R.A. (2011). Hallmarks of cancer: the next generation. Cell *144*, 646-674.

252.   Haluska, F.G., Finver, S., Tsujimoto, Y., and Croce, C.M. (1986). The t(8; 14) chromosomal translocation occurring in B-cell malignancies results from mistakes in V-D-J joining. Nature *324*, 158-161.

253.   Michaloglou, C., Vredeveld, L.C., Soengas, M.S., Denoyelle, C., Kuilman, T., van der Horst, C.M., Majoor, D.M., Shay, J.W., Mooi, W.J., and Peeper, D.S. (2005). BRAFE600-associated senescence-like cell cycle arrest of human naevi. Nature *436*, 720-724.

254.   Hemann, M.T., Bric, A., Teruya-Feldstein, J., Herbst, A., Nilsson, J.A., Cordon-Cardo, C., Cleveland, J.L., Tansey, W.P., and Lowe, S.W. (2005). Evasion of the p53 tumour surveillance network by tumour-derived MYC mutants. Nature *436*, 807-811.

255.   Zindy, F., Eischen, C.M., Randle, D.H., Kamijo, T., Cleveland, J.L., Sherr, C.J., and Roussel, M.F. (1998). Myc signaling via the ARF tumor suppressor regulates p53-dependent apoptosis and immortalization. Genes Dev *12*, 2424-2433.

256.   Serrano, M., Lin, A.W., McCurrach, M.E., Beach, D., and Lowe, S.W. (1997). Oncogenic ras provokes premature cell senescence associated with accumulation of p53 and p16INK4a. Cell *88*, 593-602.

257. Kelly, P.N., Grabow, S., Delbridge, A.R., Strasser, A., and Adams, J.M. (2011). Endogenous Bcl-xL is essential for Myc-driven lymphomagenesis in mice. Blood *118*, 6380-6386.

258. Lindeman, G.J., Adams, J.M., Cory, S., and Harris, A.W. (1994). B-lymphoid to granulocytic switch during hematopoiesis in a transgenic mouse strain. Immunity *1*, 517-527.

259. Strasser, A., Harris, A.W., Bath, M.L., and Cory, S. (1990). Novel primitive lymphoid tumours induced in transgenic mice by cooperation between myc and bcl-2. Nature *348*, 331-333.

260. Kelly, P.N., Puthalakath, H., Adams, J.M., and Strasser, A. (2007). Endogenous bcl-2 is not required for the development of Emu-myc-induced B-cell lymphoma. Blood *109*, 4907-4913.

261. Nagasawa, T. (2006). Microenvironmental niches in the bone marrow required for B-cell development. Nature reviews Immunology *6*, 107-116.

262. Hilbert, D.M., Kopf, M., Mock, B.A., Kohler, G., and Rudikoff, S. (1995). Interleukin 6 is essential for in vivo development of B lineage neoplasms. J Exp Med *182*, 243-248.

263. Hardy, R.R., Li, Y.S., Allman, D., Asano, M., Gui, M., and Hayakawa, K. (2000). B-cell commitment, development and selection. Immunol Rev *175*, 23-32.

264. Wang, H., Pierce, L.J., and Spangrude, G.J. (2006). Distinct roles of IL-7 and stem cell factor in the OP9-DL1 T-cell differentiation culture system. Exp Hematol *34*, 1730-1740.

265. Pronk, C.J., Veiby, O.P., Bryder, D., and Jacobsen, S.E. (2011). Tumor necrosis factor restricts hematopoietic stem cell activity in mice: involvement of two distinct receptors. The Journal of experimental medicine *208*, 1563-1570.

266. Sherr, C.J., and DePinho, R.A. (2000). Cellular senescence: mitotic clock or culture shock? Cell *102*, 407-410.

267. Bernad, A., Kopf, M., Kulbacki, R., Weich, N., Koehler, G., and Gutierrez-Ramos, J.C. (1994). Interleukin-6 is required in vivo for the regulation of stem cells and committed progenitors of the hematopoietic system. Immunity *1*, 725-731.

268. Reynaud, D., Pietras, E., Barry-Holson, K., Mir, A., Binnewies, M., Jeanne, M., Sala-Torra, O., Radich, J.P., and Passegue, E. (2011). IL-6 controls leukemic multipotent progenitor cell fate and contributes to chronic myelogenous leukemia development. Cancer Cell *20*, 661-673.

269. Heinrich, P.C., Castell, J.V., and Andus, T. (1990). Interleukin-6 and the acute phase response. The Biochemical journal *265*, 621-636.

270. Kane, M., Case, L.K., Kopaskie, K., Kozlova, A., MacDearmid, C., Chervonsky, A.V., and Golovkina, T.V. (2011). Successful transmission of a retrovirus depends on the commensal microbiota. Science *334*, 245-249.

271. Hirano, T. (1991). Interleukin 6 (IL-6) and its receptor: their role in plasma cell neoplasias. Int J Cell Cloning *9*, 166-184.

272. Beagley, K.W., Eldridge, J.H., Lee, F., Kiyono, H., Everson, M.P., Koopman, W.J., Hirano, T., Kishimoto, T., and McGhee, J.R. (1989). Interleukins and IgA synthesis. Human and murine interleukin 6 induce high rate IgA secretion in IgA-committed B cells. The Journal of experimental medicine *169*, 2133-2148.

273.	Yao, Z., Fenoglio, S., Gao, D.C., Camiolo, M., Stiles, B., Lindsted, T., Schlederer, M., Johns, C., Altorki, N., Mittal, V., et al. (2010). TGF-beta IL-6 axis mediates selective and adaptive mechanisms of resistance to molecular targeted therapy in lung cancer. Proceedings of the National Academy of Sciences of the United States of America 107, 15535-15540.

274.	Cheung, W.C., and Van Ness, B. (2002). Distinct IL-6 signal transduction leads to growth arrest and death in B cells or growth promotion and cell survival in myeloma cells. Leukemia : official journal of the Leukemia Society of America, Leukemia Research Fund, UK 16, 1182-1188.

275.	Kikuchi, K., Lai, A.Y., Hsu, C.L., and Kondo, M. (2005). IL-7 receptor signaling is necessary for stage transition in adult B cell development through up-regulation of EBF. The Journal of experimental medicine 201, 1197-1203.

276.	Heltemes-Harris, L.M., Willette, M.J., Ramsey, L.B., Qiu, Y.H., Neeley, E.S., Zhang, N., Thomas, D.A., Koeuth, T., Baechler, E.C., Kornblau, S.M., et al. (2011). Ebf1 or Pax5 haploinsufficiency synergizes with STAT5 activation to initiate acute lymphoblastic leukemia. The Journal of experimental medicine 208, 1135-1149.

277.	Pasqualucci, L., Compagno, M., Houldsworth, J., Monti, S., Grunn, A., Nandula, S.V., Aster, J.C., Murty, V.V., Shipp, M.A., and Dalla-Favera, R. (2006). Inactivation of the PRDM1/BLIMP1 gene in diffuse large B cell lymphoma. The Journal of experimental medicine 203, 311-317.

278.	Pasqualucci, L., Neumeister, P., Goossens, T., Nanjangud, G., Chaganti, R.S., Kuppers, R., and Dalla-Favera, R. (2001). Hypermutation of multiple proto-oncogenes in B-cell diffuse large-cell lymphomas. Nature 412, 341-346.

279.	Mullighan, C.G., Su, X., Zhang, J., Radtke, I., Phillips, L.A., Miller, C.B., Ma, J., Liu, W., Cheng, C., Schulman, B.A., et al. (2009). Deletion of IKZF1 and prognosis in acute lymphoblastic leukemia. The New England journal of medicine 360, 470-480.

280.	O'Brien, P., Morin, P., Jr., Ouellette, R.J., and Robichaud, G.A. (2011). The Pax-5 Gene: A Pluripotent Regulator of B-cell Differentiation and Cancer Disease. Cancer research 71, 7345-7350.

281.	Bryder, D., and Sigvardsson, M. (2010). Shaping up a lineage--lessons from B lymphopoesis. Current opinion in immunology 22, 148-153.

282.	Kelly, P.N., Dakic, A., Adams, J.M., Nutt, S.L., and Strasser, A. (2007). Tumor growth need not be driven by rare cancer stem cells. Science 317, 337.

283.	Hemann, M.T. (2012). The Development and Use of Genetically Tractable Preclinical Mouse Models
Genetically Engineered Mice for Cancer Research. In, J.E. Green, and T. Ried, eds. (Springer New York), pp. 477-495.

284.	Abeloff, M.D. (2008). Abeloff's clinical oncology, 4th edn (Philadelphia, Churchill Livingstone/Elsevier).

285.	Kalluri, R., and Zeisberg, M. (2006). Fibroblasts in cancer. Nature reviews Cancer 6, 392-401.

286.	Dudakov, J.A., Hanash, A.M., Jenq, R.R., Young, L.F., Ghosh, A., Singer, N.V., West, M.L., Smith, O.M., Holland, A.M., Tsai, J.J., et al. (2012). Interleukin-22 Drives Endogenous Thymic Regeneration in Mice. Science.

287. Kenins, L., Gill, J.W., Boyd, R.L., Hollander, G.A., and Wodnar-Filipowicz, A. (2008). Intrathymic expression of Flt3 ligand enhances thymic recovery after irradiation. The Journal of experimental medicine *205*, 523-531.

288. Cichowski, K., and Hahn, W.C. (2008). Unexpected pieces to the senescence puzzle. Cell *133*, 958-961.

289. Baker, D.J., Wijshake, T., Tchkonia, T., LeBrasseur, N.K., Childs, B.G., van de Sluis, B., Kirkland, J.L., and van Deursen, J.M. (2011). Clearance of p16Ink4a-positive senescent cells delays ageing-associated disorders. Nature *479*, 232-236.

290. Pasquier, E., Kavallaris, M., and Andre, N. Metronomic chemotherapy: new rationale for new directions. Nat Rev Clin Oncol *7*, 455-465.

291. Shibamoto, Y., Otsuka, S., Iwata, H., Sugie, C., Ogino, H., and Tomita, N. (2012). Radiobiological evaluation of the radiation dose as used in high-precision radiotherapy: effect of prolonged delivery time and applicability of the linear-quadratic model. J Radiat Res *53*, 1-9.

292. Barth, T.F., Leithauser, F., Joos, S., Bentz, M., and Moller, P. (2002). Mediastinal (thymic) large B-cell lymphoma: where do we stand? The lancet oncology *3*, 229-234.

293. Trikha, M., Corringham, R., Klein, B., and Rossi, J.F. (2003). Targeted anti-interleukin-6 monoclonal antibody therapy for cancer: a review of the rationale and clinical evidence. Clinical cancer research : an official journal of the American Association for Cancer Research *9*, 4653-4665.

294. Jones, S.A., Horiuchi, S., Topley, N., Yamamoto, N., and Fuller, G.M. (2001). The soluble interleukin 6 receptor: mechanisms of production and implications in disease. The FASEB journal : official publication of the Federation of American Societies for Experimental Biology *15*, 43-58.

295. Hoshida, Y., Villanueva, A., Kobayashi, M., Peix, J., Chiang, D.Y., Camargo, A., Gupta, S., Moore, J., Wrobel, M.J., Lerner, J., et al. (2008). Gene expression in fixed tissues and outcome in hepatocellular carcinoma. The New England journal of medicine *359*, 1995-2004.

296. Yang, F., Jove, V., Buettner, R., Xin, H., Wu, J., Wang, Y., Nam, S., Xu, Y., Ara, T., Declerck, Y.A., et al. (2012). Sorafenib inhibits endogenous and IL-6/S1P induced JAK2-STAT3 signaling in human neuroblastoma, associated with growth suppression and apoptosis. Cancer biology & therapy *13*.